POLITECNICO
MILANO 1863

Politecnico di Milano
Dipartimento di Scienze e Tecnologie Aerospaziali

CubeSat mission design for in-orbit environment characterisation

Master Thesis

Student:
Marco Paolo Brenna
ID:
905630
Date: **December 2020**

Supervisor:
Camilla Colombo
Co-supervisors:
Francesca Scala
Dr. Mirko Trisolini

Abstract

Space sustainability is one of the primary concern for future ability of all humanity to continue the space activities for socio-economics benefits. Years of unregulated orbit exploitation, technology demonstrations and testing have led to an exponential growth of space debris, resulting in an increased risk for satellites. Moreover, it may create a cascade effect, known as the Kessler syndrome. To secure future space exploration, it is of primary importance to understand and characterise the space debris phenomenon and develop a sustainable mission that implements end-of-life solutions. With this premises, this thesis develops the preliminary design of a CubeSat mission to characterise the debris environment in low Earth orbit. Moreover, the mission aims at testing a new concept of in-orbit autonomous collision avoidance system, that could reduce both the costs and the risk of a collision avoidance manoeuvre. At the end of the mission, the spacecraft would implement a de-orbit strategy exploiting atmosphere drag, reducing the orbit decay time. Due to the high uncertainties in the atmospheric models the reentry evolution and decay time is usually difficult to predict. To face the issues generated by the uncertain reentry models, this thesis investigates the feasibility of implementing a payload to measure and collect data regarding atmosphere temperature and pressure during the re-entry. To trace the loads effects on the spacecraft, accelerations and structures temperature and strains are registered. The objective is to validate and improve the re-entry models via post-processing of the collected data, until the break up of the satellite below 100 km altitude. This work poses the basis for future CubeSat scientific missions for Low Earth Orbit characterisation. A wide CubeSat programme could help the scientific community to work with high fidelity in-situ measurements to elaborate more accurate models. Thanks to small dimensions and low budget, CubeSat are an effective and low-cost means to improve our orbit environment knowledge, and increase awareness for better and sustainable use of space. This thesis and the mission proposal was part of the COMPASS project: Control for orbit manoeuvring by surfing through orbit perturbations (Grant agreement No 679086). This project is European Research Council (ERC) funded project under the European Unions Horizon 2020 research.

Keywords: CubeSat, LEO, Space Debris, Reentry analysis, Collision Avoidance, Space Environment

Sommario

La sostenibilità spaziale è una delle preoccupazioni principali per la futura capacità di tutta l'umanità di proseguire le attività spaziali con un vantaggio socio-economico. Anni di sfruttamento non regolamentato dello spazio, a seguito di dimostrazioni tecnologiche e test, hanno condotto ad una crescita esponenziale dei detriti spaziali, causando un aumento di rischio per i satelliti. In questo modo, si potrebbe presentare il rischio dell'innesco di un fenomeno a cascata, conosciuto come sindrome di Kessler. Per salvaguardare la futura esplorazione spaziale, è di importanza strategica comprendere e analizzare il fenomeno dei detriti spaziali, e sviluppare missioni sostenibili che implementino strategie di fine vita. In questo contesto, questa tesi presenta lo studio preliminare di una missione CubeSat volta a definire l'ambiente dei detriti nell'orbita terrestre bassa. Inoltre, la missione mira a esaminare una nuova concezione del sistema autonomo di prevenzione della collisione in orbita, che possa ridurre sia i costi sia il rischio di una collisione. Al termine della missione, il satellite implementerà una strategia di rientro, che sfrutti l'attrito generato dall'atmosfera, riducendo il tempo di decadimento dell'orbita. A causa delle elevate incertezze nei modelli dell'atmosfera, la fase di rientro di oggetti spaziali è spesso molto difficile da predire. Per affrontare i problemi generati da dall'incertezza dei modelli di rientro, questa tesi indaga la possibilità di implementare uno strumento per misurare e raccogliere dati durante la fase di rientro, principalmente la temperatura e la pressione atmosferica. Per tenere traccia degli effetti dei carichi aerodinamici sul satellite, le accelerazioni, la temperatura e le deformazioni della struttura vengono misurati e immagazzinati a bordo, fino alla distruzione del satellite ad una quota inferiore ai 100 km. Lo scopo è convalidare e migliorare i modelli di rientro utilizzando un'elaborazione a posteriori dei dati raccolti. Questo lavoro pone le basi per un futuro utilizzo scientifico dei CubeSat nella definizione dell'ambiente presente in orbita terrestre bassa. Un programma che preveda un utilizzo distribuito di CubeSats, potrebbe fornire alla comunità scientifica misurazioni in tempo reale di alta qualità, volte ad elaborare modelli più accurati. Grazie alle piccole dimensioni e al budget ridotto rispetto alle missioni classiche, i Cubesats rappresentano un mezzo efficace per migliorare la conoscenza dell'ambiente orbitale e accrescere la consapevolezza per un uso migliore e più sostenibile dello spazio.
Questa tesi fa parte del progetto COMPASS: controllo di manovre sfruttando le perturbazioni orbitali (sovvenzione No 679086). Questo progetto è finanziato dall' European Research Council (ERC) attraverso l'European Unions Horizon 2020.

Parole chiave: CubeSat, LEO, detriti spaziali, analisi di rientro, manovra anticollisione, ambiente spaziale

Contents

List of Figures

List of Tables

1 Introduction

Since 2015, all United Nations Member States adopted the 17 Sustainable Development Goals (SDGs) to recognise the vital role of social, economic and environmental sustainability for the future development of economy and technology [8]. The protection of Earth's environment, including atmosphere, forests, oceans and space, is one of the priorities of the SDGs. Sustainability has become the key driver of new technologies development. Since the beginning of the Industrial Age in the XVIII century, the unregulated exploitation of the available resources poses a threat to the sustainability of future life on Earth, and arises the consciousness that the Earth resources are limited and must be protected. This awareness have drastically changed the mankind approach to the future of Earth.
Today, the sustainability of space missions is gaining more and more importance [9]. At the beginning of space exploration, no guidelines or regulations had been developed to limit the impact of space activities on the environment. The attention was focused on technology development and new ways to improve space activity. Earth orbit capabilities have long been treated as an infinite resource and early missions did not implement end-of-life disposal strategies. The number of launches has faced an incredible growth in the last decade [10] thanks to the reduction of costs that has granted space access to an increasing number of both private and public stakeholders (i.e. SpaceX , OneWeb Constellation). The increased space exploitation drives the need for better regulations and a deeper understanding of the sustainable use of the space environment [11]. Since 1993, the Inter-Agency Space Debris Coordination Committee (IADC) [12] introduces the recommended guidelines for end-of-life mitigation strategies. If no actions are taken in this direction, in the future we could assist to a saturation of the orbits capability and an unregulated growth of the untraceable space debris, leading to a more difficult access to space. It is important that the awareness reached for the Earth preservation reflects also in space awareness, ensuring a safe and sustainable use of space that can grant future generations the possibility to continue space pursuit. The objective of this thesis is to improve the knowledge of the Low Earth Orbit environment, with a better understanding of the space debris distribution and time evolution, and more detailed atmosphere and reentry models.

1.1 Background

A significant man made particles environment has been generated by more than half a century of space flight activities. The causes of the particles environment growth can be identified in the explosions, in space collisions and breakups of space infrastructures [10], which are the primary source of debris in millimetres and centimetres size [13] . According to a definition by the Inter-Agency Debris Coordination Committee (IADC) "space debris are all man-made objects including fragments and element thereof, in Earth orbit or re-entering the atmosphere, that are non-functional" [12]. Low Earth orbit debris particle can reenter the atmosphere after few weeks, years or centuries, depending on their altitude, due to the drag and perturbing force acting on the particle that deceler-

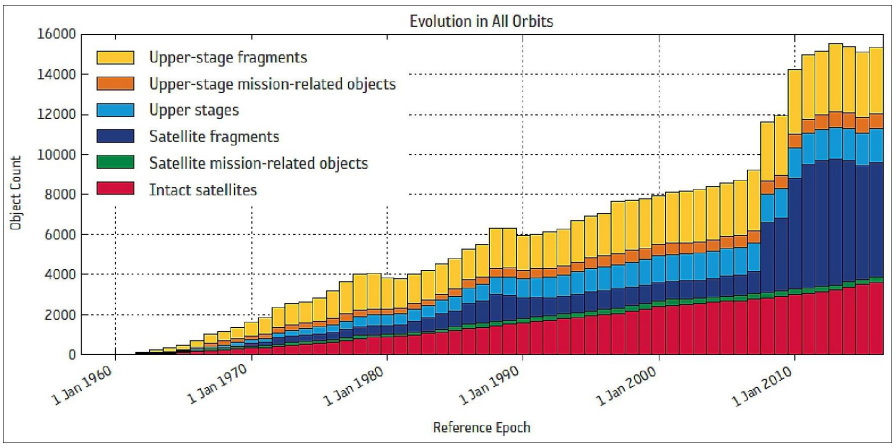

Figure 1: Evolution of the tracked and published space object population and its composition by object class -status January 2017. Credit: ESA

ate it. Air drag is effective for altitudes lower than 700-800 km; for higher altitudes the atmosphere density is less and objects generally remain in orbit for several decades. The maximum debris concentration altitude is determined by the balancing effects of debris creation and orbital decay, and can be identified in two peaks: one in the region between 800 and 1000 km, and the second at about 1400 km [14]. The debris environment characterisation is mainly based on ground-based radar and optical measurement. Routine space surveillance and tracking can recognise objects as small as 5 cm to 10 cm in LEO, which is the accepted threshold for untraceable space debris [15]. For smaller debris only in situ observations during experimental and statistical analysis can provide information and data. The information about debris objects smaller than this threshold is based on a statistical model from the national space agencies, as ESA, JAXA and NASA. However, the millimetre to centimetre size debris population is less known than the bigger size population, and debris models do not completely agree for this class. The knowledge of the debris environment is important for the space agencies to design spacecraft that can withstand impacts from small objects, and design collision avoidance systems. Furthermore, the debris models are also a tool to predict future evolution of the debris orbit environment. The knowledge of the possible future evolution and behaviour of the debris environment is essential to develop efficient space debris mitigation guidelines.

Figure 1 represents the time evolution of the tracked objects divided by class [16].

About the 57% of the catalogued objects is generated by more than 290 break-ups in orbit, explosions, and from about 10 suspected collisions [17].

The proliferation of small satellites and constellations has determined an increase in the LEO protected region space traffic. The number of orbital objects is expected to grow steadily, considering today's rate of 70-90 launch per year [18] and the increasing number of small spacecraft per launch. As a consequence, the probability of catastrophic collisions will grow accordingly. At typical collision speeds of 10 km/s in low orbits, im-

pacts by millimetre-size objects could cause local damage to an operating satellite [19], while collisions with debris larger than 1 cm can cause operative failures to spacecrafts. Finally, an impact with a debris larger than 10 cm can lead to a catastrophic break-up: the complete destruction of a spacecraft and generation of a debris cloud [20]. The worst case scenario can drive to a cascading process, the Kessler syndrome, in which each collision between objects generates more space debris. The Kessler Syndrome is a theory proposed by NASA scientist Donald J. Kessler in 1978, used to describe a self-sustaining cascading collision of space debris in LEO (Low Earth Orbit) [21]. It's the idea that satellite collisions would produce orbiting fragments, each of which would increase the probability of further collisions, leading to the growth of a belt of debris around the Earth [22]. The first documented space collision between two catalogued objects regards the Cerise satellite and a fragment of Ariane-1 H-10 in 1997. In 2009 instead was registered the first accidental collision between two intact satellites, when the communication satellite Iridium-33 collided with the Russian Cosmos-2251 military satellite, at an altitude of 776 km and with a relative speed of 11.7 km/s. Both spacecraft where destroyed, and more than 2300 collision fragments have been tracked. Some of the fragments have since reentered, but many of them are still in orbit [23]. From the consequences of this event together with other fragmentation events as the destruction of Fengyun-1C or the explosion of Briz-M in 2012, all the mission operators have seen as good practice the inclusion of the collision avoidance as part of routine operations, in order to mitigate space debris [3]. Active collision avoidance is today a routine task in space operations indeed, and validated, accurate and updated space surveillance data are available to mission operators. For a typical satellite in LEO hundreds of conjunction alerts can be expected every week [3], but only a few result in an actual collision avoidance manoeuvre. In 2018 ESA-operated satellites have performed 27 debris avoidance manoeuvre, but this number is growing every year [3]. Such an approach requires 27/7 operators availability, in order to analyse the parameters and constraints of the conjunction event. This generates high operational costs.

One important concept for conscientious space exploration is to consider the space environment as a shared and limited natural resource. The IADC (Inter-Agency Space Debris Coordination Committee), the most-recognised international entity on space debris, defined a set of mitigation guidelines, which also served as input to the space debris mitigation guidelines adopted by the UNCOPUOS (UN Committee on the Peaceful Uses of Outer Space). The key recommendations are [12]:

- limit debris release during normal operations
- minimise the potential for break-ups during operational phases
- limit the probability of accidental collisions
- refrain from intentional destruction and other harmful activities
- minimise the potential for post-mission break-ups resulting from stored energy

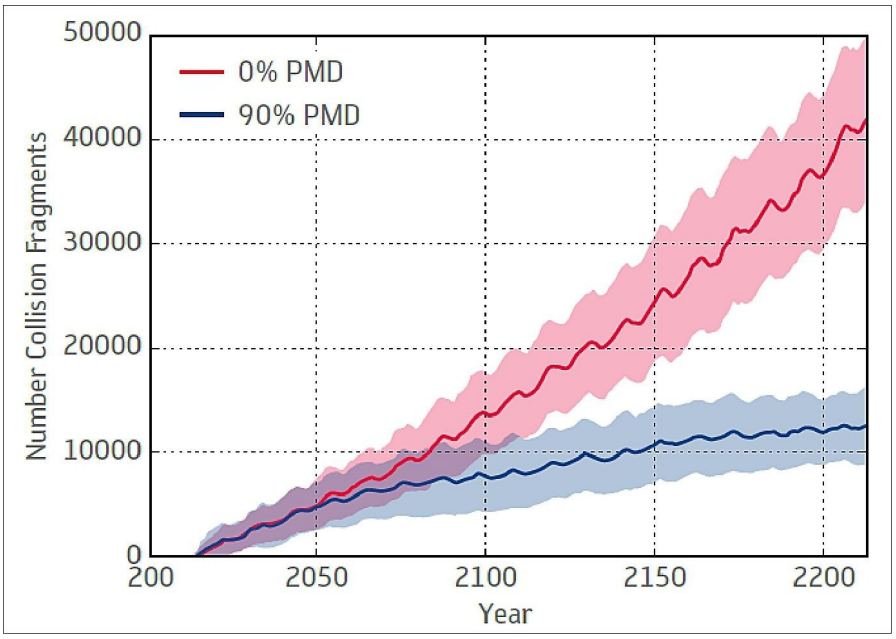

Figure 2: Projected evolution of the number of objects larger than 10 cm in LEO, depending on the adherence to PMD (Post Mission Disposal) guidelines. Credit: ESA

- limit the long-term presence of spacecraft and launch vehicle orbital stages in protected regions after the end of their missions

The future of space depends on the compliance to this guidelines. Unregulated space activities will lead to an uncontrolled increase in debris particles, having in in-space collisions its major source. To limit the permanence of man made objects in orbit after the end of mission and the consequent generation of new debris, the space agencies are developing effective Post Mission Disposals (PMD). ESA performed an investigation to analyse how the PMD compliance can affect the space debris environment. Figure 2 shows the results of this analysis, where a drastic growing of debris fragment is represented if no PMD action is taken [24]. The adoption of these new technologies to passivate and dispose missions will limit the growth of space traffic, with advantages in costs operations, collision risks and debris generation.

Roughly the 88% of small objects orbiting in altitudes lower than 800 km adhere to space debris mitigation measures because of the low altitude, and once their orbit is decayed they break up in the Earth atmosphere [11]. Only few large objects reenter Earth's atmosphere in a year, and around 75% of all the large objects ever launched have already reentered. Objects of moderate size, 1 m or above, reenter about once a week, while on average two small tracked debris objects reenter per day [25]. When an object reenters the atmosphere, it faces an increasing atmospheric density, and this determine the heating up of the object and the rise of aerodynamic forces, which lead in the majority of the case to its demise [25]. In the case of a large or very compact and

dense satellite or debris object (i.e. spent rocket bodies or large fragments), especially when a large amount of high melting point material such as stainless steel or titanium is involved, fragments of the object may reach the Earth's surface (i.e. reaction wheels). Large debris objects that reenter the atmosphere in an uncontrolled way and reach the ground pose a risk to the population, but even in this case the related risk for a human being on the ground is smaller than the risks of everyday life [26].

1.2 Thesis objectives

This thesis aims at presenting an innovative space mission concept in the field of Space Situational Awareness and Space Traffic Management activities, by addressing key areas of development in a context of a more sustainable and safer access to Space. The mission concept focuses on three main objectives:

- Characterise the sub-centimetre scale debris environment of LEO region thanks to in-situ detection.
- Test a new concept of autonomous on-board collision avoidance system.
- Retrieve data during the reentry phase.

These objectives address distinct but interlinked aspects of space sustainability. The first two objectives have a complementary purpose: the collision avoidance of traceable debris on one side and the improvement of the damage assessment from untraceable debris on the other. The reentry analysis aims at reducing the model uncertainties on the post-mission disposal, and specifically on the re-entry phase, which arise due to the atmospheric modelling (especially the solar activity) and to the satellite demise and break-up process, a process for which little to no mission-related data is currently available. An overview of the state-of-the art from previous missions is presented in section 2.

2 State of the art

2.0.1 Debris analysis

The number of debris in Earth orbit environment is highly dynamic, and their characterisation is quite challenging. The number of catalogued objects can face a drastic increase due to the combination of an accelerating launch rate and an improved space surveillance network. The objectives of the Space Situational Awareness are to locate every object orbiting the Earth, identify its provenience and predict its future orbit development [27]. Tracking and identifying in-orbit objects can be done either from space or from ground. From ground it is possible to recognise, track and catalogue space debris thanks to optical and radar observations. In a trade-off between system cost and performance, passive optical telescopes are suited mainly to observing high altitudes, whereas radars are advantageous below 2000 km [15]. In particular, in LEO the United States Space Surveillance Network (US SSN) can recognise pieces larger than 5-10 cm [28]. Objects with lower dimensions remain largely untracked, and their estimated number is about 200,000 for the range of 1-10 cm, and many millions to billions for diameters lower than 1 cm [29] [30]. There is indeed a significant gap in knowledge for particles smaller than 1 cm. Even if the particle size is reduced, the sub-centimetre particles population can significantly contribute to the spacecraft structures and subsystems degradation. A large contribution to debris particles tracking and cataloguing is due to the US Space Surveillance Network, composed by more than 30 ground station and 6 satellites, which offers a database for more than 42,000 in-orbit objects [31] [32] [33]. However, weather, atmosphere, and, in case of telescopes, daylight can limit the monitoring capabilities of ground stations.

One of the first satellite with the aim to detect space object in space was the Mid-Course Space Experiment (MSX), launched in 1996 [34]. At the beginning it had to identify and track ballistic missiles thanks to an optical instrumentation; the effectiveness of the solution allowed, in October 2000, to convert the mission to track and monitor in orbit objects, becoming the first spacecraft to successfully accomplish the task. Encouraged by the mission success, the US Department of Defence (DoD) conceived the Space-Based Surveillance System (SBSS), a satellite constellation with the aim to track space objects and accomplish space situational awareness for future control operations [35]. The satellites are equipped with optical instruments to identify the space debris environment. The first of these satellites, the Pathfinder, launched in September 2010, is covering a Sun Synchronous orbit at 630 km height. It's lifetime, originally scheduled for 7 years, was extended until 2020. The spacecraft is a 1031 kg, 840 W satellite [36].
Soon after the Pathfinder launch, also Canada started to collaborate with US DoD, and launched a minisatellite (148 kg), the Sapphire, that via optical sensors is tracking and cataloguing orbital objects, covering altitudes from 6000 to 40000 km [37].

The optical instruments have a very strong limitation in detecting small particles:

they look at the deep space, and are able to detect particles recognising their brightness from the brightness of the stars. As a consequence, small particles, with a diameter lower than 1 cm, exceed the instruments resolution capabilities. The debris population at this level can be represented only via statistical models, thanks to the analysis of impact data of specific detectors or of the surfaces' damages of satellites at the end of life. However, the latter method is inefficient due to the time and cost of retrieving a spacecraft surface after its demise. From the optical technology limit arise the need to track the currently untrackable smaller space debris and particles and provide in-situ characterisation. Specifically, it is necessary to collect information regarding the unknown population of particles versus altitude, location and time. These data can significantly improve the current models of sub-millimetre space debris and particle distribution.
The NASA Orbital Debris Program Office (ODPO) has been supporting the development of particle impact detection technologies since 2002 [38]. The objective is to provide an instrument able to perform in situ measurements to characterise the micro-meteoroid and orbital debris (MMOD) population in the sub-centimetre scale in Low Earth Orbit. The reason is that several important spacecrafts operate in this region, including the International Space Station (ISS). A key instrument parameter is the detection area, because, combined with the exposure time, determines the number of collected data, which are used to create statistical models and population sampling [7]. The ODPO has pushed for the development of a particle impact detection sensor, called the Debris Resistive/Acoustic Grid Orbital Navy-NASA Sensor (DRAGONS) [1]. The instrument is designed to detect impacts of particles in the range from 50 μm to 1 mm, to fill the measurement gap for these particles range. It is composed by two thin films located 15 cm apart and by a solid back plate below the second thin film. Multiple acoustic impact sensors are attached to the thin films and the back plate. The surface of the top film is coated with long and thin resistive lines. When a hyper-velocity MMOD particle, sufficiently larger than the thickness of the two thin films and the width of the resistive lines, hits the first film, it will cut several resistive lines, pass through the film, impact the second film, go through it, and then finally hit the back plate. The impact location on the top (or the bottom) film can be calculated with a simple triangulation algorithm based on the different signal arrival times measured by different acoustic sensors. When data from the measurements are processed and combined, information on the impact time, location, speed, direction, size of the impacting particle, and a simple estimate of the density of the impacting particle can be obtained [1]. The DRAGONS working principle is shown in figure 3 [1]. The DRAGONS is designed to be a modular low power demand, low mass and low cost instrument, and to be independent from the host spacecraft, in order to be carried as a payload on most spacecraft in both LEO and GEO. Unfortunately, DRAGONS basic design has a sensitive area of $1m^2$.

The University of Texas at Austin (UT-Austin) has developed a 3 Unit (3U) CubeSat, the Attitude Related Manoeuvres And Debris Instrument in Low (L) Orbit (ARMADILLO), with the aim to study and characterise the sub-millimetre scale orbital

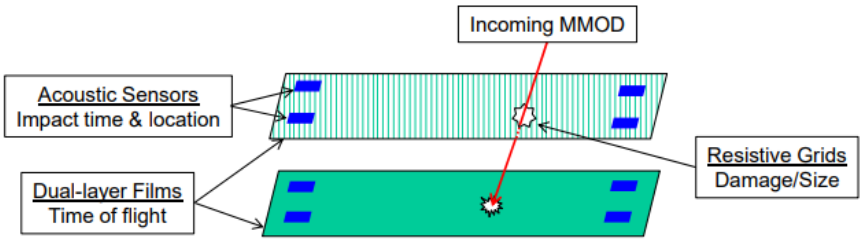

Figure 3: DRAGONS detection principles. Credit: NASA [1]

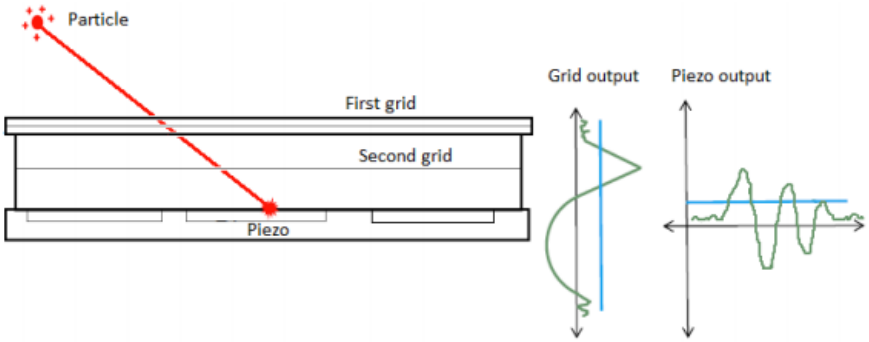

Figure 4: ARMADILLO PDD working principle. [2]

debris. The sub-millimetre space particle detection instrument is a Piezoelectric Dust Detector (PDD), which has been developed at the Center for Astrophysics, Space Physics and Engineering Research (CASPER) at Baylor University in cooperation with the Institute of Space Systems at the University of Stuttgart in Germany [2]. ARMADILLO is the first mission that has collected in-situ data on both man-made and naturally-occurring sub-millimetre size particles in Low Earth Orbit (LEO) on such a small satellite. Space debris dust detectors have flown on missions like Pioneer 10 and 11 [39], Ulysses [40], Galileo [41] and Cassini [42]. All of these missions, however, have been on satellite platforms of microsatellite size or larger, rather than the 3U CubeSat platform. The latters offer a relatively inexpensive platform on which to study the LEO space debris environment. The ARMADILLO PDD fits within the CubeSat form factor (it weighs less than 500 g and fit into 1/2 U) and measures the velocity, impulse, and time of each impact, providing information about mass and size, frequency of occurrence, source (man-made or natural) and limited information on the direction of the particle based upon the known satellite attitude. The post-processing of these data provides information on the source and nature of these particles, whether man-made or natural. The PDD instrument schematics is shown in figure 4 [2]. The minimum impact energy that can be registered by the device corresponds to at least 100 nJ. Assuming an impact velocity of 10 km/s, lower impact energies are due to impacts with particles smaller than 1 μm in diameter, and will not be detected by the instrument, being outside its

sensitivity capabilities.
The study of space debris provides crucial information for planning space operations, but there have only been a handful of missions which have investigated this problem. To improve the understanding of the debris environment a solution can be found in improving the debris detection system for CubeSats, providing an effective, low cost platform for in-situ data collection for the scientific community, and contributing to the safety of future satellites.

2.0.2 Collision avoidance manoeuvre

Currently the US 18^{th} Space Control Squadron furnish conjunction data messages (CDMs) based on an automated analysis, which give as output the approach details and an estimate of the associated collision probability [43]. The CDMs are computed considering the catalogued objects of the US catalogue and their trajectories, and details about time of closest approach (TCA), separations, state vectors, co-variances at TCA and information on the orbit determination quality are provided. When a conjunction event is marked with high collision risk probability it is carefully analysed, and assessment on mission specific processes are carried out for decision taking manoeuvre recommendations [43]. ESA typically implements optimised manoeuvres considering various constraints. Since key data are known only with limited precision, it is not possible to define for sure whether a collision will occur or not: uncertainties in object position determination and orbit propagation until the time of closest approach, determined by model uncertainties as for example drag modelling and manoeuvre performance, determine many uncertainties in the parameters of the closest approach. The key parameters that any collision avoidance strategy should have are the criteria on when to execute or not an avoidance manoeuvre. One of the most important criterion to decide if perform or not the manoeuvre is the collision risk, since it contains information on the close approach event (nominal separations, approach direction and trajectory uncertainties). However, also operational constraints have to be taken into account. To analyse the reaction threshold for the manoeuvre, it is convenient to use ESA's ARES tool [44]. It allows the estimation of overall collision risk as well as the annual frequency of close approaches with risks above levels selected by the user as a function of spacecraft size as well as the quality and age of the secondary (catalogue) orbit information. A trade-off among ignored and avoided risk can be done by selecting the risk threshold at the cost of a number of manoeuvres obtained as frequency of events having higher risk than the selected threshold. For LEO missions a risk threshold of 10^{-4} one day to the event leads to a risk reduction of around 90%, that is considered an accepted reduction factor [45]. This can be achieved in general at the expense of 1 to 3 manoeuvres per year [43].
The operational collision avoidance process at ESA/ESOC consist in the following steps, as shown in figure 5 [3]:

- Automatic download of CDMs and risk computation using CORAM software and object geometry from DISCOS [46].

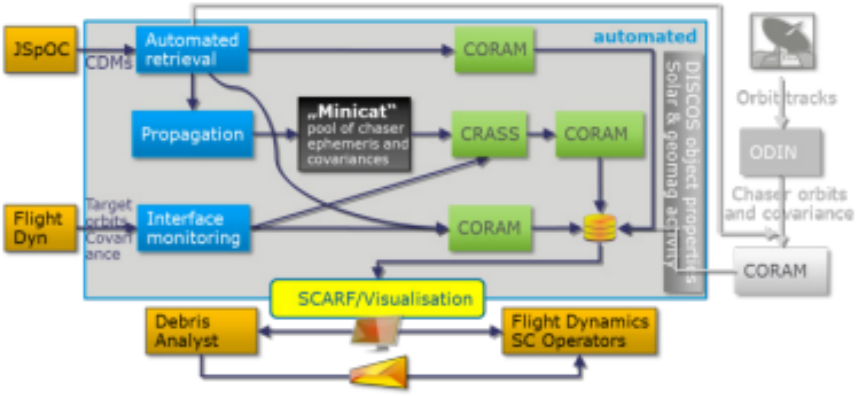

Figure 5: Extended operational collision avoidance process at ESA/ESOC with CDMs. [3]

- Propagation of the chaser state with DISCOS information. Creation of a mini-catalogue of objects close to the target spacecraft
- Risk computation based on the catalogue operating trajectories. The risk computation is fully automated, but the analyst can manually trigger extra analysis.
- High risks conjunction event are further assessed. Mission specific processes are used for decision taking and manoeuvre recommendations. This is done through the CORAM software, which can assess the optimum manoeuvre in an automatic sequence or can be configured by the analyst according to specific needs.
- External tracking data acquisition to improve the knowledge of the orbit and the associated uncertainty covariance of the chaser object using ODIN (Orbit Determination by Improved Normal Equations) software.
- CORAM (Collision Risk Assessment and Avoidance Manoeuvre) software processes the CDMs and obtain risk estimates. It is divided in two tools: CORCOS (COllision Risk COmputation Software) is dedicated to the computation of collision risk between two objects and CAMOS (Collision Avoidance Manoeuvre Optimisation Software) which is devoted to the evaluation of different mitigation strategies through the optimisation of avoidance manoeuvre parameters.
- CORCOS provides a collection of algorithms for the evaluation of the collision risk.
- CRASS (Collision Risk ASsessment Software) software screens operational ephemeris against the mini catalogue for conjunctions.
- CAMOS supports the planning of avoidance manoeuvres, optimising various objective functions. Constraints can be introduced in the manoeuvre parameters.

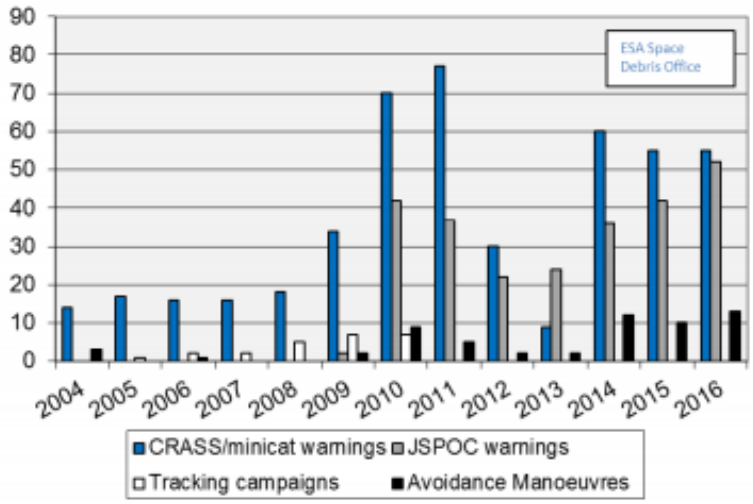

Figure 6: Collision avoidance statistics from ESA. Credit: ESA Space Debris Office

In figure 6, the number of CRASS/mini-catalogue warnings-based warnings, received Joint Space Operation Center (JSpOC) warnings (close approach notifications), tracking campaigns and avoidance manoeuvres is shown for the time period between 2004 and 2016 [3]. It is clear that the conjunction data messages and the required collision avoidance manoeuvres face an increasing trend, which will grow faster and faster in the future.
To support these activities the Space Debris Office develops and maintains an infrastructure of debris environment and risk analysis tools, such as the Meteoroid and Space Debris Terrestrial Environment reference model (MASTER) and the DRAMA tools suite and the Database Information System Characterising Objects in Space (DISCOS) database which provides information on on-orbit objects. ESA's proposal for a Space Safety Programme to start in 2020 includes a cornerstone "Collision Risk Estimation and Automated Mitigation (CREAM)" [47]. CREAM entails the development of technologies for automating collision avoidance and its demonstration with a suitable newly developed or existing flying platform. CREAM has three central objectives:

- reducing manpower efforts, in particular for large constellations
- reducing the number of false alerts
- reducing the time between manoeuvre decision and close approach

CREAM will develop the needed techniques towards automated decision, planning, and execution of collision avoidance actions, and will demonstrate these developments [47]. ESA has signed a data sharing agreement with the US, and thanks to this agreement information on several hundreds of conjunction alerts per spacecraft and week are furnished to ESA [43]. After further analysis and risk assessment, only about two of these

events are marked as actionable alerts. To process these actionable alerts, considering several constraints and applying different methods and tools, an analyst is needed [45]. Not all the actionable alert determine the execution of the manoeuvre. The ratio on executable manoeuvre and actionable alert is about 5-10 actionable alerts per conducted avoidance manoeuvre [45]. The classical process contributes with considerable costs to the overall mission operations effort. In 2018 ESA estimated that every year about 14 MEUR are spent worldwide on manoeuvring spacecraft in LEO in response to false alerts [48].

Space activity is accelerating, with more and more object inserted in LEO, as depicted in figure 7 [4]. Space Surveillance Networks will soon be delivering catalogues of up to 200k objects [36]. If no improvement in the automated processes is made, the classical approach for collision avoidance manoeuvre will be an unmanageable task for the operators [46]. New manoeuvre decision criteria and automated approaches should be investigated to face the increasing space traffic management challenge. Some proposed alternatives can be the implementation of low-thrust manoeuvring or the use dedicated devices or attitude changes to control the effective drag. Both can make it possible to implement a continuous collision avoidance process in replacement of the classical impulsive manoeuvring [49]. CREAM will approach automation by employing and maturing machine learning approaches to replicate expert decisions [47]. The machine learning techniques will be applied also considering artificial intelligence techniques for automated manoeuvring decisions. This gives the opportunity to accelerate the avoidance process and reduce the time between decision and event, as manoeuvre sequences can be pre-optimised and stored already onboard in a generic form, ready for a late go/no-go decision [47].

If a conjunction event involves different entities, the coordination between the parts can result as cumbersome. With the deployment of large constellations the current practice of ad-hoc coordination through human interface to operator processes could become inefficient [47]. To allow more immediate and quicker relations between the involved parts, CREAM will develop communication protocols for manoeuvring coordination. The final target is to have a completely autonomous system. If on-board decision is possible, the information required for a decision have to be uplinked. The on-board decision has then to be downlinked and communicated to other concerned spacecraft [47]. To distribute traffic information the most promising option are the Iridium receivers or similar alternatives [47]. In this way it is possible to link the coordination efforts with on-board trajectory estimation, the realisation of a global optimisation to reduce the collision risk comprehensively for all upcoming events and spacecraft, and the use of pre-optimised manoeuvres stored on-board that are triggered for execution through alternative communication channels.

2.0.3 Reentry model validation and testing

The reentry phase is always a critical part in the mission design, because it is influenced by the uncertainties in the atmospheric model, orbital perturbations, and thermomechanical and breakup properties of the spacecraft. The design of atmospheric entry

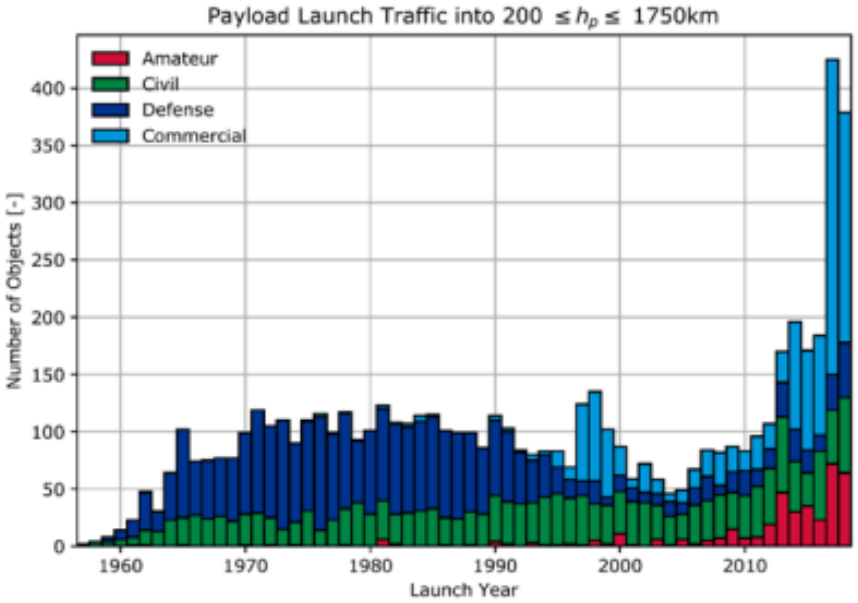

Figure 7: Evolution of payload launch traffic. [4]

system technologies relies heavily on simulation tools of different fidelity. Following initial trade studies using low-to-mid fidelity systems-level simulation tools, high fidelity computational fluid dynamics (CFD) simulations are used to define the aerothermal environment that an entry vehicle's thermal protection system (TPS) will experience. Thanks to their coupling with material thermal response codes using appropriate boundary conditions, high fidelity simulations become powerful and sophisticated tools for the design and sizing of a vehicle's TPS that must withstand the entry environment. These models are validated and developed thanks to in-situ measurement or tests in appositely designed facilities, that reproduce the flight environment. However, in these facilities only partial replication of the real environment that the spacecraft is subjected to is possible. For this reason, flight experiments remain the benchmark for end-to-end validation of simulation tools. Optical instruments are commonly used to analyse and then post-process the atmospheric data and the break-up models, to improve the re-entry analysis of spacecrafts at the end-of-life. This modus operandi has been privileged by NASA since 1990. NASA's utilisation of airborne assets and spectral imaging instrumentation for observation of super-orbital reentry events traces its heritage to airborne astronomy and meteor observations. The flight are performed at a nominal altitude of 12 km, which is above 80% of the atmosphere and 99% of the atmosphere's water vapour. Almost all potential obscuring cloud cover is avoided at that altitude, and optical absorption due to atmospheric constituents is greatly diminished [50].

In 2006, the Stardust capsule re-entered the Earth's atmosphere with a re-entry speed of 12.8 km/s [51]. This was the fastest re-entry of a human made space vehicle ever.

The possibility to retrieve heat shield erosion and plasma characterisation data is very valuable for the design of future interplanetary missions, since the reentry conditions are close to the hyperbolic re-entries for sample return missions. Unfortunately, on the capsule no instrument dedicated to reentry analysis was installed. The only way to obtain information on heat shield and re-entry plasma was provided by passive optical methods. NASA prepared an observation mission with the help of the NASA DC-8 airborne observatory [52]. The capsule's descent through the atmosphere produced optical emissions from the capsule's surfaces, the high temperature gases surrounding the vehicle, and gases and dust in the vehicle's wake. The surface emitted radiation in the grey-body spectrum, whose magnitude is characterised by the surface's temperature and emissivity [52]. The gas emission derives from the interaction in the boundary layer between the excited states of the atmosphere gases and other gases deriving from the ablation of the heat shield of the capsule. The intensity of the gas radiation depends on the number densities of the emitting states and spectroscopic factors that govern their radiative properties. Wake radiation, when present, originates from species with long-lived excited states, also populated by shock heating, that have become entrained in the wake of the vehicle. Thermal radiation from the capsule surface was expected to dominate the emitted spectrum. The study of American, Japanese and German scientists led to the definition of 11 different set ups, in order to achieve spectrally resolved datain different wavelength ranges and with different time resolution [53]. For the optical instruments onboard the airplane manual tracking was adopted, and this was possible thanks to the precise trajectory prediction and airplane navigation. The airplane was meant to fly a 15 km wide and 45 km long observation loop at an altitude of 14 km above the area of Nevada [52]. Stardust data was acquired during about 30 s of the re-entry starting at Stardust altitudes of about 84 km over ground down to altitudes of 45 km [52]. The setup of the observation did not allow to achieve spatial resolution of the radiation data, thus all measured values represent an integration both on the visible part of the glowing heat shield and the plasma in the post shock region. Planck temperatures were determined assuming a constant temperature over the whole heat shield.

Another study performed on an atmospheric reentry of a space object was done on the 29^{th} of September 2008, when the European spacecraft ATV-JV (Automated Transfer Vehicle Jules Verne) had a safe destructive reentry into the South Pacific Ocean Uninhabited Area (SPOUA) after having successfully completed its mission [5]. The reentry have been observed by two aircrafts equipped with a large number of optical instruments, and furthermore the reentry was observed also from the International Space Stations (ISS). The ATV-JV was the first ATV mission, and the objective of the observation were the assessment of the breakup altitudes with accuracy better than 5 km, the identification of explosion events and the analysis of the trajectories, size and temperatures of the fragments [5]. The observation manoeuvre was the result of a coordination effort between the trajectory design of the ATV-JV, the two aircrafts and the ISS attitude, in order to satisfy the observation conditions. The cooperative design of multi-vehicle trajectories and the synchronised exchange of trajectory data have con-

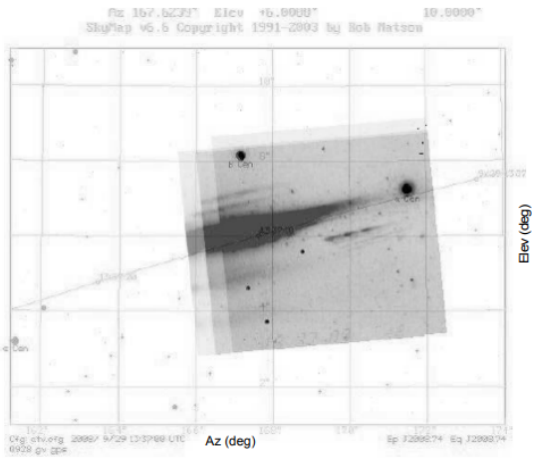

Figure 8: ATV fragment images from DC-8 Observation overlapped to Nominal Trajectory and star field. [5]

tributed to the success of ATV-JV reentry observation campaign. It was the first time that four vehicles have synchronously manoeuvred to maximise the re-entry visibility from and to optimal observation conditions for the optical instruments mounted on the ISS and on the two aircrafts. Figure 8 [5] shows a shot of the ATV-JV break-up.

The Hayabusa mission was designed to retrieve a fragment from the asteroid 1998 SF36 "Itokawa", and in the 13^{th} of June 2010 the Hayabusa sample return capsule reentered the Earth atmosphere over the Woomera Prohibited Area in southern Australia, performing a successful reentry [54]. This was the third sample return mission after NASA's Genesis and Stardust mission. For this reason, its atmospheric reentry was an appealing opportunity to collect aerothermal data at superorbital speeds [55]. Even in this case, the reentry analysis was not foreseen at the time of the mission design, and the heatshield of the reentry capsule did not contain a reentry analysis payload instrumentation. For this reason, remote observation was the only option to observe and retrieve data during the reentry. The observation objectives consist in the characterisation of the aerothermodynamic environment during the reentry thanks to time-resolved measurements of the optical emissions of the SRC surface, shock heated gases and the trailing wake. The reentry observation of the Hayabusa capsule took as baseline the previous reentry observation campaigns for the Genesis, Stardust and ATV missions. The observation mission team successfully executed the airborne observation campaign [54]. The NASA DC-8 used for the reentry observation was equipped with 25 science instruments, in order to analyse the incoming SRC and the break-up of the spacecraft bus. Many of the instruments consisted in slitless spectrograph that utilised transmission gratings [54]. Other instruments employed fiber-coupled slit spectrographs or cameras with band pass filters to realise spectral resolution. Three instruments were devoted to high resolution colour video documentation. Twenty-three out of 25 scientific instruments on-board the DC-8 returned useful data [54]. However, because of the distance between the SRC

reentry and the observing aircraft and the small dimensions of the SRC, spatial distribution of the emitted SRC surface and surrounding gas radiation was not distinguishable by the imaging instruments used in the observation [54], and the SRC appeared to the instruments as a point source of light. The total observation time from first detection to loss of signal was approximately 70 seconds and corresponded to the SRC's descent from approximately 85 km to 35 km altitude. The emission data collected during the observation provided insight into the aerothermodynamic processes of atmospheric entry and the performance of the capsule's thermal protection system [54].

Reentry analysis is important to collect information on thermal protection systems to test them, but also to retrieve information on the reentering objects break up events. The knowledge of the break up process of reentering objects is important to estimate the risk at ground associated with a surviving debris reentry. As a matter of fact, after the launch of a spacecraft, some of the launch hardware reenter the atmosphere and can reach the ground after the satellite is deployed, and the spacecraft itself can return to the atmosphere at the end of life. Today, computer tools are used to estimate the ground hazard associated with reentries, as for example the Range Safety Assessment Tool (RSAT) [56]. These tools have been developed and calibrated using limited data derived from visual evidence and analysis of recovered hardware [57]. The reentry analysis however highlight the presence of high uncertainties in the reentry event, and show that the phenomenon is not well understood. It is then desirable to perform in-situ measurement during the reentry and break up of a space object. However, the challenges related to such a system design are multiples:

- Aerodynamic heating can melt aluminium and other materials and deceleration loads can exceed 7 g's.
- The reentering object is surrounded by a plasma field which includes small fragments and particles of melted metal, which makes broadcasting data during breakup very difficult.
- High uncertainty in the re-entry location on ground, within the latitude band defined by the orbit's inclination.
- Targeting a reentry requires ground communication of commands to the vehicle and precise manoeuvre capability of the deorbiting hardware, as well as a propulsion system to effect the deorbit, potentially expensive additions to a stage or hardware.
- Multiple data from different reentries are required to help understand the variation that might be expected.
- In case the satellite is equipped with a re-entry box, to store the data, a proper target of the re-entry area is important to retrieve the recording device.

A different approach rather than the optical observation of the reentry uses dedicated sensors placed on the heat shield of the spacecraft. This method has been studied by

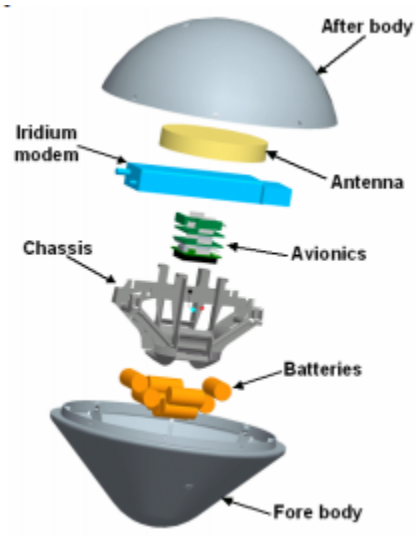

Figure 9: Exploded view of REBR without heat shield. [6]

the Aerospace Corporation, that in partnership with NASA's Ames Research Center has developed a prototype for a new system for collecting and returning data collected in the stressing reentry environment [58]. The sensor package was called the Re-Entry Breakup Recorder (REBR), consisting in a small, disposable reentry vehicle (shown in figure 9 [6]) that can collect data on new thermal protection system materials and concepts and on space hardware demise during reentry, and return data via a commercially-available communication system [6]. The REBR weighed approximately 2 kg and contained a data recorder, a customisable sensor suite, batteries, GPS, antenna, and a modem that enables communication with the Iridium satellite network, all protected from the reentry environment by a thermal protection system. The device collected data during reentry and then broadcasts the data via the Iridium communications system prior to ground impact. The device requires no services (power or communications) from the host vehicle and recovery of the device is not required. It can be configured to either release from the host early in the reentry heating process or to remain attached and collect data during breakup of the host [6].

A better understanding of the reentry phenomenon is necessary to improve the guidelines to design missions with safe end of life de-orbiting. A proper validation and improvement of the currently existing models and tools could enable researchers and engineers to build confidence in the use of these design tools, mature their development, and reduce risk in future heat shield designs.

2.1 Contribution to the scientific community

The objectives of this thesis, as already described in 1.2, follow ESA's Space Safety Programme [59]. Established in 2009, the Programme has defined a number of ambitious goals [60]:

- A tested and exercised early warning system on Space Weather events providing actionable information to users
- The capability to provide early warnings for asteroids larger than 40m, three weeks in advance
- The ability to deflect asteroids smaller than 1km, if known 2 years in advance
- The demonstrated capability to rendezvous, capture, service and de-orbit defunct space objects in a controlled fashion with a commercial perspective
- To achieve sustainable European space traffic including debris avoidance and disposal in an economically viable way

It is mainly the last point that the thesis addresses to. ESA's plans focus on enhancing both space debris monitoring and reentry risk models. In addition, it is planned to develop on-board technology to improve European compliance with collision avoidance requirements in an economically viable way.

The mission proposed in this thesis aim at contributing to all three the previous mentioned ESA's objectives. The mission will develop three different payloads, as described in three different payloads, described in section 6.5, which would allow the spacecraft to collect collect in-situ data on sub-centimetre scale debris distribution in some particular LEO regions; thanks to an on-board algorithm, the satellite will perform autonomous collision avoidance decisions and manoeuvres, after receiving an alert from ground; at the end of the mission, a specifically designed payload will retrieve information on the reentry environment and dynamics. The possible outcomes of the mission will be available to the scientific community, and will significantly contribute to validate and tune the space debris models, improving the comprehension and the characterisation of the environment. Also, the reentry data retrieved can be used to develop more accurate reentry models, refining both the debris dynamics comprehension (i.e. when a debris is destroyed by the atmosphere) and also the understanding of last instants of the reentry spacecrafts, including the break-up events, which are typically characterised by high uncertainties. Regarding the space traffic management, in the context of ESA's CREAM project [47], the autonomous collision avoidance system developed and proposed for this mission is an effective solution to reduce manpower effort and costs for manoeuvre decisions and inter-satellite organisation, and poses the basis for a future where space traffic management will be completely a computer task.

2.2 Thesis organisation

This thesis presents the preliminary design for a CubeSat mission, discussing a solution to fulfil the mission objectives and dealing with the most significant issues the mission has to face. In section 3 the preliminary mission requirements are described, focusing on the most important requirements that the mission has to comply with, discussing the alternatives and justifying the final choice. In section 4 a preliminary selection of the concept of operations of the mission is presented, introducing how the mission will develop and the organisation of the mission phases. Then, after this two introductory chapters, in sections 5 and 6 is described the design process that led to the results of this work, focusing on the mission analysis and orbit selection, and the preliminary system design, with particular attention to the attitude control system, which is the most peculiar subsystem for this type of mission. In subsection 6.5 the preliminary payloads selection process and characteristics are described, proposing a solution to accomplish the task in an optimum way. A preliminary mass and power budget is then given at the end, relying on off the shelf components selection where possible. In section 7 a summary of the mission results and main open points is presented, together with a description of some of the most important next steps for the design of the mission.

3 Mission requirements

The first important task to accomplish in the mission design is the definition of the requirement document. It states the mission purpose, what the spacecraft shall do and how it shall be done. There are two types of system requirements: mandatory (M), and preference or nice to have (NH). Mandatory requirements ensure that the system satisfies the operational needs; they states the minimal requirements necessary to accomplish the objectives. They must be passed or failed, there is no middle ground. Preference requirements are evaluated to determine the best designs. They should be evaluated with a multi-criteria decision technique, because none of the feasible alternatives is likely to optimise all the criteria and there will be trade-offs between these requirements. There are different requirement categories: functional (F), mission (M), interface (I), environmental (E), physical (PH), operational (O), human factors (HF), payload (PY), logistic (L), product assurance (PA), design (D), configuration (C) and verification requirements (V). This chapter describes the most relevant requirements for the CubeSat mission under analysis and their main motivations.
The functional requirements specify what is the functionality of each subsystem and or component. The three objectives of the mission are formalised in requirements F-030, F-060 and F-160.

F-030	*M*	*T*	The debris detection subsystem shall be able to detect debris between 1e-6 m to 1e-3 m	*Above 5 cm scale the debris can be detected from ground. There is a significant gap in knowledge for particles smaller than 1 cm [10]*
F-060	*M*	*A,T*	The spacecraft shall perform at least 3 collision avoidance demonstration manoeuvres, everyone referring to a different warning time	*It is important to test the system in different warning conditions, to test its capabilities in different scenarios and check the robustness*
F-160	*M*	*A,T*	The reentry analysis shall be performed from 200 km to 100 km altitude	*Under 200 km the atmosphere density increase significantly, and the aim is to study the effect on the dynamics for reentry objects [25]*

The F-030 refers to the debris analysis phase. It states that the spacecraft must be able to perform statistical debris analysis, detecting space debris in a selected range. The trade-off on the detected debris dimensions is a results from both the needs to investigate the sub-centimetre scale debris and the instrument capabilities. The lower limit is chosen according to payload sensitivity, but also for practical reasons: since the aim is to study the hazardous debris environment, which can pose a threat to operational satellites, it is an unjustified effort to try to detect too small particles, because it is very unlikely that they can represent a relevant threat to spacecraft and subsystems [61]. The upper limit

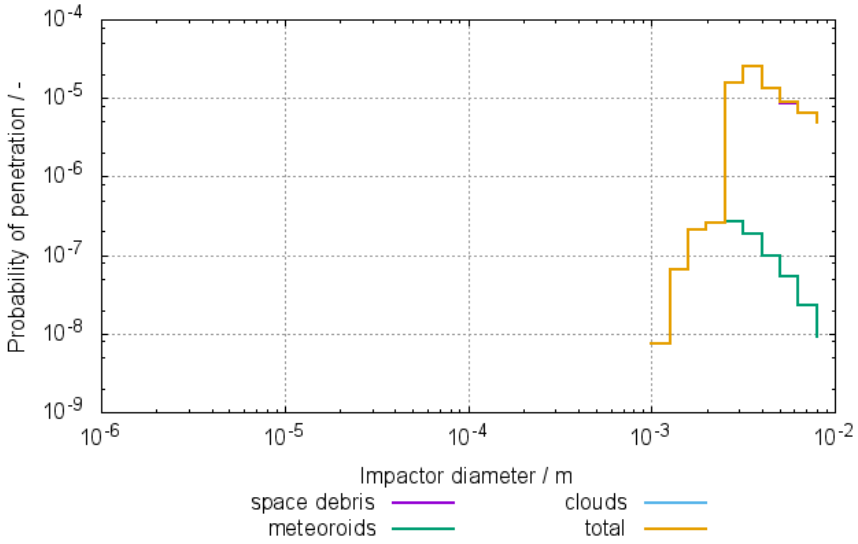

Figure 10: Probability of penetration in ESA's triple wall with respect to object diameter

instead is defined by the exigency to detect debris below 5 cm, resulting from ground station capabilities, but also from the capacity of the spacecraft and the sensor to bear impacts. Indeed, for a CubeSat an impact with a 5 cm particle at LEO speed can result in a fatal accident. This is formalised in requirement F-050.

F-050	*M*	*T*	The debris detection subsystem shall be able to detect and bear impacts up to 300 J	*Limit selected to avoid payload break-ups*

The value of the impact energy of 300 J is computed according to a statistical analysis of the impacts on the spacecraft. Using MASTER and DRAMA software, a collision analysis has been performed (see section 5 for the detailed analysis). The orbit is a 800 km quasi circular Sun synchronous orbit. The analysis has been carried out for 1 year, from October 2020 to October 2021, considering particles in the range between of 1e-6 m and 1e-2 m, both natural and man-made. Considering as baseline shielding the ESA triple wall [62], no particle with a diameter lower than 1 mm is able to penetrate it, as shown in figure 10. Considering the case of an impact probability of 1e-4 particles per year, that is an acceptable collision probability level, and a surface of 0.2x0.2 m, the maximum value of velocity reached is about 20 km/s and a mass of the order of 1e-6 kg, as shown in figures 11a, 11b and 12. Considering these limit values, the resultant impact energy would be 200 J. Adding 50% safety margin on this value, it results the 300 J requirement.

From the analysis on the probability of penetration, in figure 10, it is derived the upper limit of particles dimension as 1e-3 m as preliminary selection. It is unwanted that the spacecraft is lost or damaged in contact with dangerous particles, so the preferred action is to foresee the possibility of collision avoidance manoeuvre avoiding the

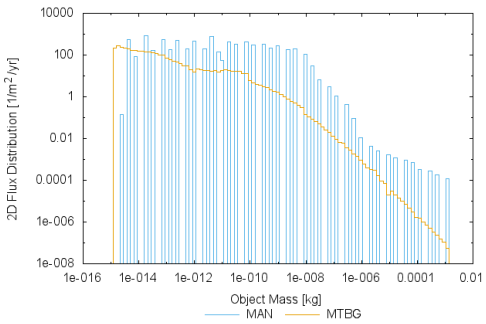

(a) Flux distribution with respect to object mass.

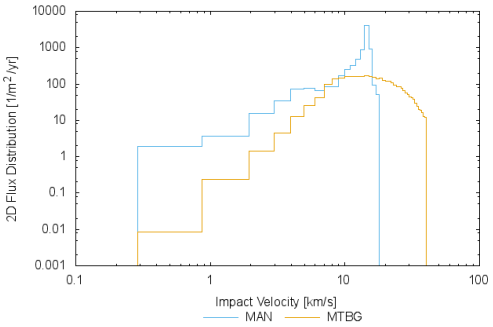

(b) Flux distribution with respect to impact velocity.

Figure 11: Flux distribution of orbital debris and meteoroid particles

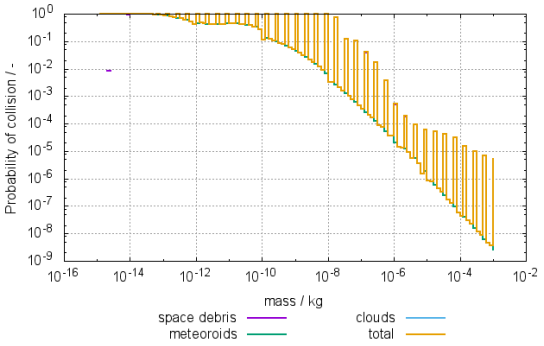

Figure 12: Probability of collision with respect to mass

centimetre scale ground detected particles. This range however is still a preliminary parameter, because further analyses on payload and shielding will be assessed for the final selection.
A "nice to have" specification for the debris analysis is the possibility to distinguish whether the impact has been caused by a man-made debris or a natural meteoroid. This would help to better characterise the LEO environment, and to analyse the population difference between man-made and natural dust particles. Furthermore, to better describe debris evolution processes, it is important to not overestimate the data considering also natural dust particles as specified in F-040.

F-040	*NH*	*T*	The debris detection subsystem shall distinguish between the dust and man made debris	*To better characterise the environment*

Requirement F-060 specifies the need to test the autonomous collision avoidance system, which is one of the mission objective, in different scenarios. The system must be robust, and it is important to grant the functionality of the collision avoidance with different warning scenarios, for example changing the available time from the collision message to the crossing, that would determine different manoeuvre requirements. Furthermore, for statistical reasons it is important to perform more than one test, to have enough data to assess the system performance. Typically a 90% success probability is taken as satisfying value to be compliant with the guidelines to limit debris growth in LEO [63]. This is expressed in requirements F-100 and F-110.

F-100	*M*	*T*	The on-board collision avoidance system shall have at least 90% success probability	*To be compliant with guidelines for debris mitigation [63]*
F-110	*M*	*A*	The collision avoidance demonstration manoeuvre shall be performed at least 3 times during the main phase of the mission and 3 times during the reentry phase	*To have statistical results*

For safety reasons, in order to prevent a collision with the colliding debris caused by a malfunctioning of the autonomous collision avoidance system, real conjunction situations shall be managed in a "classical" way from ground. Section 6.5.2 describes the design process for the autonomous collision avoidance system. To check the proper functionality of the autonomous collision avoidance system during the manoeuvre, it is necessary to gather information on satellite position and velocity during all the CAM. Moreover, it is important to downlink the output of the on-board collision avoidance algorithm, to check if the actuation is compliant with the on-board decision. Furthermore, in this thesis an innovative algorithm for an autonomous on-board decision making for the collision avoidance manoeuvre is proposed, which has to respect the requirements specified in the F-071, F-080, F-090 and F-150.

F-071	*M*	*A, T*	Before the CAM, the satellite shall send to ground the information regarding the optimal manoeuvre, and during the CAM shall monitor and store the information on the satellite position and velocity	*To check the results of the CAM payload*
F-080	*M*	*A, T*	The orbit position and velocity of the spacecraft shall be checked with an accuracy of at least 10 m and 0.25 m/s during all the manoeuvre	*To check the compliance of the actuators with the algorithm output and the effectiveness of the manoeuvre*
F-090	*M*	*A, T*	Real collision avoidance situations shall be handled from the ground segment	*For mission safety*
F-150	*M*	*A, T*	The on-board autonomous collision avoidance manoeuvre's software shall be able to be modified from ground and uploaded to the spacecraft	*To make modification to the software if necessary*

Requirement F-160 defines the minimum boundaries in which the reentry analysis shall be performed, in order to have a satisfying amount of data retrieved for model validation and testing. The most interesting and significant part of the analysis is in the altitude range of 200 km to 100 km, because measurements in that altitudes are suffers from significant atmospheric effects. The spacecraft starts heating due to atmospheric drag, and the the control system could not be able to maintain the control accuracy required for the atmospheric analyses. Thus in this thesis, the pointing capability to avoid an uncontrolled tumbling effect is presented. In that situation, both measurement effectiveness and data upload can be degraded, until it becomes an impossible task under a certain altitude limit, defined by spacecraft capabilities. In this thesis a preliminary attitude control analysis has been performed (see section 6.3), and it was simulated the spacecraft control effort down to 100 km, to assess the capability to avoid an uncontrolled re-entry. The need to transfer the stored data to the ground station before the loss of the spacecraft and telecommunication systems is explained in requirement F-170.

F-170	*M*	*A, T*	The re-entry analysis data shall be downloaded to the ground station once per orbit, during the re-entry analysis from 200 km to 100 km	*It is of great importance to retrieve measurement data before loosing the spacecraft*

In F-020 is specified the need of controlling the pointing vector during all the mission phases, with different accuracy requirements. The spacecraft will implement a three

axis control to accomplish all the tasks: debris analysis requires velocity pointing, CAM requires 3 axis control to push the satellite in the desired direction, and reentry analysis is very challenging from the tumbling viewpoint. See section 6.3 for attitude specifications.

F-020	*M*	*A,T*	The attitude of the spacecraft shall be controlled during all the mission phases, with different accuracy	*To perform the required analysis and testing*

This work wants to propose a mission concept based on space sustainability, thus it is important to be compliant with the debris with the debris mitigation guidelines. As in requirement F-010, even if the spacecraft experiences a failure, it must be able to lower the perigee and ensure passive reentry in maximum 1 year. This is important to limit the permanence in space of uncontrolled objects, that can become dangerous for operating satellites.

F-010	*M*	*A,T*	In case of failure, it shall be ensured that the satellite can lower the perigee down to at least 200 km, to ensure passive reentry in maximum 1 year	*To limit debris generation in LEO region*

Another important step in the analysis and design of the mission concept is the definition of the mission requirements. They define specific subsystems requests, and can state "how well" the requirement should be satisfied.
From the debris analysis viewpoint the noteworthy requirements are the P-MA-010, P-MA-020 and the P-ADCS-010.

P-MA-010	*M*	*A*	The orbit altitude of the satellite shall be between 500 km and 900 km altitude. The orbit shall be a Sun Synchronous orbit	*To analyse the most polluted LEO region*
P-MA-020	*M*	*A*	The orbit altitude of the satellite shall be chosen in order to have a minimum number of man made debris impact per year of at least 100	*To have enough impacts for statistical analysis*
P-ADCS-010	*M*	*A,T*	The ADCS subsystem shall ensure 1° pointing accuracy during the debris analysis phase in the velocity direction	*To face the debris detection payload towards velocity direction, where the debris flux is higher*

The orbit of the mission has been selected thanks to different considerations and simulations, as a trade-off between debris analysis and reentry needs as described in section 5.

An altitude among 500 to 800 km could provide a sufficient number of debris impact on the spacecraft and at the same time is low enough to reduce the propellant consumption in the deorbit phase, granting the spacecraft reentry in less than 25 years also if the worst case scenario is considered. Requirement P-MA-010 states the limit in which the most concentrated debris population can be found, and P-MA-020 is the requirement that decide if a particular orbit can be chosen or not, depending on the impact probability per year. During debris analysis it is important that the payload face the velocity direction with at least 1° accuracy, in order to maximise the flux on the instrument and retrieve a bigger amount of data. A preliminary study on the payload position has been carried out, considering the chosen orbit and a 12 U CubeSat, along a Sun synchronous 800 km orbit, which represent the peak in the debris density distribution with respect to altitude, as described in section 5. The sensitive area of the payload is set as 0.04 m^2, in order to fit the side face of a 12 U CubeSat. The results show a higher flux in the frontal direction, on the surface positioned toward the velocity direction, as depicted in figure 13. The position of the debris analysis payload is described in the requirement C-010, placed in the configuration requirements. This requirement is derived from the flux analysis shown in figure 13. The velocity direction face is indeed the one with the higher number of impacts.

C-010	*M*	*T,I*	The debris detection instrument shall be directed toward velocity direction and keep that attitude during all detection phase with 1° deg pointing accuracy	*To ensure the maximum debris flux possible*

For the autonomous CAM testing phase, the most stringent requirements are on the ADCS and OBDH subsystems. For the propulsion system, the ΔV required is not comparable to the ΔV necessary to de-orbit the satellite, since the former is in the order of 5 m/s, and the latter is around 120 m/s. See section 6.2 for more details on the ΔV budget of the mission. The requirements are P-OBDH-010, P-OBDH-020, P-PS-010 and P-ADCS-030.

P-OBDH-010	*M*	*A,T*	The OBDH shall be able to process TBD Kb/s	*To compute the optimum collision avoidance manoeuvre*
P-OBDH-020	*M*	*A,T*	The OBDH shall store TBD Kb	*To store the algorithms and the data*
P-PS-010	*M*	*A*	The PS shall have at least 150 m/s ΔV budget	*To deorbit and CAM*
P-ADCS-030	*M*	*A,T*	The ADCS s/s shall provide at least a 0.07 deg/s slew rate during CAM phase	*To direct the motor in the right firing direction in time for the manoeuvre*

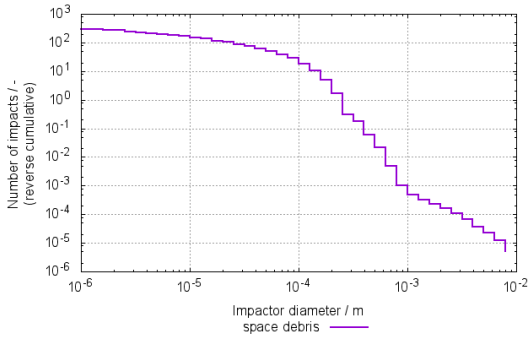

(a) Impacts on velocity direction surface

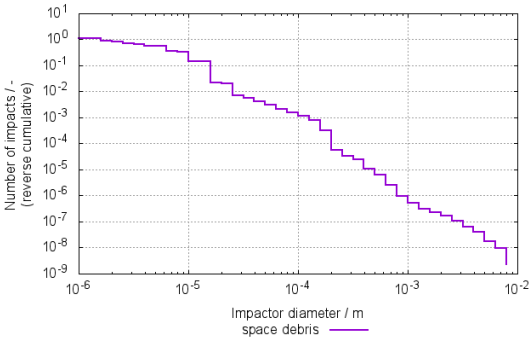

(b) Impacts on back surface

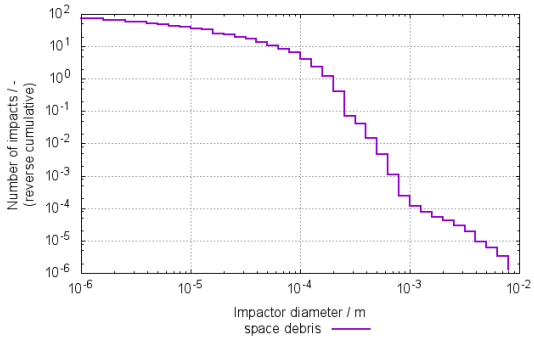

(c) Impacts on right surface

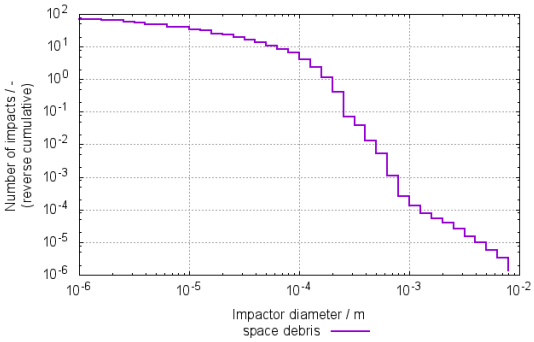

(d) Impacts on left surface

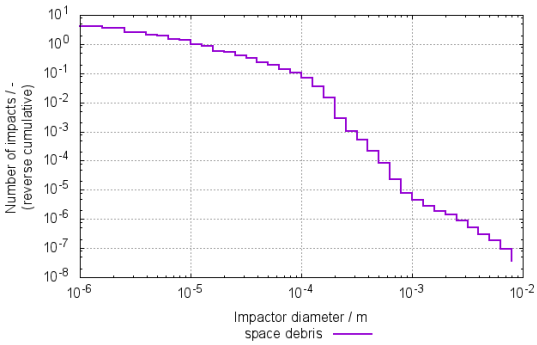

(e) Impacts on top surface

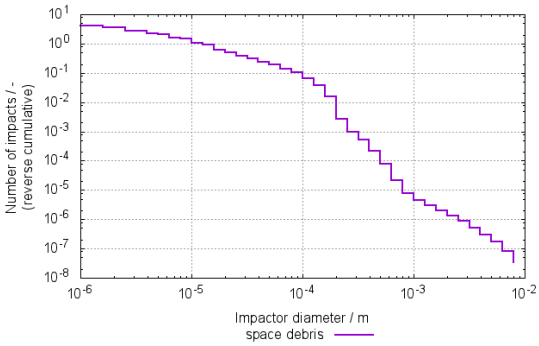

(f) Impacts on bottom surface

Figure 13: Debris impacts on payload sensitive surface placed in different spacecraft positions

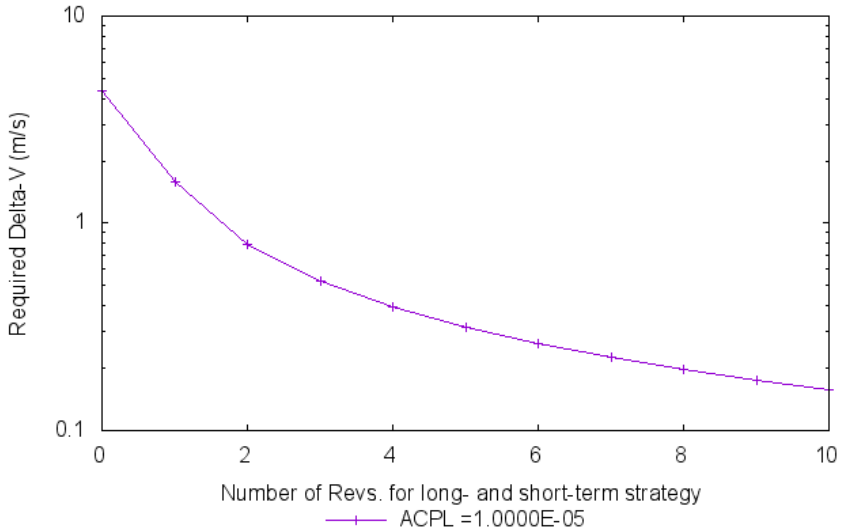

Figure 14: ΔV requirement for collision avoidance

The optimum collision avoidance manoeuvre is computed on-board, and this shall be done in a reasonable time - about 1 orbit - to allow the manoeuvre to be performed with enough time before the conjunction. Requirements P-OBDH-010 and P-ADCS-030 ensure that the spacecraft is ready to perform the manoeuvre in time, allowing also a low thrust possibility if the conditions allows it and the time before collision is enough. The ΔV due to collision avoidance manoeuvres has been computed using ARES software, for a 600 km quasi circular Sun synchronous orbit, which has been selected as the operative orbit for the mission (see section 5 for the description of the decision process) and an accepted collision probability level of 1e-5, as shown in figure 14. Furthermore, shall be considered also the ΔV dedicated to the autonomous CAM testing manoeuvres. Hence the requirement P-PS-010, in which is also considered the ΔV necessary for the reentry, about 115 m/s, and the total is marginalised by 20%. See section 6.2 for more insight in the ΔV budget determination.

During the re-entry phase it is important that the spacecraft survives at least until an height of 100 km, without breaking-up. Along the re-entry, the satellite retrieves the data thanks to the reentry payload, sending them to ground before the break-up of the spacecraft and the loss of communication possibilities. To do that in an effective way, the attitude control system shall be able to control the attitude of the spacecraft during this phase. Requirements P-STR-010, P-TMTC-010, P-TMTC-020 and P-ADCS-040 describes these needs.

P-STR-010	*M*	*A,T*	The spacecraft structure shall withstand aerodynamics loads during the re-entry phase between 200 km and 100 km altitude	*To avoid spacecraft loss before reentry data are retrieved*
P-TMTC-010	*M*	*A,T*	The TMTC subsystem shall be able to send the reentry analysis data to a TBD ground station	*The spacecraft shall download the data before loss of communications*
P-TMTC-020	*M*	*A*	The TMTC subsystem shall be able to download at least TBD Mbit/s and upload at least TBD Kbit/s	*The time available to transfer the data is limited, so a minimum data rate must be granted*
P-ADCS-040	*M*	*A,T*	The ADCS s/s shall ensure ensure 5° deg of pointing accuracy during re-entry analysis phase	*To increase the effectiveness of reentry measurement and data transfer*

Moreover, the physical requirements are introduced to specify the dimensions of the spacecraft.

PH-010	*M*	*A,T*	The mass at launch shall be of maximum 10 Kg	*To reduce costs and to be considered a nanosat [64]*
PH-020	*M*	*A,T*	The volume at launch shall be of maximum 23x24x36 cm	*The volume of a 12 U standard deployer [65]*

The decision of a 12 U nanosat was taken after a preliminary mission budgets have been evaluated, and taking into account the necessity to equip the spacecraft with 3 different payloads and a propulsion system. Considering the mission objectives, a first iteration on the subsystems components has been performed, deriving the mass, dimensions and energy budget for the mission. The design process that led to the mission budgets is better described in section 6.6. The starting idea was to consider a 12 U standard CubeSat, but during the preliminary design phase also a 8 U structure was considered. However, the latter was soon discarded, due to the components and payloads dimensions, that could not fit in a 8 U CubeSat. See section 6 for an insight in components selection and mission budgets. Even if a 12 U CubeSat can weight up to 24 kg, the design choice is to keep it in 10 kg, possibility confirmed by the preliminary design and components selection.

From the environment viewpoint, the spacecraft is subjected to an hostile surrounding, both during the debris analysis phase and the reentry phase. The orbit is specifically chosen to pass through one of the most polluted LEO regions. This results in a stressful environment on the spacecraft structures and subsystems, that would for sure face a multiplicity of impacts with debris particles. Debris particles bigger than 5 cm are subjected to tracking and are registered in the US Space Surveillance Catalogue. If a

conjunction with such a particle is expected, a collision avoidance manoeuvre is performed. For smaller debris a forecast of collision can not be expected. It is important that the spacecraft does not break or have any fatal loss of functionalities in such an event, as in requirement E-020. During the reentry, the spacecraft experience a heating due to the atmosphere friction. Before reaching the ground, usually at an height of 80 km, reentering CubeSats burn up completely in the atmosphere. It is mandatory for the mission purpose however that the spacecraft does not have loss of functionalities before reaching at least 100 km altitude, in order to complete the analysis and sent data to a ground station, as in requirement E-010.

E-010	*M*	*A, T*	The spacecraft shall withstand TBD temperature of reentry	*To allow reentry analysis*
E-020	*M*	*A, T*	The spacecraft shall withstand impacts up to 20 kJ	*To prevent loss of the spacecraft due to debris particle impact. Energy value is computed from the results shown in figures 11a, 11b, 12.*

Operational requirements specify which actions shall be performed during the mission operation activity and how to handle them. Regarding the operational life of the satellite, it is important to select the length of the mission. This influences the spacecraft design and component selection, for example batteries, propellant mass budget and solar panels. The length of the mission is driven by the necessity to recover a minimum amount of debris data in order to have statistical measurements to allow model validation, as specified in requirement O-010. Since the mission retrieves information on the environment thanks to its payload, it is important to establish a proper communication link with ground to download the data and allow the on board memory to free new space, as described in requirement O-040.

O-010	*M*	*A, T*	The operational lifetime of the mission shall be at least 1 year	*To allow statistical representation of debris environment*
O-040	*M*	*A*	The spacecraft shall be able to send to ground the data retrieved every TBD time in TBD time	*To not rack up data*

To accomplish the mission's tasks, the spacecraft is equipped with three different payloads. For every instrument, it is necessary to specify the requirements for its design or choice, depending on the strategy of customising it or buying it off the shelf. General payload requirements as PY-010, PY-020 and PT-030 are necessary to keep the payloads compliant with the mission budgets.

PY-010	*M*	*A, T*	The power consumption of the payload shall be limited to 4000 W	*To not exceed spacecraft energy capabilities*
PY-020	*M*	*A, T*	The maximum weight of the payloads shall be of 3.5 Kg	*To stay in weight limit*
PY-030	*M*	*A, T*	The maximum space occupied by payload shall be of 4 U	*To fit in the structure and deployer*

For the single payload instrument, it is important to report what it shall accomplish and its performance characteristics. For the debris detection sensor, requirements PY-050, PY-060 and PY-100 state the impact characteristics that the sensor must detect. The requirements are based on the MASTER and DRAMA analysis already described in figures 11a, 11b, 12 and 10, and will be further explained in section 5.

PY-050	*M*	*T*	The debris detection subsystem shall be able to determine the energy of the impact up to 300 J	*Energy range of target debris particles*
PY-060	*NH*	*T*	The debris detection subsystem shall be able to determine the velocity of the impact, with a range from TBD to 20 km/s	*Velocity range of LEO debris*
PY-100	*M*	*T*	The debris detector shall bear impacts of particles up to 20 km/s and 300 J energy	*The sensor shall keep working even after several impacts with no damages*

A possible feature that can be implemented on the debris sensor is the possibility to reconstruct the orbit of the debris. This can be done after post-processing information on the debris direction and velocity. This would allow to better understand the debris environment, and retrieve information on the origin of the debris, or help to perfect the models on debris orbit evolution. The related requirements are the PY-040, PY-060 and PY-070.

PY-040	*NH*	*T*	The debris detection subsystem should be able to reconstruct the orbit of the debris using the impact direction and velocity	*To have more information on the debris origins*
PY-070	*NH*	*T*	The debris detection subsystem should be able to reconstruct the direction of the debris	*To allow orbit reconstruction*

The reentry analysis payload must perform the measurements necessary to retrieve information on the atmosphere and its interaction with the spacecraft. The uncertainties in

the reentry can be of various type, both on atmospheric model and also in the spacecraft break-up process. To check the atmosphere characteristics, its pressure and temperature will be measured. To reconstruct the break-up process of the spacecraft, both temperature and accelerations on the structure will be measured, to have the thermodynamic behaviour of the spacecraft. This analysis will be used to improve the models for spacecraft reentry. Requirements PY-110, PY-120 and PY-130 formalise the role of the payload in collecting these information.

PY-110	*M*	*T*	The reentry validation subsystem shall measure atmosphere density with TBD accuracy	*To reconstruct atmospheric model*
PY-120	*M*	*T*	The reentry validation subsystem shall measure atmosphere temperature with TBD accuracy	*To reconstruct atmospheric model*
PY-130	*M*	*T*	The reentry validation subsystem shall measure accelerations acting on the spacecraft during the reentry down to 100 km altitude	*To have information on the structural loads and spacecraft interaction with atmosphere*

4 Concept of Operations and Mission Architecture

This chapter describes the preliminary analysis performed to define the concept of operation and the mission architecture of the CubeSat mission. Specifically, the preliminary analysis that led to the architecture definition is described, and the most important mission phases have been organised in the concept of operations.

4.1 Preliminary analysis

For every mission objective and payload, a preliminary analysis and technology assessment has been studied.
First, an analysis on possible debris detection device is carried out, considering the requirements and constraints for the analysis and characterisation of the orbital environment. Literature review and different payloads comparison (see section 6.5) have led to three different possibilities, as shown in figure 15:

- impact detector (figure 15a)
- non-impact detector (figure 15b)
- formation flight with optical detection (figure 15c)

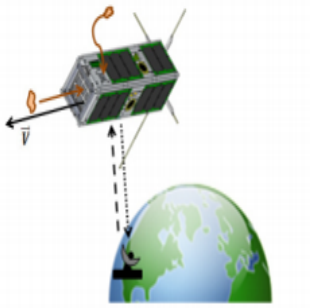

(a) Impact detector. Credit: ARMADILLO mission [2]

(b) Non-impact detector. Credit: US Naval Research Laboratory [66]

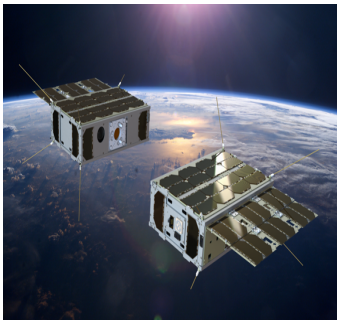

(c) Formation flight detection. Credit: ESA - RACE double CubeSat mission

Figure 15: Debris detection mission architecture possibilities

Advantages and disadvantages of these possible detection strategies have been analyse for a proper trade-off of the baseline device for the mission. First, an impact detector has a consolidated flight heritage, a easy implementation and a low power requirement [67]. However, the detection rely on a small area, reducing the impact probability. The data that can be extrapolated are instrument dependent; more advanced sensors allow to retrieve information not only about the number of the impacts, but also on the dimension, mass, speed and direction of the debris particle (see section 6.5). On the other hand, a non-impact detector is based on optical instruments that allows to

identify nearby particles. This determines a broader sensitive area, increasing the detection probability and debris flux through the sensitive surface [7]. For this instrument, the detectable particles are bigger with respect to the ones of an impact detector, that can identify smaller debris, and more energy is required. Furthermore, no information on particle characteristics except dimensions can be retrieved. This type of technology does not have a flight heritage yet flight heritage, and is still in development. Finally, another approach relies on the combined benefit of the optical detection with CubeSat formation flight. The idea is to use one spacecraft with an optical transmitter coupled with another spacecraft equipped with a receiver (as done for the RACE mission [68]). The resulting covering area can be wide, with dimensions depending on the optical instrument capabilities. Implementing this approach, information on the direction and velocity of the debris particle can be retrieved. Yet this would require a more advanced attitude control and relative flight dynamics, that would increase mission complexity and costs.

A second analysis is carried out to analyse the possible different approaches to implement an on-board collision avoidance algorithm. Specifically, during the mission, the on-board autonomous collision avoidance system will be tested. Different approaches to the test have been considered and discussed:

1. The system would perform a real collision avoidance manoeuvre.
2. An apposite built "debris" is detached and inserted on a conjunction trajectory with the CubeSat, and the system would perform an avoidance manoeuvre to avoid the "debris".
3. The system would perform a collision avoidance manoeuvre after receiving a warning message of a collision with a "synthetic" debris. The "synthetic" debris orbital parameters and uncertainties are based on a real debris of the LEO region

The real collision avoidance option has not been considered, because an error in the manoeuvre can lead to a crash with the consequent loss of the spacecraft and new debris generation in the LEO region, eventuality that must be avoided as required by the debris mitigation guidelines. Moreover, to test the system it is needed to wait until a conjunction warning is found, and this can lead to a very long waiting time for the tests to be performed. The decision process of a collision avoidance manoeuvre depends on many different factors, based on statistical orbit uncertainties parameters on both the satellite and the debris. To prove the effectiveness of the decision algorithm and to reduce the waiting time of the tests, the use of an appositely created debris could be implemented. This debris would detach from the satellite and would be inserted in an orbit which have a conjunction with the orbit of the satellite itself. In this way, real tracking information on both the satellite and the debris can be used to make a conjunction message and observe the response of the autonomous collision avoidance system. This however would generate a real risk for the spacecraft, with the same disadvantages of the first case, and

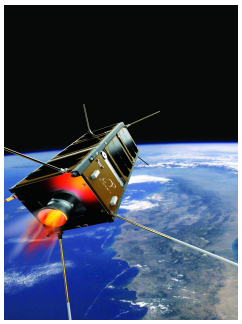

(a) Chemical propulsion system. Credit: D-Orbit

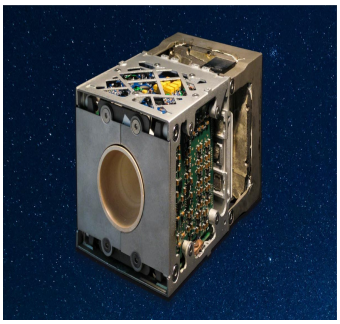

(b) Low thrust system. Credit: T4i

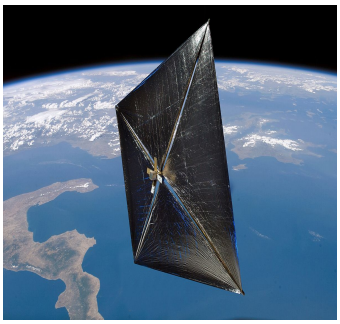

(c) CubeSat solar sails device. Credit: NASA Nanosail D2 mission

Figure 16: De-orbit strategies

also in case of success the LEO environment would have been enriched by one more uncontrollable object, contributing to increase the debris number. To decrease the risk and mitigate the consequences of a failure in the autonomous manoeuvre decision strategy, but at the same time to make possible an evaluation of the on-board algorithm, the last alternative suggests to perform the collision avoidance manoeuvre based on a collision message that is synthetic, but representative of real debris element. In this way it is possible to combine the advantages of the previous proposals, with a limited risk to the debris environment.

A final analysis is performed to analyse the possible strategies for the final part of the mission , before the atmospheric analysis phase. Specifically, at the end of the mission, the spacecraft will perform a manoeuvre to de-orbit from its operative altitude to a perigee altitude of about 200 km. To reduce the permanence orbit time and to be compliant with the debris mitigation guidelines, an upper limit of 6 months before re-entry has been considered. The trade-off on the possible propulsion strategy considers four different architectures:

1. A chemical propulsion system for impulsive manoeuvres (figure 16a).
2. A low thrust electric propulsion system red(figure 16b).
3. A solar sail de-orbiting device (figure 16c).
4. A combination of a solar sail device and a chemical or low thrust propulsion system.

For the first strategy, the impulsive manoeuvre could rely on cold or warm gas engine. The target orbit can be achieved either using a single or multi impulsive strategy. Once the required ΔV is known, the number of manoeuvres is decided considering the amount of ΔV per manoeuvre. Adopting multiple manoeuvres strategy is a safer decision, because if one of the manoeuvre is not performed as scheduled, the error can be limited

and using the remaining firings it is possible to adjust the orbit and remedy to the error. However, the number of manoeuvre shall be compliant with the restarting capabilities of the engine, and the motor efficiency shall be verified on too small ΔV manoeuvres. In the design of the spacecraft, the required volume and weight for the necessary propellant will be considered. Moreover, if the engine provides high levels of thrust, it is of primary importance to check that the attitude control system is able to keep the pointing of the spacecraft during the firing, otherwise the manoeuvre could result in the loss of the satellite. The power demand of the engine is contained, even in the case of warm gas systems, and can be supplied by the spacecraft solar arrays. On the other hand, the electric low thrust propulsion systems are more compact and are able of higher specific impulses. A low thrust approach can realise a constant and controlled orbit lowering. This strategy allows a continuous control of the descent orbital trajectory, avoiding the risk related to a high thrust technology. However, they typically require a high energy demand, and they are used on CubeSats in combination with large deployable solar panels and high capacity batteries, resulting in an increase of complexity and weight. Another strategy to reduce the orbit decaying time is to exploit the solar radiation pressure acting on the satellite, with an increased reflective surface. A solar sail device could be introduced for this purpose. At the end-of-mission it should be deployed, enhancing the spacecraft natural de-orbit. However, solar sails effectiveness in reducing significantly the decay time of the spacecraft without generating further debris from collisions during reentry has to be demonstrated. This mission could improve the current technology level for CubeSats solar sails. Since the thrust generated by the solar effect on the sails is very low and it is should be demonstrated the feasibility to produce de-orbit in a short time period as the 6-month target, it was also proposed to couple the sails effect with a propulsion system. The latter possibility would require at least two CubeSat unit dedicated to propulsive and de-orbiting system, increasing the weight and the complexity of the system. In addition, during the reentry data collection, solar sails interaction with atmosphere could generate unexpected torques on the spacecraft, making it unfeasible by the attitude control system, with the risk of a failure in the reentry data collection or transmission phase.

Finally, for the reentry analysis phase, three main mission architecture have been investigated:

- An on-board distributed network of sensors, burning during reentry (figure 17a).
- A "black box" re-entry payload, surviving the spacecraft break-up, that do not need to be collected on ground (figure 17b).
- A daughter satellite that orbit above the reentering spacecraft to collect video data and use them to post process information. (figure 17c)

During the reentry, the spacecraft is subjected to aerodynamic forces, that induce vibrations and loads on the structure, and to a thermal load that results in the burning of the CubeSat before reaching the ground, usually at about 80 km altitude [69]. Subsystems functionalities can be compromised, and the data measurement and transmission

(a) CubeSat hardware for reentry analysis. Credit: Surrey Space Center

(b) Rentry payload. Credit: Terminal Velocity Aerospace

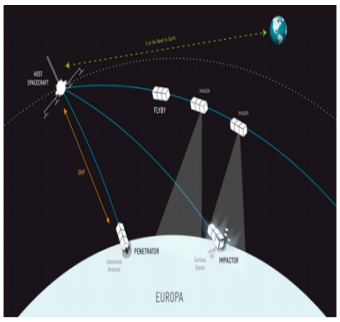

(c) Formation flight to film reentry. Credit: NASA Europa Clipper Mission

Figure 17: Reentry analysis strategies

in this environment can result very difficult. However, as described in section 6.3, the spacecraft control can be ensured until 100 km altitude, giving the chance to perform reentry analysis inside the mission requirements boundaries. The advantage of using the main spacecraft equipment to accomplish the task is a more compact and simple design, with benefits in terms of space and weight. One alternative could be the employment of a reentry independent payload that register the aero-thermodynamic loads and the break-up process, and before reaching the ground sends the collected data thanks to its own telecommunication system. Usually this payloads are heavy due to the heat shield required to protect the payload and make it survive during the descent. Moreover, the use of a reentry surviving payload could require a controlled reentry to manage the risk at ground. The aim is to keep the ground risk negligible. For this reason, its use on a CubeSat must be carefully evaluated. Based on NASA's reentry observation of different missions using an aircraft equipped with different optical cameras, a third option could be considered. A secondary spacecraft equipped with a multi-spectral camera, with an orbit above the main CubeSat, could be used during the reentry. This allows to observe from a close distance the break-up process of the satellite, with the possibility of recover information about atmosphere and structures, via post-processing of the images. The drawback of this option is a more complex mission analysis design and the need to build a second independent spacecraft, which would increase costs and mass budget.

4.2 Mission Architecture

The final mission architecture has been chosen between the proposed alternatives. The spacecraft is a CubeSat-dimension satellite with a maximum volume of 12 U, as a trade-off result on the three payload dimensions and weighs. For the debris analysis, the main driver for the technology selection has been the TRL of the payload. Non-impact detectors are still in their development phase, while the impact based debris payload has flight heritage, and has proven its effectiveness in many different missions, for example Cassini or Rosetta missions (see section 6.5). This thesis aims at demonstrating the feasibility of

debris analysis and reentry validation using a 12U CubeSat, opening up a wide range of future possibilities to improve scientific knowledge of the LEO environment. Formation flying has been discarded due to high costs, complexity and risk; however, it can be a valid step forward to increase debris detection capabilities, and shall be implemented in future missions. During the main phase of the mission, an autonomous on-board collision avoidance system will be tested. The strategy chosen is the test manoeuvre based on the synthetic debris collision message, thanks to its reduced risk compared with the others and to its fidelity to a real case scenario. The creation of more debris in a busy LEO orbit has to be prevented indeed, and the other options would not respect the debris mitigation guidelines, jeopardising the mission itself. At the end of the main phase, the deorbit is performed thanks to a multi impulse manoeuvre, with the aid of a warm gas thruster. Solar sails are not implemented because of their complexity and the high folding volume required. One of the three mission objectives, the reentry analysis, depends on the de-orbiting strategy, and an failure of solar sails would jeopardise the mission. The low thrust electric engine has been evaluated, but the high amount of power needed is not sustainable by the CubeSat, without increasing the area of the solar panels with large wings. This would add more stress in the attitude control system, in particular during the reentry phase, and would determine more uncertainties in a crucial part of the mission. For this reason, the chosen alternative has been the chemical thruster. Both single manoeuvre and multiple manoeuvre have been taken into account, A trade-off analysis has been performed to both minimise the ΔV for the de-orbit and maximise the time spent in the region between 200 and 100 km altitude. In addition, the risk related to each strategy has been evaluated. To reduce the risk derived by a failure or uncertainties during the firings, the ΔV has been divided into multiple impulse, being able to correct possible errors in the manoeuvres with the subsequent ones. For the reentry analysis, the selection was to implement a spacecraft hardware to perform the task, equipping it with accelerometers, temperature and pressure sensors. The surviving reentry capsule has been discarded for weight and dimensions reasons, in addition to the casualty risk derived by the surviving payload reaching the ground. There are some implemented payloads with the right functionalities, but their weight is not less than 2 kg, and their dimensions are comparable to the 12 U CubeSat structure, as for example the Reentry Breakup Recorder (REBR) [6]. Finally, the formation flight alternative has been already discarded for the debris analysis, and for the same reasons is not considered also during reentry. Its added complexity, weight and cost do not justify the output of the analysis, which would be similar to what done in the past by NASA's aircraft missions.

4.3 Concept of Operations

Once the objectives of the mission and the high level concept architecture have been defined, it is important to define a preliminary concept of operations that the mission should follow. The concept of operations presented in this section aims at defining the characteristics of the main mission phases of the CubeSat mission concept.

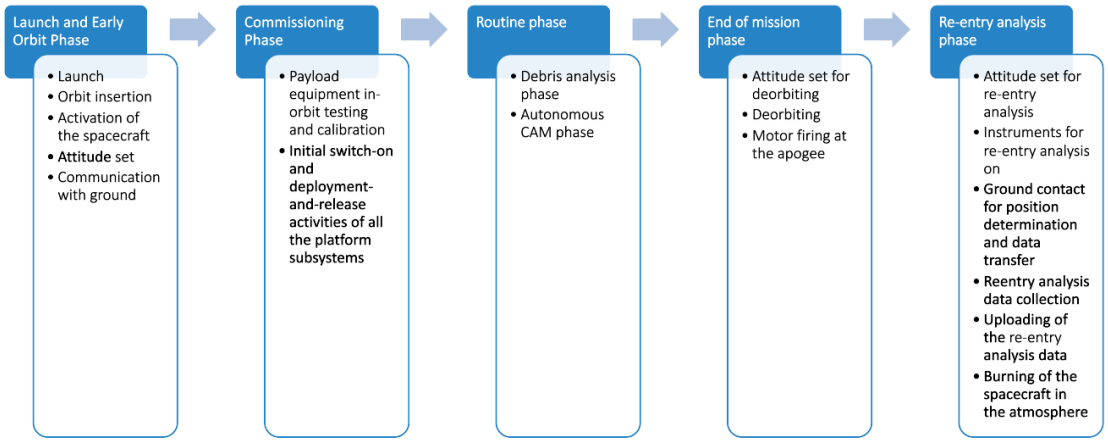

Figure 18: Preliminary mission phases

The mission would be divided in five main phases, as shown in figure 18:

1. Launch and early orbit phase
2. Commissioning phase
3. Routine phase
4. End of mission phase
5. Reentry analysis phase

The first phase is the launch and early orbit phase [70]. The launch phase expected duration is some some hours. After the launcher last stage has delivered its payloads, the deployer unloads the CubeSat to its operative orbit. At this point, the spacecraft starts to activate all its operative systems. This operation can lasts from hours to days, in which the spacecraft shall deploy its appendages, activate the OBC and ADCS subsystems and perform a detumbling manoeuvre. When the detumbling phase is complete, solar panels are opened (if deployable solar panels are present), and generate and accumulate electric energy in batteries. Once the spacecraft is functioning, the attitude determination and control system has to acquire the satellite attitude and perform a slew manoeuvre to set the spacecraft in the correct attitude for ground link. At this point, communication with ground begins and spacecraft parameters, functionalities and correct orbit positioning are checked.

1. Launch and early orbit phase
    1 Launch
    2 Orbit insertion
    3 Activation of the spacecraft

4 Attitude set

5 Communication with ground

The commissioning phase prepares the spacecraft to accomplish its tasks. This phase for a CubeSat can last up to one month, in which all the spacecraft subsystems are switched on, checked and made operational. The functionalities of the payloads are checked, and every payload is tested and calibrated if necessary. In this phase it is important to check if the spacecraft or some parts have suffered from damages during the launch phase. Once the commissioning phase is terminated, the spacecraft is ready to start the routine phase.

2. Commissioning phase

    1 Payload equipment in orbit testing and calibration

    2 Initial switch-on and deployment-and-release activities of all the platform subsystems

In the routine phase the spacecraft carries out the debris analysis, and the on-board autonomous collision avoidance manoeuvre is tested. The debris analysis will last several months, to collects enough data to allow statistical modelling of the debris environment. During the debris analysis, the collected data will be sent to ground, at least once a day. During this phase, the spacecraft receives the synthetic conjunction messages from ground. At this point, the CubeSat would stop the debris analysis, establish ground communications and upload the data. Precise orbit position of the spacecraft is acquired. Communication and position tracking shall be ensured during the whole duration of the CAM test. The on-board software compute the optimal manoeuvre to be performed by the satellite, and give the command to the on-board actuators. At the end of the manoeuvre, both the on-board decision and its actuation are evaluated, and eventual correction or improvements to the on-board software are sent to the spacecraft. Once the test is complete, the spacecraft set its attitude for scientific debris analysis again, the debris payload is restarted and the debris phase continue. This sequence is repeated a desired number of time, depending on the number of CAM tests that have to be performed. In this case the minimum tests required from the requirements has been set to three.

3. Routine phase

    1 Debris analysis phase

        i Debris analysis on

        ii Communication with ground every TBD time

        iii Debris analysis off

        iv Scientific data upload

    2 Autonomous CAM phase

        i Sending false collision warning message from ground

ii Precise position determination of the spacecraft
iii Communication with spacecraft
iv Autonomous collision avoidance manoeuvre
v Check on the state of the spacecraft and the manoeuvre
vi Download of the correction of the software (if necessary)
vii Attitude set

At the end of the debris science phase, the spacecraft begins the de-orbiting phase, by lowering the perigee via multiple ΔV at the apogee. After 5 manoeuvres at the apogee, the perigee is lowered to about 200 km altitude. The impulsive manoeuvres are separated about 10 days from one to another, to allow orbit correction or recalculation if needed.

4. End of mission phase

    1 Attitude set for deorbiting
    2 Deorbiting
    3 Motor firing at apogee

As soon as the s/c orbit lower its perigee below 200 km, the reentry analysis phase starts. During this phase, the spacecraft shall control the attitude profile and switch on the reentry payload. The spacecraft shall be tracked to check the orbit positioning and the effect of the atmosphere on the orbit evolution. Communications with ground shall be ensured to transfer the data retrieved. The spacecraft permanence under 200 km before the reentry has been computed to be about 9 days. The orbit lowering continue mainly due to aerodynamic drag, that at first has the effect of circularising the orbit, and then starts a progressive decay. Under 100 km height the attitude control system is no more able to ensure the control of the spacecraft, and the CubeSat starts decay: the spacecraft will burn-up and completely destroy in the atmosphere, below about 80 km of altitude.

5. Reentry analysis phase

    1 Attitude set for reentry analysis
    2 Instruments for reentry analysis on
    3 Ground contact for position determination and data transfer
    4 Reentry analysis data collection
    5 Uploading of the reentry analysis data
    6 Burning of the spacecraft in the atmosphere

5 Orbit selection

This chapter describes the analyses performed for the selection of the nominal orbit for the 12U CubeSat mission concept. The key parameters that drive the analyses are the number of debris particles that can be detected and the compliance with the re-entry analysis under 200 km of altitude. The orbit then must be chosen to allow a proper data collection for the scientific payloads. For the debris analysis, the key parameter that must considered, is the number of man made particles that impact the payload. For the reentry payload, the main goal of the mission analysis is to provide enough residence time in the region between 200 km and 100 km altitude. Moreover, the 25-year rule of the space debris policy will be considered in the trade-off analyses, to ensure a proper re-entry even in case of satellite failure. Furthermore, at the end of the mission, the deorbit time should be less than 6 months, and the propellant used for the manoeuvre shall be minimised.

5.1 Debris analysis

To perform debris analysis, ESA's MASTER v8.0.2 and DRAMA v3.0.3 have been used. MASTER (Meteoroid and Space Debris Terrestrial Environment Reference) "*allows to assess the debris or meteoroid flux imparted on a spacecraft on an arbitrary earth orbit. MASTER also provides the necessary computational and data reference for DRAMA*"; DRAMA (Debris Risk Assessment and Mitigation Analysis) "*is a comprehensive tool for the compliance analysis of a space mission with space debris mitigation standards. For a given space mission, DRAMA allows analysis of*" [71]:

- *Debris and meteoroid impact flux levels (at user-defined size regimes)*
- *Collision avoidance manoeuvre frequencies for a given spacecraft and a project-specific accepted risk level*
- *Re-orbit and de-orbit fuel requirements for a given initial orbit and disposal scenario*
- *Re-entry survival predictions for a given object of user-defined components*
- *The associated risk on ground for at the resulting impact ground swath*

The first survey performed at the beginning of the selection process is a density analysis of debris with respect to orbit altitude. The objective of this first simulation is to understand debris orbit distribution, and identify the LEO region with the larger debris population.A MASTER simulation via the spatial density tool has been performed. The simulation time has been set between the 1^{st} of October 2020 and the 1^{st} of October 2021. The parameters of the simulation are reported in table 1. The results of the simulation, shown in figure 19, highlight a peak of man made debris density at about 800 km altitude. The minimum debris density is found at 400 km, and increases until the peak. After the maximum value, the man made particles have a slow but constant descent, until the

parameter	**min**	**max**	**type**
particle size [m]	1e-6	1e-2	-
altitude [km]	400	1500	-
declination [deg]	$-90°$	$90°$	-
right ascension [deg]	$-180°$	$180°$	-
debris sources	-	-	condensed
meteoroid sources	-	-	Grün

Table 1: Input parameters to MASTER for debris density vs altitude analysis

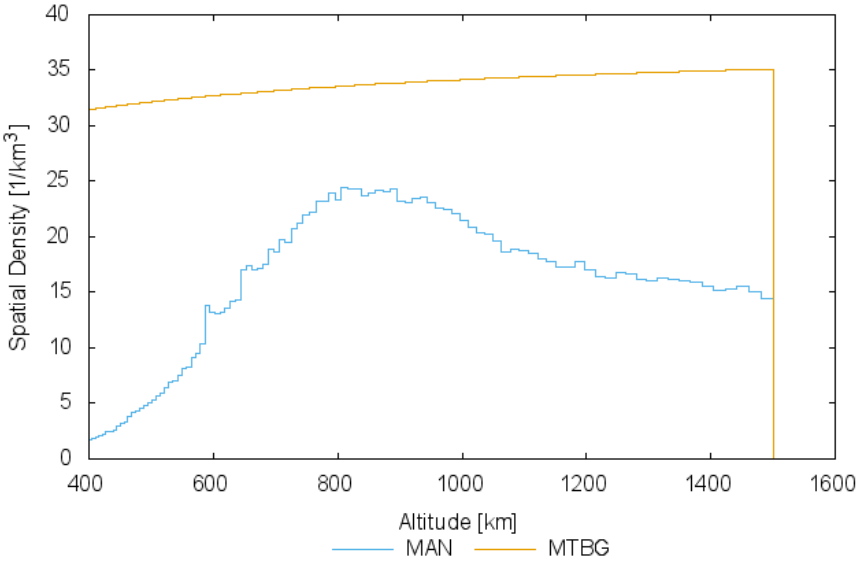

Figure 19: Debris density vs orbit altitude

upper altitude considered. This is compliant to what expected from literature [11]. The natural meteoroids flux is almost constant throughout all the altitudes of the simulation. From the analysis, the highest impact probability corresponds to an orbital altitude of about 800 km. However, the orbit selection does not only depend on the number of man made particles impacts, a more refined analysis has been performed for different altitude, ranging from 500 to 1200 km. The objective of the study is to identify the orbit inclination range that are more subject to debris pollution. Furthermore, not only the number of man made particles impacts are investigated, but also the ratio between man made and natural source debris is considered. The first simulation is performed with MASTER to evaluate the flux distribution for the considered orbital range. MASTER's input, except from orbit height and inclination, are the same for the whole analysis, and are shown in table 2. The simulation is performed computing the flux on a flat surface with the normal oriented in the velocity direction. This choice has been done considering that the majority of debris impacts is concentrated on the velocity direction spacecraft

parameter	**min**	**max**	**type**
selection	-	-	Earth-bound
argument of true latitude [deg]	0°	360°	-
epoch [y/m/d]	2020/10/1	2021/10/1	-
eccentricity	-	-	0.001
right ascension of the ascending node [deg]	-	-	0°
argument of perigee [deg]	-	-	0°
resolution [months]	-	-	1
particles size [m]	1e-6	1e-2	-
debris sources	-	-	condensed
meteoroid sources	-	-	Grün - Taylor distribution
target surface	-	-	normal in flight direction

Table 2: Input parameters to MASTER for debris flux analysis

surface, as shown in section 3 and figure 13.

For every different altitude considered, inclinations between 0° and 180° deg have been investigated, with a step of 10° deg between them.
Figures 20a and 20b show the results of the analysis for a 500 km orbit. At this altitude, the total flux of the meteoroids is from 2 to 6 times higher than the man made debris source for all the orbital inclinations. This scenario is not recommended for the mission, because the majority of the impacts on the scientific payload would be from natural sources and the results of the mission can be misrepresented, with a drastic consequence in the case in which the payload is not able to recognise the source of the impacting particle. The higher man made debris flux in the region can be found between an inclination of 80° and 90° deg; here the cumulative flux is dominated by the meteoroid in the lowest dimensions. For bigger particles, the flux on the surface is comparable, and the maximum value is about 100 particles per square metre per year, for dimensions of about 1e-5 m. The flux is quite low, considering also that they are given as particles per square metre, and it must be weighted by the sensitive surface area of the instrument; statistical analysis from this scattered data can result as scant.

Similar considerations can be done for the results of the analysis at 550 km. The results for the 80° deg and 90° deg inclination can be seen in figure 21a and figure 21b respectively. These inclinations have been chosen because for this orbital planes the higher flux has been registered. The predominance of the natural meteoroids on the cumulative flux is present for both orbital planes considered. Also in this case, the maximum flux of man made particles is reached between inclinations of 80° and 90° deg, where the flux of bigger man made particles is the same order of magnitude with respect to the one of the meteoroids of the same size.

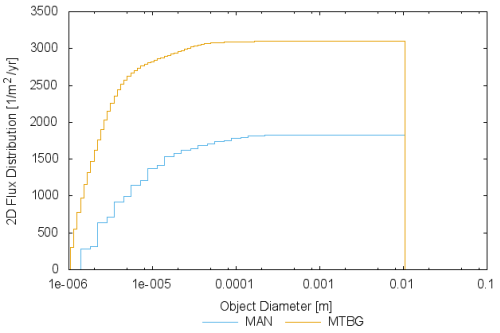

(a) Cumulative impact flux vs particle diameter for 500 km altitude and 80° deg inclination

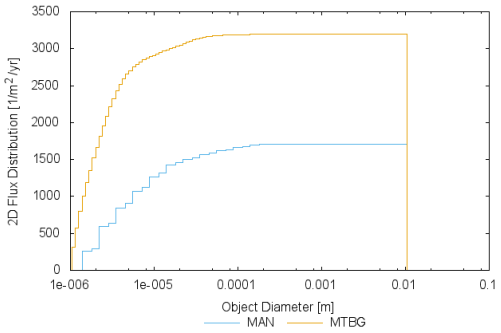

(b) Cumulative impact flux vs particle diameter for 500 km altitude and 90° deg inclination

Figure 20: Higher particles fluxes for 500 km altitude quasi circular orbit

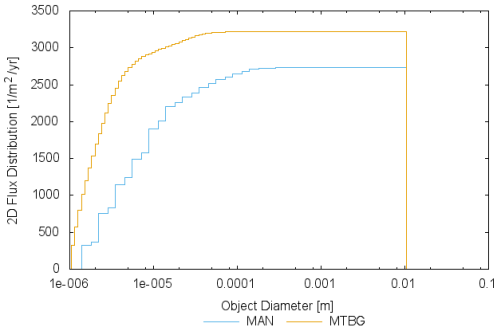

(a) Cumulative impact flux vs particle diameter for 550 km altitude and 80° deg inclination

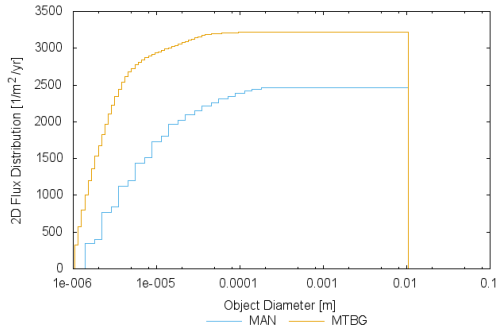

(b) Cumulative impact flux vs particle diameter for 550 km altitude and 90° deg inclination

Figure 21: Higher particles fluxes for 550 km altitude quasi circular orbit

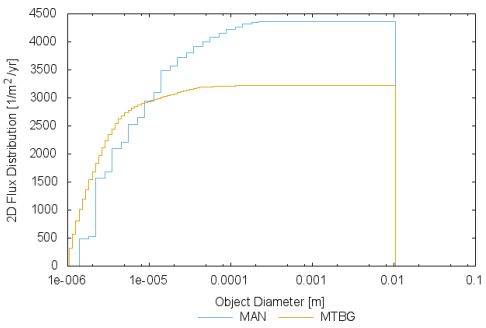

(a) Cumulative impact flux vs particle diameter for 600 km altitude and 80° deg inclination

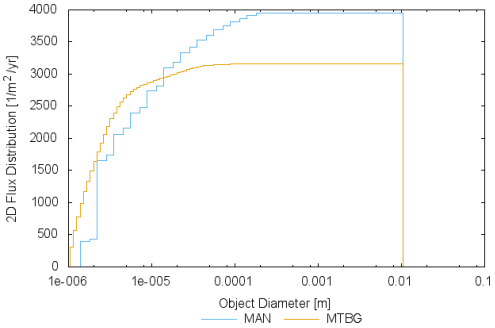

(b) Cumulative impact flux vs particle diameter for 600 km altitude and 110° deg inclination

Figure 22: Higher particles fluxes for 600 km altitude quasi circular orbit

When the region of 600 km is considered the situation is getting better from the ratio viewpoint; the cumulative flux of man made debris is higher than the meteoroids flux, and if the flux for specific particles dimensions is considered, the one of the debris bigger than 1e-5 m is one order of magnitude higher than the meteoroids one, and the separation increases with increasing particles dimensions. The higher flux is concentrated in inclinations ranged from 80° deg and 110° deg, and the output of the analysis for these boundaries is reported in figures 22a and 22b. In this region an impact analysis can generate enough impact data to satisfy the requirement of the mission, that corresponds to at least 100 debris impacts detected. A comparison between different orbit region predicted number of impacts can be found in table 4.

For a height of 700 km, the cumulative debris flux is nearly double with respect to the meteoroid one, but if a more detailed insight in particle dimensions is sought it is possible to state that for particles bigger than 1e-5 metres there is a sharp predominance of man made debris flux. Total flux of almost 6000 debris per square metre per year is reached for a orbit inclination of 80° deg, and this value remains constant until an inclination of 100° deg. The results for these 2 orbital planes are reported in figure 23a and figure 23b; the difference in the man made objects and meteoroid fluxes is now incremented, with the man made debris number that reaches 6000 impacts per square metre per year.

At 800 km height the maximum flux of debris is reached. In the orbital planes between 80° deg and 100° deg of inclination the debris flux value is greater than 100 particles per square metre per year up to debris dimensions of the order of 0.1 mm. The cumulative flux of man made particles is higher than the meteoroid one from a dimension of 1e-5 m and reach a value that is more than 2 times higher than the meteoroid flux. This is a positive scenario for the impact detector, that would retrieve a predominant amount of data from man made objects, with minor influence from the natural dust. Furthermore, in this region are present more "big" particles, in the order of 1e-4 m, which study is more interesting from a damage risk assessment viewpoint. The results

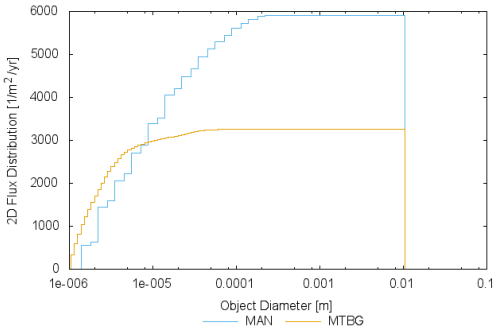

(a) Cumulative impact flux vs particle diameter for 700 km altitude and 80° deg inclination

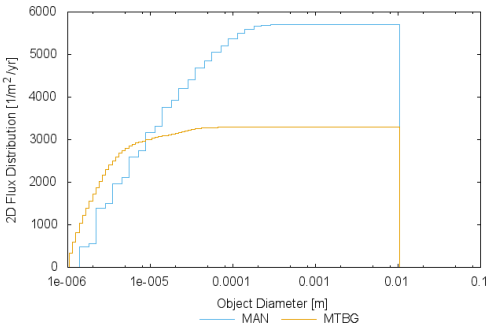

(b) Cumulative impact flux vs particle diameter for 700 km altitude and 100° deg inclination

Figure 23: Higher particles fluxes for 700 km altitude quasi circular orbit

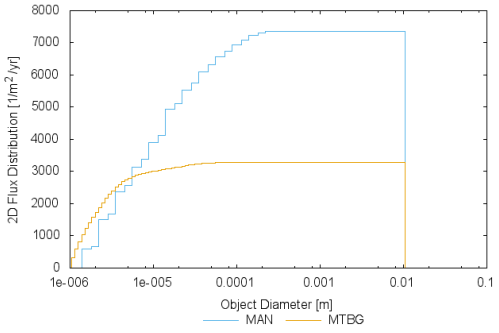

(a) Cumulative impact flux vs particle diameter for 800 km altitude and 80° deg inclination

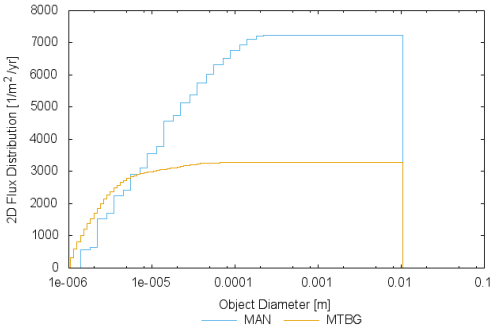

(b) Cumulative impact flux vs particle diameter for 800 km altitude and 100° deg inclination

Figure 24: Higher particles fluxes for 800 km altitude quasi circular orbit

for orbital planes of 80° deg and 100° deg are shown in figure 24a and 24b.

Expanding the analysis to 900 km orbit, similar values to the 800 km case can be found. The debris density is still in its peak region, as shown in figure 19. Similar considerations to the previous case can be assessed, and also in this case the more polluted planes are the one laying between 80° and 100° deg inclination. The results of the analysis are shown in figure 25a and 25b.

Orbit region of 1000 km altitude has been investigated also. The inclination planes of the highest fluxes in this region can be identified between 90° deg and 100° deg. The total amount of man made debris starts lowering with respect to the peak, in particular for bigger particles, that are also the more interesting to retrieve. However, even if the flux experiences a decrease with respect to the peak, the region is more suited for debris analysis than the 500 km and 600 km regions. The results for the two extreme inclinations are reported in figure 26a and figure 26b.

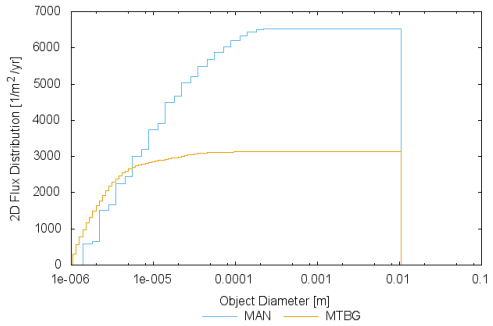

(a) Cumulative impact flux vs particle diameter for 900 km altitude and 80° deg inclination

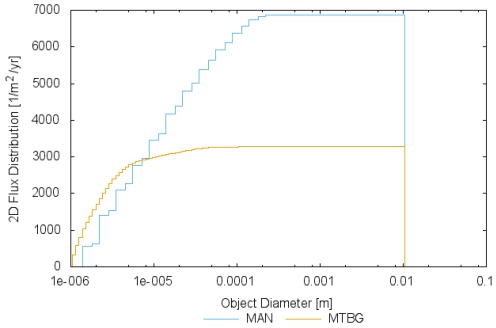

(b) Cumulative impact flux vs particle diameter for 900 km altitude and 100° deg inclination

Figure 25: Higher particles fluxes for 900 km altitude quasi circular orbit

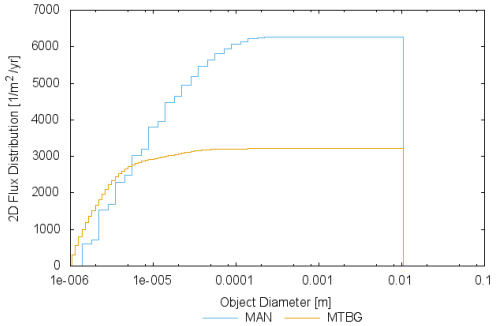

(a) Cumulative impact flux vs particle diameter for 1000 km altitude and 90° deg inclination

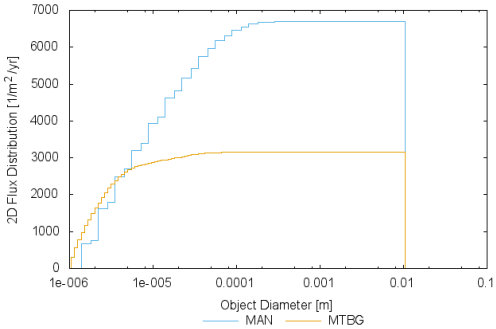

(b) Cumulative impact flux vs particle diameter for 1000 km altitude and 100° deg inclination

Figure 26: Higher particles fluxes for 1000 km altitude quasi circular orbit

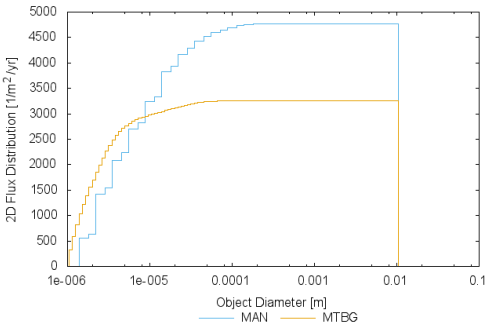

(a) Cumulative impact flux vs particle diameter for 1200 km altitude and 90° deg inclination

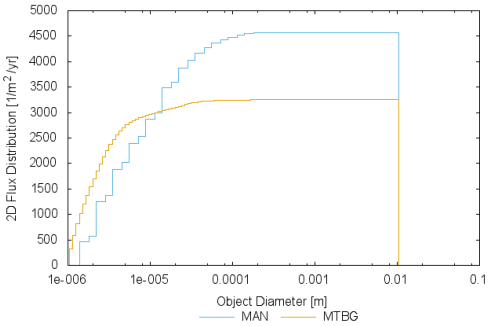

(b) Cumulative impact flux vs particle diameter for 1200 km altitude and 110° deg inclination

Figure 27: Higher particles fluxes for 1200 km altitude quasi circular orbit

As last orbital flux analysis, the region of 1200 km altitude is considered. The altitude is well above the peak, and this can be seen in the analysis results shown in figure 27a and figure 27b. The total flux value is reduced, and it is only 50% greater than the meteoroids in the upper dimension range. In this case, the best cases are concentrated in the orbital planes lying between 90° deg and 110° deg inclination.

This first preliminary analysis on the orbital selection has been done for different altitudes. Moreover, the inclination range among 80° to 110° deg ha been identified as the region with higher debris flux per unit surface. Except from 500 km and 550 km orbits, all the analysis identified the maximum in an inclination range comprehensive also of the Sun synchronous orbit. Since these orbits are very busy and of major interest for many missions, and there are many launch opportunities that deliver on this orbits, it has been decided to choose the Sun synchronous orbit as target for debris analysis. To refine the analysis in these specific orbits, an impact analysis through DRAMA software has been performed. Inside DRAMA, the MIDAS (MASTER-based Impact Flux and Damage Assessment) tool has been used. The analysis regard the selected most polluted zones of the previous case study, and assess the number of impacts on the sensitive surface of the debris payload, that is hypothesised to be 20x20 cm. The input to the software have been summarised in table 3.

Similarly to the previous analysis in MASTER, the first altitude that was considered is 500 km. The Sun synchronous inclination for circular orbits at this altitude is 97.4° deg. Since the maximum flux is concentrated in inclinations between 80° and 90° deg, a double analysis is performed in this case, one considering the 80° deg orbital plane and one considering the Sun synchronous orbit. This is done in order to compare the two outputs, and verify that in the case a 500 km orbit is chosen for the mission, the Sun synchronous inclination can be chosen without penalising too much the debris science. In case this is not verified, the selection shall turn toward an orbital plane in the local optimum region. In the 80° deg inclination orbit the number of impacts is very low; the total number of impacts during 1 year simulation does not reach the target requirement

parameter	**min**	**max**	**type**
simulation date [y/m/d]	2020/10/1	2021/10/1	-
eccentricity	-	-	0.001
right ascension of the ascending node [deg]	-	-	0°
argument of perigee [deg]	-	-	0°
spacecraft cross sectional area [m^2]	-	-	0.08
spacecraft mass [kg]	-	-	10
drag coefficient	-	-	2.4
particles size [m]	1e-6	1e-2	-
debris sources	-	-	condensed
meteoroid sources	-	-	Grün - Taylor distribution
target surface area [m^2]	-	-	0.04
surface orientation	-	-	normal in velocity direction

Table 3: Input parameters to DRAMA for debris impact analysis on payload sensitive area

of 100 impacts per year. The number of impacts on the instrument is higher than 1 only under 0.1 mm scale. Similar situation is for the Sun synchronous 500 km orbit, with the difference that the number of impacts are a bit lower also in the smaller size region; however, the two orbits give similar results and none of them is acceptable for the mission requirements, since they do not guarantee 100 impacts on the detection sensor. It is necessary then to discard the option of the 500 km orbital region from the possible orbit pool for the mission. The results of the two analysis are shown in figure 28a and figure 28b.

For 550 km the Sun synchronous orbit lays on an inclination plane of 97.59° deg. Also in this case, the Sun synchronous orbit is outside the local optimum range found as included between 80° and 90° deg. As for the previous case, a double analysis considering 80° and 97.59° deg has been performed, to check if the Sun synchronous orbit can be a too penalising choice. For the 80° deg inclination orbit the target value of 100 is barely reached. However, it is equal to the number of meteoroid impacts on the instrument. The man-made debris impacts compared to the meteoroid ones are in similar number throughout the whole size range of the simulation. From the debris analysis viewpoint this is not desirable, even if the number of man made debris impacts reached the required value. Even in this case the situation is reflected by the Sun synchronous case, with no relevant differences between the two cases. The choice of the Sun synchronous 550 km orbit then would be acceptable for the mission requirements, but if possible shall be avoided to get cleaner data from the debris payload. The results are shown in figure 29a and figure 29b for 80° and 97.59° deg respectively.

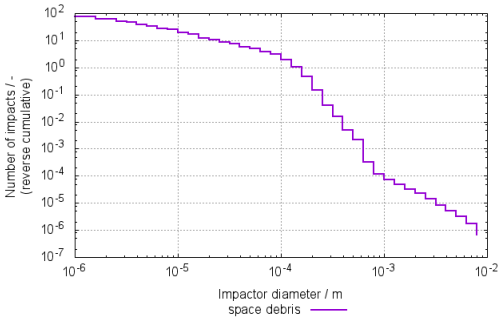

(a) Cumulative number of impacts vs particle diameter for 500 km altitude and 80° deg inclination

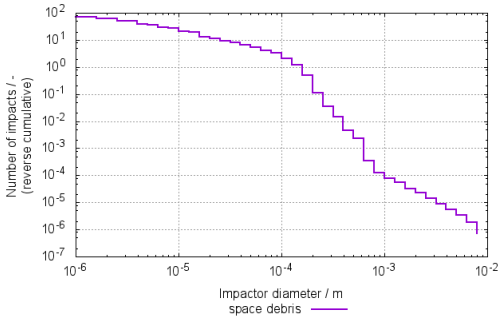

(b) Cumulative number of impacts vs particle diameter for 500 km Sun synchronous orbit

Figure 28: Particles impacts for 500 km altitude quasi circular orbit comparison between 80° deg inclination and Sun synchronous orbit

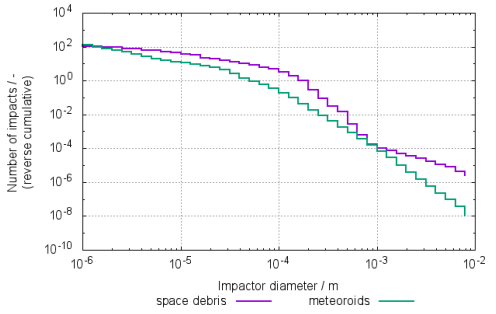

(a) Cumulative number of impacts vs particle diameter for 550 km altitude and 80° deg inclination

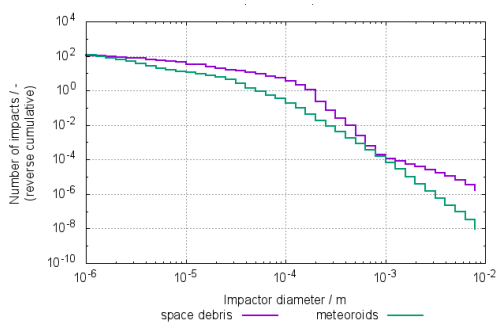

(b) Cumulative number of impacts vs particle diameter for 550 km Sun synchronous orbit

Figure 29: Particles impacts for 550 km altitude quasi circular orbit comparison between 80° deg inclination and Sun synchronous orbit

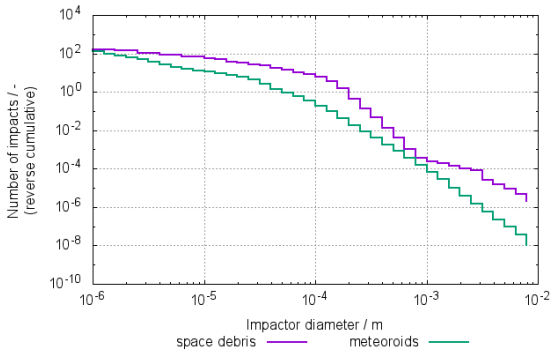

Figure 30: Cumulative number of impacts vs particle diameter for 600 km Sun synchronous orbit

For 600 km the Sun synchronous orbit inclination is 97.78° deg. This is in the band of maximum debris flux for the region. Previous analysis identified a majority of man-made particles with respect to natural meteoroids, in particular for the bigger sizes. In DRAMA analysis this trend is confirmed, and the number of impacts for man made particles bigger than 1e-5 m is one order of magnitude bigger than the impacts number of meteoroid source for most of the sizes. However, the total impacts remain relatively low, and, even if the cumulative number of debris impacts is higher than the meteoroids, there is no significant distinction between the two values: about 180 debris particles and 130 meteoroid particles impacted on the sensitive surface of the instrument as shown in figure 30. Even though the total number of impacts is similar, in the upper particles size range there is a clear distinction between the two fluxes, and a scientific payload that can compute at least the size of the impacting particle can filter the results to have a more precise measurement of man made debris. Therefore this orbit can be taken into account for the mission.

Getting closer to 800 km the space debris density is reaching its maximum. For 700 km Sun synchronous orbit, that would be at inclination of 98.18° deg, the increase in the man made particle impact number resulting from DRAMA analysis is evident, as in figure 31. In this region the total number of impacts is in majority due to man made particles. The average size of detected particle is increasing, facilitating the debris payload task.

At 800 km the peak is reached. The estimated number of detected particles exceeds the 300 units for man made objects, and it is almost three times the number of meteoroids that would impact the sensitive surface (see table 4). Furthermore, the number of particles bigger than 1e-5m increases as well. This is the ideal situation for the science phase, and the Sun synchronous 98.6° deg 800 km orbit would be the best choice from the debris analysis viewpoint. The impacts on the debris detector are shown in figure 32.

For the 900 km Sun synchronous orbit a similar behaviour as for the 800 km one is present. The debris density is still in its maximum range, and the polluted environment

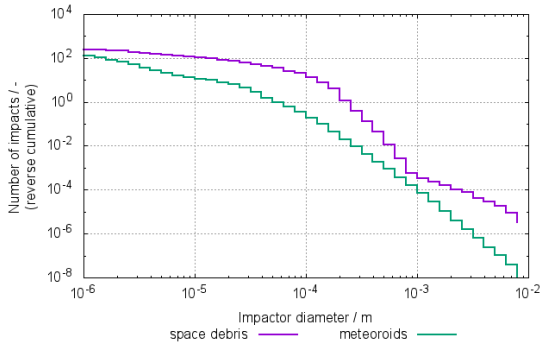

Figure 31: Cumulative number of impacts vs particle diameter for 700 km Sun synchronous orbit

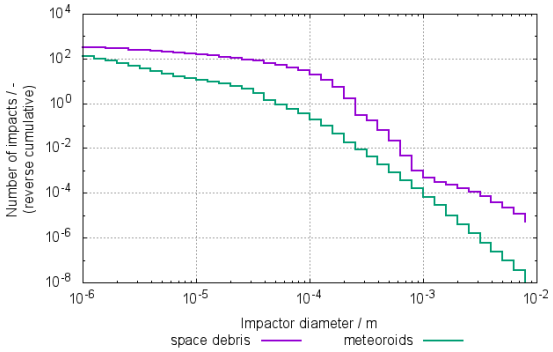

Figure 32: Cumulative number of impacts vs particle diameter for 800 km Sun synchronous orbit

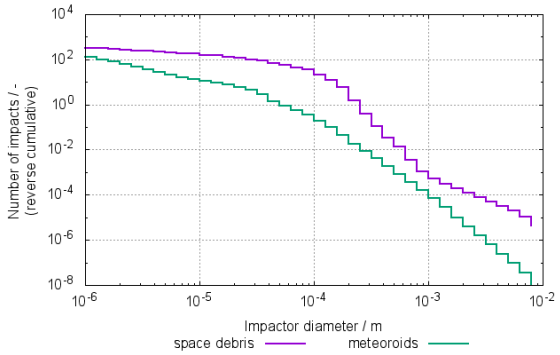

Figure 33: Cumulative number of impacts vs particle diameter for 900 km Sun synchronous orbit

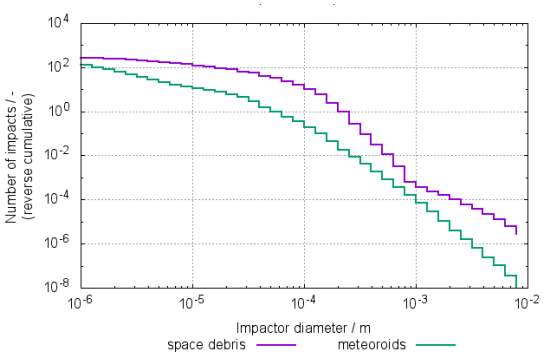

Figure 34: Cumulative number of impacts vs particle diameter for 1000 km Sun synchronous orbit

favours the debris science phase, due to an higher impact probability. The results of the 900 km 99.03° deg orbit DRAMA simulation is shown in figure 33.

For the LEO region above 900 km the debris spatial density decreases. Both the total number of man-made debris that impact the sensor and the average dimension of the particles detected is lower than the previous two cases. However, the number of man made objects impacts is still well above the requirement, and there is a clear distinction between the man made and meteoroid particles. The results of DRAMA simulation for the 1000 km Sun synchronous orbit (99.47° deg) are shown in figure 34.

Last DRAMA simulation performed concerns the 1200 km Sun synchronous orbit. The debris population is similar to the environment at 700 km, as expected from the debris spatial density diagram in figure 19. Although the number of impacts and particles dimension is reduced from the optimum case, the region satisfies the debris requirement target, and the impacts number separation between the man made and natural particles is still positive for the analysis. Figure 35 illustrates DRAMA analysis results for 1200 km 100.4° deg orbit.

In conclusion, from the MASTER and DRAMA analyses, the better options in terms

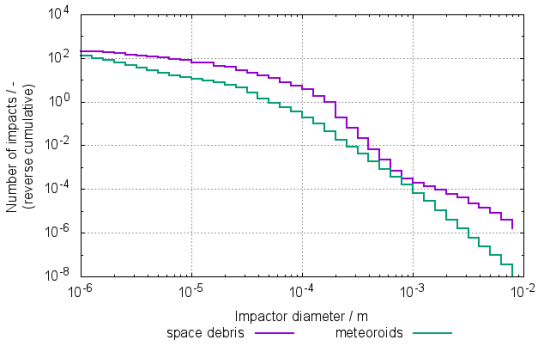

Figure 35: Cumulative number of impacts vs particle diameter for 1200 km Sun synchronous orbit

height [km]	**meteoroids**	**debris**	**total**	**debris/meteoroids ratio**
500	$\sim$ 130	$\sim$ 70	$\sim$ 200	0.54
550	$\sim$ 130	$\sim$ 100	$\sim$ 230	0.77
600	$\sim$ 130	$\sim$ 180	$\sim$ 310	1.4
700	$\sim$ 130	$\sim$ 240	$\sim$ 370	1.85
800	$\sim$ 130	$\sim$ 320	$\sim$ 450	2.46
900	$\sim$ 130	$\sim$ 270	$\sim$ 400	2.08
1000	$\sim$ 130	$\sim$ 250	$\sim$ 380	1.92
1200	$\sim$ 130	$\sim$ 190	$\sim$ 320	1.46

Table 4: Impacts per year comparison on the debris payload sensitive surface (0.04 m^2) for different altitudes

of number of impacts of space debris results in Sun Synchronous Orbits between 800 km to 900 km. However, with different impact levels and characteristics, Sun synchronous orbits ranging from 550 km to 1200 km can possibly satisfy the requirement of the mission. For a more immediate comparison between the possible orbit pool, a comparison between the total number of impacts, due to both man made and natural objects and their ratio can be done, as in table 4. The meteoroid flux is constant throughout the region considered; on the other hand, the number of debris impact ranges from a minimum of 70 impact at 500 km to a maximum of 320 impact at 800 km of altitude, for a Sun synchronous orbit, with a man made/natural particles ratio of 2.46.

5.2 Reentry

The final part of the mission requires a proper manoeuvre to start the re-entry analysis, after the debris science phase and the CAM phase. The aim of the reentry payload is to analyse the atmosphere and its interaction with the satellite in the region between 200 km and 100 km. It is important then that the spacecraft remains in this region for a sufficient amount of time, to allow the payload to collect a satisfying amount of data.

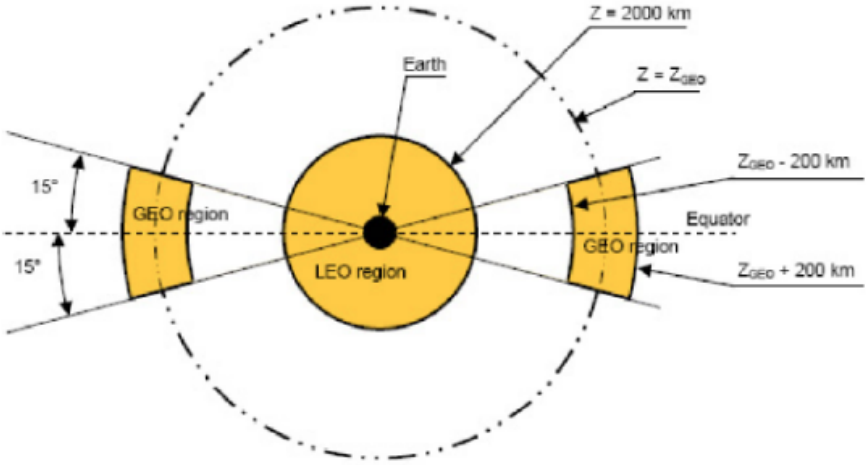

Figure 36: Orbital protected regions, Space Debris Mitigation Standards. Credit: IADC

Moreover, the spacecraft operates in the LEO region, which is subjected to the IADC space debris mitigation guidelines [72], as shown in figure 36. It is important then to de-orbit the spacecraft in a fast and secure way. In order to be able to perform the reentry analysis during the mission estimated lifetime of an year and to not exceed the CubeSat lifetime that in general can be assessed to about two years, it is important to guarantee the reentry in at most 6 months, to reduce the residence time of the spacecraft in the region once the tasks are completed. Moreover, the reentry phase should be designed in order to minimise the required propellant, because the small dimensions of the spacecraft and the reduced weight do not allow big propellant tanks. The analysis is based on the required ΔV, and for the mission considered a literature research on off the shelf CubeSat components allows to define an acceptable level of total on board ΔV set around 150 m/s (i.e. Hyperion Technologies, Vacco, NanoAvionics).

5.3 Orbital model

To investigate the re-entry strategy and perform an optimisation analysis, a MATLAB model has been developed. The model considers a perturbed two body problem, under the effect of the atmospheric drag an Earth gravitational perturbations. The atmosphere density for different altitudes has been computed using an exponential atmospheric model (see eq. 1), where ρ_0 is the reference density, h is the spacecraft altitude, h_0 is the reference altitude and H is the scale height [70]. For the density model, the U.S. Standard Atmosphere (1976) [73] for 0 km, the CIRA-72 for 25-500 km and CIRA-72 with $T_\infty = 1000K$ for 500-1000 km have been used [74].

$$\rho(h,t) = \rho_0 e^{-\frac{h-h_0}{H}} \tag{1}$$

For drag computations, the spacecraft parameters taken into account are the cross sectional area, of 226.3x340.5 mm for a 12 U CubeSat (see section 6.3 for explanations),

the spacecraft weight of 10 kg, and the drag coefficient of 2.2 [70]. The area to mass ratio for the spacecraft is 7.705515e-9 km^2/kg. The drag acceleration is computed as in equation 2.

$$\overline{a}_{drag} = -\frac{1}{2} A_m C_D \rho v_{rel}^2 \frac{\overline{v}_{rel}}{\|\overline{v}_{rel}\|} \tag{2}$$

Where a_{drag} is the acceleration acting on the spacecraft, A_m is the area to mass ratio, C_D is the drag coefficient, ρ is the atmosphere density and v_{rel} is the relative velocity between the spacecraft and the atmosphere.
During this analysis, the Earth was not considered a perfectly symmetric sphere. In fact, it is more like an oblate spheroid with an equatorial bulge and flattening at the poles. In addition, Earth has a slight pear shape at the equator and a variety of minor mass anomalies (i.e. continents, mountains). Mathematically, this is included by expanding the geopotential function at the position (r, θ, ϕ) in a series of spherical harmonics [70]:

$$\begin{aligned} U(r,\theta,\phi) = & \sum_{n=0}^{\infty} (\frac{r}{R_E})^{n+1} J_n P_{n0} \cos\theta + \\ & \sum_{n=1}^{\infty} \sum_{m=1}^{n} (\frac{r}{R_E})^{n+1} [C_{nm} \cos m\phi + S_{nm} \sin m\phi] P_{nm} \cos\theta \end{aligned} \tag{3}$$

where J_n is defined to be C_{n0}, which is called as the zonal harmonic coefficient. R_E is the Earth radius at the equator, P_{nm} are Legendre polynomials, r is the geocentric distance, θ is the latitude and ϕ is the longitude. Terms with m=0 are called zonal harmonics, terms with n=m are called sectoral harmonics and terms with $m \neq 0$ and $m \neq n$ are called tesseral harmonics. The J_2 term is, by far, the most of the geopotential terms; it is an oblateness term, since it represents the mass distribution of the equatorial bulge. It has a important effects for the orbit, causing the right ascension of the ascending node and the argument of perigee to rotate at rates of several degrees per day. Typically the effects of the higher order harmonics are extremely small, except for special circumstances. For these reasons, in the model only the J2 effect has been taken into account, as $J_2 = 0.0010826359$.
The reentry analysis rely on the described orbital model to integrate the perturbed orbit. During the reentry, one or more impulsive manoeuvres are performed, depending on the strategy, in order to lower the perigee altitude of the spacecraft and reduce the decay time. To do that, the impulsive manoeuvres are performed at the apogee of the orbit. The orbit integration is appositely equipped with an event function that stops the integration if two conditions are met simultaneously: the first condition is the arrival of the spacecraft at the apogee of the orbit; the second condition is that between two consecutive manoeuvres, at least ten days have to be spent. When this happens, the model compute the target orbit parameters, based on the current orbit and position of the spacecraft. At this point, both the current velocity and the target velocity of the spacecraft are available. The required ΔV is then computed, and the natural decay starts again with the new orbital parameters, until the new manoeuvre conditions are met. If this not happen, the spacecraft continues its natural decay, until the stopping

conditions of for the reentry event function are met; this happens when the spacecraft reaches an altitude of 100 km. The manoeuvres perigee targets are given as an input to the model, which performs the different strategies selected, giving as output the ΔV of every single manoeuvre and the total ΔV for the different strategies. For the last optimisation on the reentry strategy, a genetic algorithm has been used, in order to optimise the cost function in a predefined range of altitudes targets (see section 5.3.1 for the optimisation details).

5.3.1 Results

The first analysis performed is a parametric study regarding the end of life strategy. The objective is to have a first guess on the key parameters of the reentry phase, which have been identified as the time until the reentry, the residence time between 200 km and 100 km altitude and the required ΔV, and their dependence from the reentry orbit strategy. A first simulation has been performed, considering a single impulsive manoeuvre at the apogee of the operative orbit. The initial orbit has been chosen considering the output of the space debris orbit selection study in section 5.1. The manoeuvre is performed starting from an initial Sun synchronous circular orbit at different altitudes, ranging from 550 to 1200 km; different perigee altitude are then taken as targets, and a single impulse firing has been computed to reach that target. After the firing, the spacecraft keeps its free motion until reentry, which is considered to happen at 100 km. The simulation's output is the required ΔV, computed as the difference in the velocities of the initial orbit and the target orbit, the total time until reentry and the time spent under 200 km, and are shown in figure 37. From the single impulse analysis three important considerations can be done:

- to maximise the time time spent under 200 km, a final perigee altitude around 200 km shall be targeted.
- no perigee altitudes above 280 km ensure reentry in at least 180 days.
- to have a deorbit ΔV of no more than 150 m/s, no orbit above 900 km altitude can be considered.

The further step in the reentry design, is to divide the ΔV in more than 1 firing. For a CubeSat a single ΔV manoeuvre generates too much risk to be considered. If the manoeuvre is considered impulsive, then the firing time shall be reduced. This requires high thrust if high ΔV is needed, so the attitude system can be unable to grant the pointing accuracy of the CubeSat, leading to an uncontrolled engine firing and a consequent fatal accident that pose a serious threat to the mission and the other satellites, generating an uncontrollable CubeSat size debris in a busy LEO region. If low thrust is used, too much firing time is requested, the manoeuvre can not be considered impulsive anymore and problems regarding attitude and accuracy of the manoeuvre can arise. If this is the case, no further correction is possible, since the spacecraft expend all the propellant in a single manoeuvre, and the mission is jeopardised. For this reasons

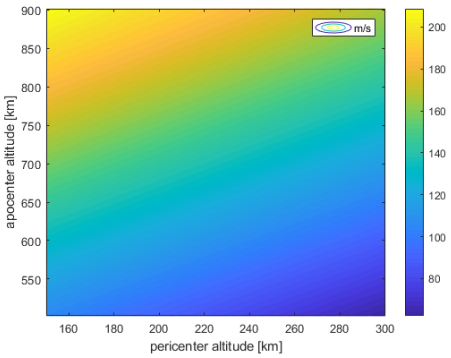

(a) Single impulse manoeuvre ΔV [m/s] to de-orbit.

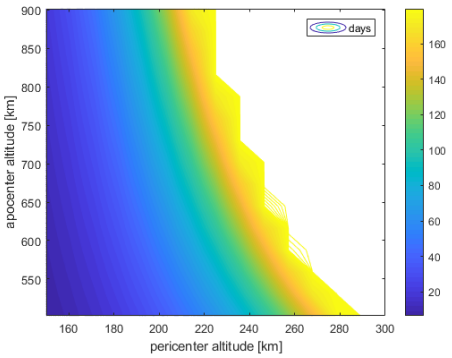

(b) Number of days before reentry (100 km) for different initial and target altitudes

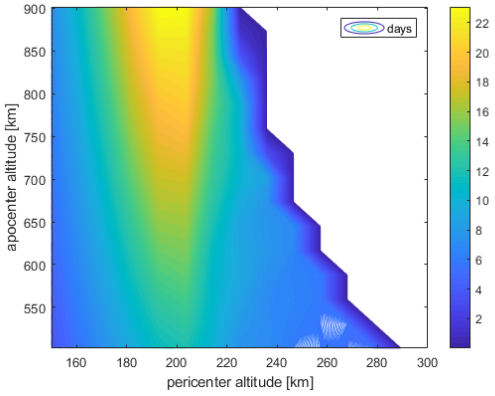

(c) Number of days spent under 200 km for different initial and target altitudes

Figure 37: Single impulse manoeuvre to de-orbit. The y-axis reports the initial altitude, the x-axis the target altitude.

Manoeuvre No.	**option 1 [km]**	**option 2 [km]**
1	400	450
2	300	350
3	200	250
4	150	180

Table 5: Caption

H_0 **[km]**	**steps [km]**	ΔV **tot [m/s]**	ΔV **[m/s]**	Δt_{tot} **[days]**	$\Delta t_2 00$ **[days]**
500	400-300-200-180	85.05	32.3-27.4-23.5-1.74	61.8	2.09
500	400-350-200-180	85.2	32.3-13.14-38-1.7	61.9	2
635	400-300-200-180	121.8	68.4-27.3-23.8-2.3	63.1	0.23
635	450-300-250-180	121.9	54.4-41.4-9.4-16.9	63.2	0.24
770	400-300-200-180	157.1	103.3-27.3-24.1-2.3	64.3	0.1
770	450-300-250-180	157.2	89.4-41.2-9.7-16.9	64.4	0.08
900	400-300-200-180	191.1	137.1-27.3-24.4-2.3	65.3	0.02
900	450-300-250-180	191.2	123.3-41.2-10-16.8	65.3	0.02

Table 6: Results for different deorbiting strategies for 4 impulses

a multi impulse strategy is considered. A first simulation for a multi impulse reentry strategy has been performed considering 64 different scenarios. The simulation consists in 4 different firings, always at the orbit apogee. Between 2 consecutive firings, at least 10 days have to pass, in order to check the manoeuvre outcome and be able to organise the following manoeuvre also if errors in the previous one caused an unexpected orbit track. Furthermore, the waiting time allows to exploit natural perturbances to lower the orbit apogee and reduce the required ΔV. As first guess, four different orbit altitudes are considered: 500 km, 635 km, 770 km and 900 km. For every manoeuvre there are two different alternatives: For every starting altitude, the sub-optimum result is reported in table 6. It is possible to notice that to have a total ΔV below 150 m/s, it is necessary to stay on an orbit under 770 km. Furthermore, the best results in terms of time of flight under 200 km are obtained for the orbits with the lower initial altitudes.

Another limiting factor in the mission orbit altitude is the requirement of natural de-

Parameter	**Value**
Altitude	600 km
inclination	97.78° deg
eccentricity	0
anomaly of perigee	0
right ascension of the ascending node	0

Table 7: Selected orbit parameters

cay in at most 25 years. The CubeSat is operating in a polluted and busy orbital region. A failure of the propulsion system or a fatal collision with a space debris would cause the generation of a great threat to other operating satellites. To reduce the effects of a system failure, the chosen orbit shall be chosen in order to be compliant with the space debris mitigation guidelines even if no propulsion system is available. This correspond to a natural decay time of 25 years. For a 10 kg spacecraft, the maximum altitude that guarantees a 25 years decay is about 600 km if best case scenario is considered, otherwise it can last up to 60 years [75]. This poses an important constraint to the eligible orbit.

5.4 Final mission orbit profile

The final orbit profile of the mission is based on the considerations of both the debris analysis and the reentry analysis, and propose a trade-off solution that satisfy mission requirements and at the sane time optimise the drivers of the selection. To maximise debris impacts on the detector, the best choice was an orbit between 800 km and 900 km. However, the ΔV required to deorbit from such altitudes exceeds the target ΔV of 150 m/s, and such performance would be a burden for the propulsion system. Furthermore, to ensure a safe mission and compliance to mitigation guidelines, a maximum altitude boundary of 600 km shall be set. From the previous debris impact analysis, in the range between 500 to 600 km, the best option is to choose the maximum value. With these considerations the operative orbit of the mission is settled to 600 km. This altitude is at the boundaries for a 25 years reentry, and even if there is the possibility that in the worst case scenario the spacecraft decay time is more than 25 years, it is taken as an acceptable risk, privileging the improved science possibilities that the 600 km orbit offers with respect to the 550 km one. However, a more detailed risk analysis should be performed for future mission design steps, and the possibility to lower the operative orbit to 550 km should be evaluated carefully.

To reduce the propellant consumption during reentry and, at the same time, to maximise the time passed under 200 km, an optimisation of the multi impulses strategy has been performed using a genetic algorithm. The function is similar to the previous one: every manoeuvre is performed at apogee, and the time between to consecutive manoeuvre is at least 10 days. The ΔV is given instantaneously, and then the spacecraft follow its natural motion. After further considerations on manoeuvre failure risk, has been decided to add 1 impulse to the previous 4. The first ΔV demand was too high

h_a **[km]**	h_p **[km]**	ΔV **[m/s]**
588.34	450.5	36.98
588.1	389.9	14.47
587.3	282.8	34.78
585.3	225.9	20.81
564.1	199.1	6.04

Table 8: Firing targets and relative ΔV for reentry phase

to ensure safe operations during the firing, and an error in the first manoeuvre could jeopardise the reentry phase. The aim is to reduce the first impulse ΔV which was too high for the 600 km orbit. An even distribution of ΔV between the manoeuvres guarantees safer operations and the possibility to recover from a pointing or firing error. The cost function to minimise used for the optimisation is a combination between the total ΔV expressed in metres per second and the time passed under 200 km, in days. The two parameters are then weighted and multiplied by a scaling factor, in order to have the same order of magnitude, as reported in equation 4.

$$J = 0.7\Delta V_{tot} - 3t_{low} \tag{4}$$

The input to the genetic algorithm consists in the range of the target altitudes for the 5 firings. For the first firing a range between 400 and 500 km has been chosen. As previously said, the altitude has been increased to reduce the first ΔV. The second altitude range is 300 - 400 km, the third 250 - 300 km, the fourth 200 - 250 km and the last 180 - 200 km. The final altitude has been increased too because once the spacecraft reaches 150 km the drag becomes so intense that the time spent under 200 km is less than 1 day, and this would results in an insufficient amount of data retrieved by the reentry analysis payload.

The optimal deorbit strategy starting from a 600 km circular Sun Synchronous orbit is reported in table 8, in which the altitude steps and the relative ΔV are reported. The total ΔV for the reentry is 113.08 m/s, and the time spent between 200 and 100 km with this strategy is 8.61 days. The total time elapsed between the first impulsive manoeuvre and the reentry at 100 km is 99.85 days, less than the 180 days decided in the requirements.

During the reentry the spacecraft pass from a circular orbit to an elliptical orbit, with eccentricity of 0.027, through the impulsive manoeuvre, and then the orbit perturbations force again the orbit evolution toward a circular orbit. When all the orbit develops inside 200 km, the altitude continues to decrease due to the action of the drag force, until the boundary line of 100 km is reached and the mission is considered ended. In figure 38 the altitude evolution of the reentry after the last firing is shown, and in figure 39 an extract of the reentry is presented, focusing on the circularisation process that low the apogee from 600 km down to 200 km and lower. Only the last part of the reentry is reported, after the last firing, and the orbit passages above 200 km are reported in blue, while when the altitude is lower than 200 km the orbit is represented in red. The complete

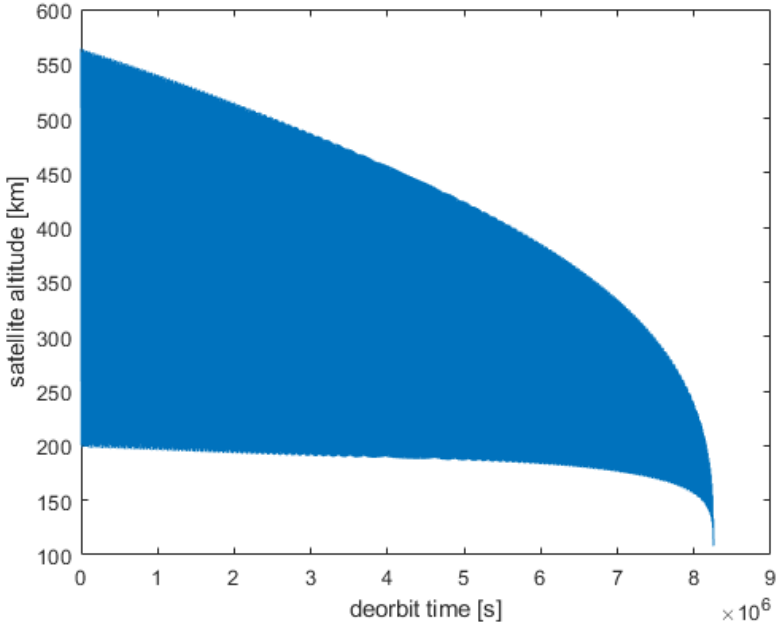

Figure 38: Spacecraft altitude during reentry

deorbiting phase is shown in figure 40, where with different colours are represented the different parts of the reentry phase, and with the red stars the location in which the firings occur.

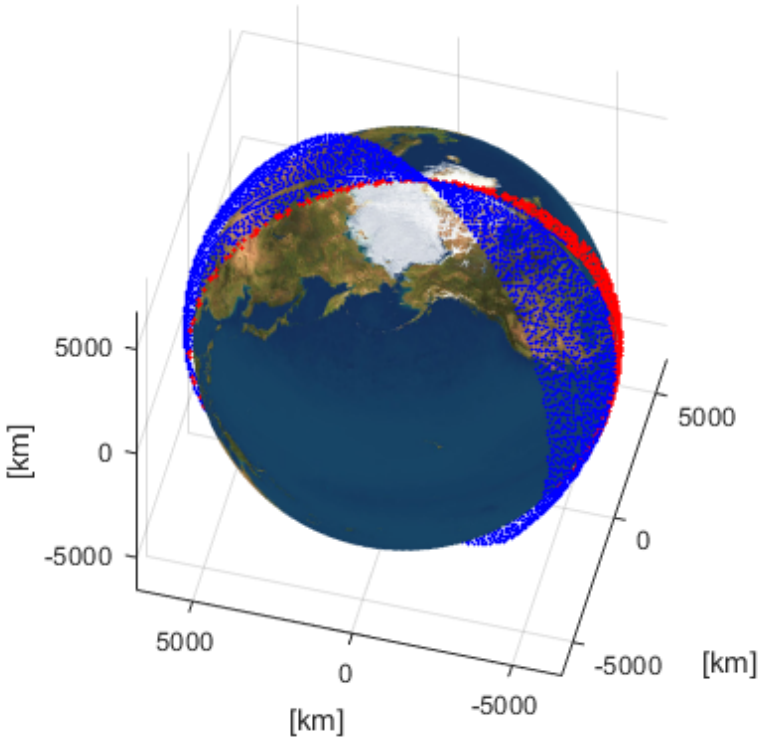

Figure 39: Natural decay of the orbit after the last manoeuvre. The blue part identifies the altitudes above 200 km, the red part the altitudes under 200 km

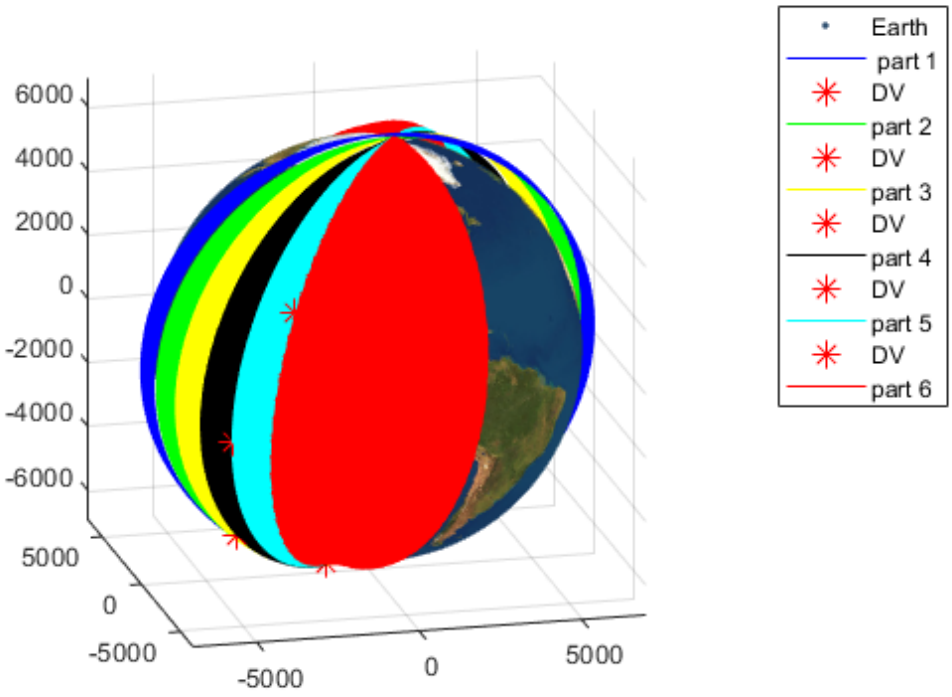

Figure 40: Reentry phase orbit profile. In blue is represented the operative orbit evolution at 600 km, in green the orbit after the first firing, in yellow after the second firing, in black, azure and red the orbit after the third, forth and fifth firing respectively.

6 System design

In this section a preliminary system design for the mission is described. The aim is to describe the most relevant subsystems for the mission and their design drivers, creating simple models or preliminary analysis to allow the definition of the performance that need to be satisfied, and offering some off the shelf alternatives in the components selection. Furthermore, the three payloads of the mission are presented, explaining their baseline, and the optimum choices for the current mission. In the end, a preliminary iteration on the mass and power budgets is proposed.

The mission concept consists in a CubeSat carrying three different payloads. Traditionally, the space industry produced large and sophisticated spacecraft having high budgets that only a large government-backed institutions can sustain. However, over the last decade, the space industry experienced an increased interest towards smaller missions and recent advances in commercial-off-the-shelf (COTS) technology miniaturisation enhance the development of small spacecraft missions based on the CubeSat standard. CubeSats were initially envisioned primarily as educational tools or low cost technology demonstration platforms that could be developed and launched within one or two years [76]. Recently, however, more advanced CubeSats missions have been developed and proposed, indicating that CubeSats started to transition from being educational and technology demonstration platforms to offering opportunities for low-cost real science missions with potential high value in terms of science return and commercial revenue. The CubeSat standard was introduced by Stanford and California Polytechnic State Universities in 1999 [77] [78], and it specifies that a standard 1U unit is a 10 cm cube (10x10x10 cm^3) with a mass of up to 1.33 kg [79]. A 1U CubeSat could either serve as a standalone satellite or could be combined together to build a larger spacecraft. One of the main advantages of this standardisation is to allow launch vehicle producers to adopt a common deployment system independent on the CubeSat manufacturer.

6.1 Structures

Structure is the primary chassis of spacecraft, which mechanically supports all the spacecraft subsystems as well as it might serve as thermal and radiation shielding for sensitive components. Custom built and off-the-shelf structures are the two main options for a CubeSat structure. The main advantage of Commercial Off-The-Shelf (COTS) structures is their simplicity and flight heritage, whereas custom built ones could be adopted for a specific mission complexity, payload and subsystem requirements, with the drawback of a higher cost due to test and qualification campaign. Typically, CubeSat structures are made in aluminium [80] but recently 3D printed CubeSat structures are gaining some interest among developers, and several missions, including for example 3U Tomsk-TPU-120 [81], 1U PrintSat [82], 2U QB50 UNSW EC0 [83], started to utilise 3D printed structures.

For this preliminary analysis of the mission concept, the baseline is to use commercial-off-the-shelf components where possible. Debris science and autonomous CAM testing do not burden on the structure specifications. The spacecraft is flying through a densely

Properties	**SM12**	**8-Unit**
form factor	12 U	8 U
measures	340.5x226.3x226.3 mm	226.3 x 226.3 x 227mm
primary structure mass	1430 g	1333 g
full structure mass	1750 g	1871 g
stack layout	PC/104	PC/104

Table 9: SM12 and 8-Unit structures properties

populated zone of space debris, but the normative and the mission requirements specify that close conjunction with debris bigger than 1 cm scale should be avoided. On the other hand, smaller particles can pose a threat for the performance of specific subsystems, but from the structure point of view they do not represent a possible source of failure [84]. For the reentry analysis the main concerns are the aerodynamic heating and the break-up altitude. The reentry analysis target is to recover measurement data in the region between 200 and 100 km altitude, and be able to send the data to ground. Passed the Karman line, the spacecraft becomes uncontrollable [85] and the mission is considered ended, because would be impossible to continue to register and transmit data. Once the mission objective is reached, the spacecraft continues in its decay, and the increasing density determines an continuous heating of the satellite, until aerodynamic forces and thermal action destroy the spacecraft at about 80 km [26]; at this point, all the components are burned in the atmosphere. For CubeSats with standard components, complete burning before reaching the ground is ensured (only some very dense metallic part can survive, but the risk associated with that is negligible) [26], and no controlled reentry is necessary. The limiting elements in the reentry then are identified as the temperature reached, which problem has to be faced by the thermal control system and protective coatings, and the attitude control. The structure break-up is is the decisive event determining the end of science. For these reasons, a commercial-off-the-shelf CubeSat structure can be taken into account.
There are multiple companies, such as Pumpkin, ISIS, Radius Space and NPC Spacemind among others, providing off-the-shelf structures ranging from 1U to 27U class CubeSats. The dimensions of the spacecraft have to be chosen according to the payloads and subsystems accommodation. In section 6.6 a preview on the mission budgets is given. Considering the preliminary systems iteration on mass and volume of the components, the possible choice on CubeSat platforms reduces to 8 U or 12 U. Thanks to CubeSat standards, the supplier choice is very wide. In this work, the 12 U structure the Italian NPC Spacemind SM12 [86] has been selected as baseline; the SM12 was selected above other thanks to its light weight, only 1750 g with respect to a competitors average of 2 kg, and its versatility in configuration and COTS compatibility. The 8U structure is less common between constructors, and there are only few companies in Europe that offer it off the shelf. The ISIS 8-Unit CubeSat structure [87] is an example, with a weight of 1871 g, and its flexibility in the design, allowing customisation and adaptation for the payloads if necessary. In table 9 a comparison between the two structures

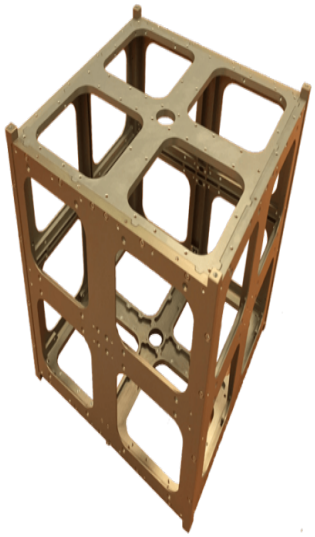

(a) ISIS 8U CubeSat structure. Credit: ISIS

(b) NPC Spacemind SM12 structure. Credit: NPC Spacemind

Figure 41: CubeSat structure possible baselines for the structure of the CubeSat mission concept

characteristics is presented. The NPC Spacemind structure offers more flexibility in the design, and it is lighter than the 8 U structure. Furthermore, the 12 U structure is more widely used with respect to the 8 U configuration, and the actual standard Canisterized Satellite Dispensers (CSD), which are used as a standardised launch device, do not have an 8 U option [88]. The standard CSD for 12 U satellite allows a maximum spacecraft mass of 24 kg and size envelope of 23x24x36 cm. This set a constraint on maximum weight and maximum storage configuration dimensions for the design of the spacecraft. The results of the preliminary mass and volume budgets do not express the need to use the 12 U structure at the expense of the 8 U one, however, thanks to the better performance and customisation allowed on the NPC Spacemind structure, the final selection for the structure hangs for the SM12. From the mass budget viewpoint, this decision allows to save at least 100 g and have more space to organise the payload and necessary instruments.

6.2 Propulsion system

The preliminary design of the propulsion system is based on the ΔV budget for to the reentry phase, the CAMs and the testing of the autonomous CAM system. The ΔV required for the reentry phase to de-orbit the spacecraft is described in section 5.2, and is equal to 113.08 m/s. Applying a 20% margin to this value, the delta-v budget increase to 135.7 m/s. The propellant for the collision avoidance manoeuvre has been estimated thanks to DRAMA ARES tool. It allows to compute the required ΔV for

Parameter	**value**
Date	2020/10/01
semi-major axis	6980 km
eccentricity	0.001
inclination	97.8° deg
right ascension of the ascending node	0° deg
argument of perigee	0° deg
spacecraft diameter	0.3 m
particles size	0.01-100 m
warning time	1 day
global scaling factor for position uncertainties	1
uncertainties	based on CDM data
position uncertainties epoch	from catalogue uncertainties
ACPL value	1e-5
target collision probability level	0.1

Table 10: DRAMA ARES input parameters for collision avoidance ΔV computation

collision avoidance manoeuvres of the mission, after specifying the mission parameters, the acceptance collision probability level (ACPL) and the manoeuvre strategy. The conjunction warnings are based on the MASTER database. To perform the simulation, the inputs to the software are reported in table 10. The orbital parameters given correspond to the nominal orbit profile of the mission, the 600 km Sun synchronous orbit. The conjunction warnings are based on particles visible from ground. To identify them, ARES uses the radar equation reported in equation 5, where D_{min} represent the minimum detectable particle dimension, the reference diameter $D_{ref} = 0.32\,m$, the reference altitude $h_{ref} = 2000\,km$ and the exponent value $Exp = 2$.

$$D_{min}(h) = D_{ref}\left(\frac{h}{h_{ref}}\right)^{Exp} \tag{5}$$

The output gives the ΔV depending on the number of revolution between the manoeuvre and the conjunction event, and the number of manoeuvre to be performed according to the defined ACPL. The analysis results in the need to perform 2.04 collision avoidance manoeuvres, and the ΔV required with respect to the number of revolution before conjunction, as shown in figure 42. In the worst case scenario with zero revolutions between the manoeuvre and the event, corresponding to a minimum forewarning to the conjunction event, a maximum delta-v of 5 m/s is needed. Moreover, it is necessary to add the 5 m/s ΔV required by the testing of the autonomous collision avoidance system. The ΔV budget is then reported in table 11,together with the 20% marginalised values.

To deal with the ΔV requirement, different propulsion technology have been taken into account. To avoid adding complexity on the attitude control system due to high thrust level, the maximum thrust for the on-board engine should not be higher than 1 N level.

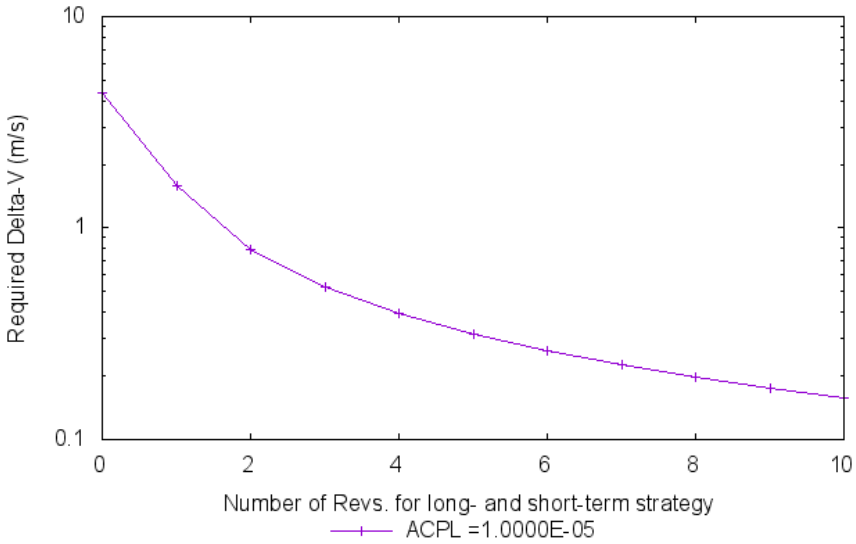

Figure 42: ΔV necessary for collision avoidance manoeuvres with respect to revolution before event

requirement	ΔV **[m/s]**	**20% margin** ΔV **[m/s]**
reentry	113.08	135,7
CAM	5	6
autonomous CAM testing	5	6
total	123.08	147.7

Table 11: Preliminary ΔV budget

Parameter	**EPSS-C1**	**CubeSat propulsion module**
mass [g]	1000	1410
dimensions [U]	1.3	1
power [mW]	9600	12500
I_{sp} [s]	213	≥ 285
I_{tot} [Ns]	400	≥ 850
thrust [N]	1	0.35-1
technology	monoprop. ADN-based	biprop. N2O and C3H6
TRL	7	8
company	NanoAvionics [89]	Dawn Aerospace [90]

Table 12: Possible CubeSat engine and their characteristics

Some possible alternatives are a mono-propellant Ammonium Dinitramide (ADN)-based motor of NanoAvionics specifically designed for CubeSats, and a bipropellant engine of DawnAerospace. Table 12 summarise the main engine characteristics and performance. The objective is to choose a small and light system with 150 m/s ΔV capabilities.

6.3 Attitude Determination and Control system

The attitude determination and control system should be able to keep the velocity pointing of the spacecraft during the science phase with a required accuracy of 1° deg, and to guarantee a quick 90° deg slew manoeuvre to ensure collision avoidance capability even if a radial firing is needed. The minimum slew velocity for the aim is set in order to obtain the 90° deg slew in at least one quarter of orbit revolution. For the selected orbit, this results to a angular velocity of 1.09e-3 rad/s. At the end of the mission, during the reentry, the spacecraft should not tumble and it should keep a velocity pointing attitude to perform the reentry analysis phase. This is the most demanding phase for the attitude control system, and an analysis should be done to assess whether the on-board actuator could maintain the attitude control for the satellite up to 100 km of altitude.
The attitude component selection takes as baseline the attitude control system of ARMADILLO [91], a 3U CubeSat with a similar payload dedicated to LEO debris analysis, adapting it the performance demand of a 12 U satellite, which has an higher inertia, and the peculiar reentry environment. The system utilises a set of 3 gyroscopes, two sun sensors, and a magnetometer for basic attitude determination. An external star tracker provides a more accurate attitude determination. A set of 3 reaction wheels is used for three-axis attitude control of the spacecraft. To satisfy the mission attitude requirements, as attitude sensors a preliminary selection of three to six sun sensors, placed on different faces to keep the Sun in the field of view whatever the attitude and have a robust attitude determination system. Then 2 star trackers are selected for redundancy, together with three gyroscopes, one for every axis for angular velocity measurement, and a magnetometer to measure Earth magnetic field in body axes. A preliminary selection of possible off the shelf components is presented in table 13. The selection has been

Figure 43: D-Sense module. Credit: D-Orbit

made after a research on CubeSat off-the-shelf components, where the performance, dimensions, mass and power consumption of the instruments have been compared. The components selected are identified as baseline for the 12U CubeSat mission, but could be iterate during the phase A of the mission. The combination of sensors proposed are compliant with the pointing requirement accuracy for attitude determination. A different possibility could be the selection of a multi-sensor module for the attitude determination system. This allows to reduce the total mass and power consumption, thanks to a synergy system appositely assembled in a single optimised module. One example is the D-Orbit D-Sense [96], shown in figure 43, which is a multi-sensors module that has the capability to track the position of the Sun, the Earth's horizon, the magnetic field, and the angular rate of the spacecraft. It also includes a camera that can be used to take photos and videos, and operate as a star tracker. The instrument has its own microcontroller, and is fed by a single pair of power and data line, simplifying the design of the attitude system. The overall weight of the system is 0.2 kg for a dimension of 70x70x55 mm; the power consumption is 500 mW.
To control the spacecraft, a set of 4 reaction wheels has been considered, disposed one along each axis and one redundant wheel in the bisector of the three axes. Since the off-the-shelf GOM wheels are in a pyramid configuration, this would require a custom configuration from GOM actuator. The reaction wheels are used to keep the pointing during the science phase and to perform the slew manoeuvre for the CAM. For wheels desaturation and spacecraft detumbling during LEOP, a set of two orthogonal magnetorquers and a cold gas thruster on the spare axis have been considered. Also for the actuators a proposed selection of instruments is presented in table 14. Reaction wheels can provide the pointing accuracy requirement even during the reentry phase, thanks to the high control moment they can provide to the spacecraft.

For the preliminary design of the attitude control system the CubeSat has been modelled as a parallelepiped with dimensions equal to the structural ones. The total

Sensor	**Mass [g]**	**Dimensions [mm]**	**Power [mW]**	**performance**	**Company**
NCSS-SA05 (Sun sensor)	5	33x11x6	10	update rate: $\leq$ 10 Hz ; $\geq$0.5° deg RMS error over FOV	NewSpace Systems [92]
ST200 (star tracker)	106	50x50x83	670	slew rate: 1°/s ; update rate: 5Hz ; accuracy pitch/yaw: 10 arcsec , roll: 70 arcsec	Berlin Space Technologies [93]
STIM202 (gyroscopes)	55	38.6x44.75x20	1500	125-1000 samples/s ; ARW 0.15 ; customisable filter on every axis	Sensonor [94]
NMRM-Bn25o485	85	99x43x17	750	update rate: $\geq$18 Hz ; $\geq$ 8nT noise density	NewSpace systems [95]

Table 13: Sensors selection for attitude determination system

parameter	**iMTQ (magnetorquer)**	**NanoTorque GSW-600**
mass [g]	196	940
dimensions [mm]	95.9x90x17	95x95x61.6
power [mW]	1200	2500 x wheel
torque	max dipole moment $0.2Am^2$	max torque 1.5 mNm
accuracy	actuation envelope error $\geq 5\%$	accuracy 0.5 rpm
characteristics	2 torque rod + 1 air core torquer	max momentum storage 19 mNms ; max wheel speed 6000 rpm
company	ISIS [97]	GOMspace [98]

Table 14: Actuators selection for attitude control system

weight of the spacecraft has been assumed as 10 kg, according to the final target weight. The inertia matrix has been computed considering a uniform mass density inside the spacecraft, therefore the result is a diagonal inertia matrix:

$$I = \begin{vmatrix} 0.1434 & 0 & 0 \\ 0 & 0.1434 & 0 \\ 0 & 0 & 0.08789 \end{vmatrix} kgm^2 \tag{6}$$

The attitude control system should provide velocity pointing of the debris payload, Sun pointing for solar panels and Earth pointing for the telecommunication system. To do that, a 3-axes control is needed. Since the CubeSat is in a low Earth orbit (see table 7), and the aim is to keep velocity pointing of the payload, a passive stabilisation configuration through gravity gradient is adopted. However, due to the small dimensions of the spacecraft, it is not enough to guarantee the pointing of the spacecraft, and active control shall be adopted. To have passive stabilisation in the local-vertical local-horizon frame, the axes of the spacecraft shall be directed as follow [99]:

- minor axis of inertia shall be directed along x axis of LVLH (radial direction)
- maximum axis of inertia shall be directed along z axis of LVLH (normal to the orbital plane)
- intermediate axis of inertia shall be directed along y axis of LVLH (velocity direction)

For this reason, the debris payload is placed in one of the four side panels of the CubeSat (2x3 unit) . A schematic image of the spacecraft desired attitude is shown in figure 44.

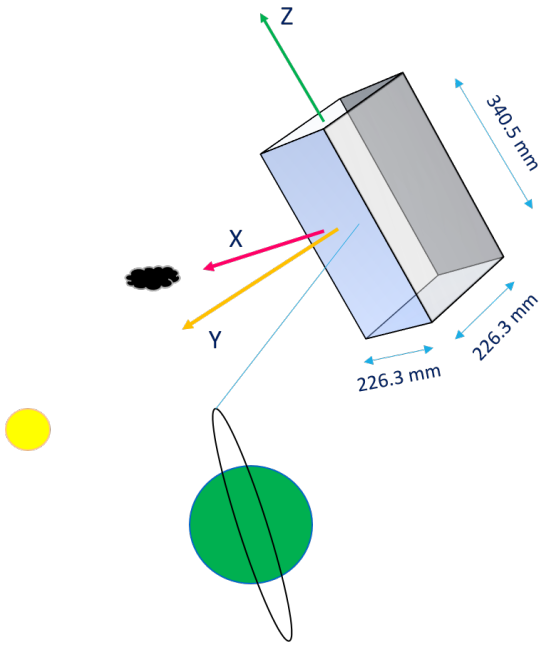

Figure 44: Desired attitude of the CubeSat during velocity pointing condition

6.3.1 Attitude and orbital dynamics model

To model the attitude dynamics of the spacecraft different perturbations have been considered:

- aerodynamic drag of the Earth atmosphere
- parasitic magnetic torque caused by Earth magnetic field
- radiation exposure (i.e. Solar radiation pressure, Earth infrared radiation), that is responsible for radiation pressure over the surfaces
- Earth gravity perturbations that cause gravity gradient on the spacecraft

In the simulation, the following approximation have been made; the Earth motion around the Sun is considered as a circular restricted two-body problem; the initial date is assumed to be the vernal equinox, thus at the beginning of the simulation the Earth and the Sun are aligned in the Vernal equinox axis. The motion of the spacecraft around Earth is a perturbed two-body problem, considering J2 and aerodynamic drag effects. To model the aerodynamic torque and the radiation pressure torque, the centre of pressure of the surface is set shifted 1 cm from the geometric centre.

The aerodynamic torque on the spacecraft is computed considering the aerodynamic force acting on each of the faces of the CubeSat, and the momentum harm is considered as the distance of the centre of pressure of the surface from the centre of mass of the satellite. Only the surfaces that directly face the velocity direction are considered in the

computation of the aerodynamic torque. Since all the surfaces are flat panels, all the drag coefficients are assumed equal $C_D = 2.4$. In equation form, the air drag momentum torque is computed as:

$$F_D = -\frac{1}{2} C_D \rho v_r^2 \frac{v_r}{\|v_r\|} (n_s \frac{v_r}{\|v_r\|}) A \tag{7}$$

where F_D is the aerodynamic force in Newton acting on the surface having normal n_s and area A, ρ is the air density computed with an exponential model (see section 5) and v_r is the relative velocity between the satellite and the atmosphere in body frame, computed as in equation 8, where Ω_E is the rotation vector of the Earth and r is the spacecraft position in inertial frame.

$$v_{rel} = v_{s/c} - \Omega_E \times r \tag{8}$$

This is done for the surfaces that are in the velocity direction, where the dot product between v_r and n_s is greater than zero. Then the aerodynamic moment with respect to the centre of mass is computed as:

$$M_D = \sum r \times F_D \tag{9}$$

where r is the distance between the centre of pressure of the surface and the centre of mass of the satellite in m, and M_D is expressed in Nm.

In LEO the spacecraft experiences a relatively strong magnetic field. It can be exploited to perform manoeuvres using magnetorquers, although it can be responsible for the generation of undesired torques on the satellite. For this reason it is important to model the Earth magnetic field to both predict the disturbances on-board the spacecraft and to have an on-board model to compute the control for the desired manoeuvre. For this purpose, the Earth magnetic field is hereby modelled using the magnetic dipole approximation. The Earth magnetic field can be approximated in the Earth inertial frame by a magnetic dipole model using equation 10 [70].

$$b_N = \frac{R^3 H_0}{r^3} [3(\hat{m} \cdot \hat{r})\hat{r} - \hat{m}] \tag{10}$$

Where b_N is the magnetic field in the inertial frame, R is the Earth equatorial radius equal to 6371.2 km, r is the position vector of the spacecraft in inertial frame, $\hat{m}$ is the unit vector along the dipole axis and $\hat{r}$ is the unit position vector. H_0 is a constant defined as

$$H_0 = \left((g_1^0)^2 + (g_1^1)^2 + (h_1^1)^2 \right)^{\frac{1}{2}} \tag{11}$$

where the Gaussian coefficients are taken from the international geomagnetic reference field, depending on time. For this analysis the 2020 coefficients of the NOAA database [100] have been taken into account. The interaction of the Earth magnetic field with the residual magnetic induction due to currents in the satellite determines the arise of a torque on the spacecraft. This torque can be modelled to approximate the real in-orbit disturbances using:

$$M = m \times b_B \tag{12}$$

where M is the undesired torque in Nm, m is the parasitic induction of the spacecraft, which for this case is considered equal to $\begin{bmatrix}0.1 & 0.1 & 0.1\end{bmatrix}^T$ Am^2 to represent the worst case scenario for a CubeSat, and b_B is the Earth magnetic field in body coordinates. It is computed rotating b_N by the attitude matrix $A_{B/N}$: $b_B = A_{B/N} b_N$.
There are three main sources of radiation pressure that act over the satellite surfaces [101]:

- direct solar radiation
- solar radiation reflected by the Earth
- Earth radiation

Part of the incoming radiation after illuminating the surface is absorbed, part is reflected specularly and part reflected with diffusion. To model this behaviour are defined 3 parameters, ρ_a, ρ_s, ρ_d respectively. These radiations generate a force on the surface illuminated, which resultant is positioned in the centre of pressure. The force for a flat surface of area A can be computed using equation 13 [70]:

$$F = -PA(\hat{S} \cdot \hat{n}_s)\Big[(1-\rho_s)\hat{S} + (2\rho_s(\hat{S} \cdot \hat{n}_s) + \frac{2}{3}\rho_d)\hat{n}_s\Big] \tag{13}$$

where P is the average pressure due to radiation, evaluated as the power per unit surface F_e divided by the speed of light c

$$P = \frac{F_e}{c} \tag{14}$$

$\hat{S}$ is the unit vector representing the direction of the source of the radiation in body coordinates and $\hat{n}_s$ is the normal to the surface. The coefficients of reflectivity and absorptivity depend on the type of the surface. At this design level common values for CubeSats have been taken into account, choosing $\rho_s = 0.5$ and $\rho_d = 0.1$ for the spacecraft body [70]. The force arises only over the surfaces directly illuminated by the source, so the torque is computed when $\hat{S} \cdot \hat{n}_s > 0$. In this case, the total torque acting on the satellite is computed as

$$T = \sum r \times F \tag{15}$$

where r is the distance from the centre of mass of the satellite and the centre of pressure of the surface. The power per unit surface depends on the distance from the source. At 600 km their values are around 1358 W/m^2 for solar radiation, 600 W/m^2 for the solar radiation reflected by the Earth and 150 W/m^2 for direct Earth radiation.

Earth gravity field acting on the satellite is not uniform, and this determines the onset of undesired torques on the spacecraft. This is true in particular for large satellites, but even for small CubeSats it is worth to take that into account if its effect over a long time is investigated. The torque generated by the elementary force f due to gravity acting on the elementary mass dm is:

$$dM = -r \times \frac{Gm_t dm}{\|R+r\|^3}(R+r) \tag{16}$$

where r is the distance of the infinitesimal mass from the centre of gravity, G is the gravity constant, m_t is the mass of the Earth and R is the radius of the orbit. After performing some computations and simplifications, and if it is considered the origin of the body reference frame centred in the centre of mass, it is possible to have the total momentum torque acting on the satellite in the form:

$$M = \frac{3Gm_t}{R^5} \int_B (r \cdot R)(r \times R) dm \tag{17}$$

To evaluate the effect of the torque on the satellite dynamic, this has to be evaluated in body fixed coordinates. To do that, R can be rotated as $R_B = \|R\| A_{B/L} \begin{bmatrix} 1 & 0 & 0 \end{bmatrix}^T$. This is equal to write $R_B = \|R\| \begin{bmatrix} c_1 & c_2 & c_3 \end{bmatrix}^T$ where $\begin{bmatrix} c_1 & c_2 & c_3 \end{bmatrix}^T$ is the first column vector of $A_{B/L}$. Performing the integration and expressing in body coordinates, the momentum torque on the spacecraft is then :

$$M = \frac{3Gm_t}{R^3} \begin{Bmatrix} (I_z - I_y)c_2c_3 \\ (I_x - I_z)c_1c_3 \\ (I_y - I_x)c_1c_2 \end{Bmatrix} \tag{18}$$

The total disturbance torque which the spacecraft is subjected to is then the sum of the previous torques. Figure 45 shows the total disturbance torque acting on the spacecraft orbiting at the 600 km Sun Synchronous orbit.

6.3.2 Nominal debris analysis phase

During debris analysis phase the attitude control system shall ensure velocity pointing of the debris payload, that is mounted on the CubeSat face with normal in the x-axis of the body frame, as shown in figure 44. The desired attitude matrix can be computed with the first row given by the velocity direction unit vector, the second row given by the cross vector product of the velocity direction unit vector and the inverse of Earth direction vector, and the third row is written as the cross vector product between the first and second row. In this way the spacecraft has one lateral face, the one with normal in x-axis direction in body frame, facing velocity direction, one lateral face that has coarse pointing in Sun direction and the bottom face, along z-axis of body frame, that is directed toward the Earth. The desired attitude matrix is reported in equation 19.

$$A_D = \begin{vmatrix} \hat{v} \\ \hat{v} \times \hat{r} \\ \hat{v} \times (\hat{v} \times \hat{r}) \end{vmatrix} \tag{19}$$

Where $\hat{v}$ is the unit vector in velocity direction and $\hat{r}$ is the unit position vector. It is possible also to define a desired angular velocity ω_D as:

$$\Omega_D = -\dot{A}_D \cdot A_D^T \tag{20}$$

$$\omega_D = \begin{vmatrix} -\Omega_D(2,3) & \Omega_D(1,3) & -\Omega_D(1,2) \end{vmatrix} \tag{21}$$

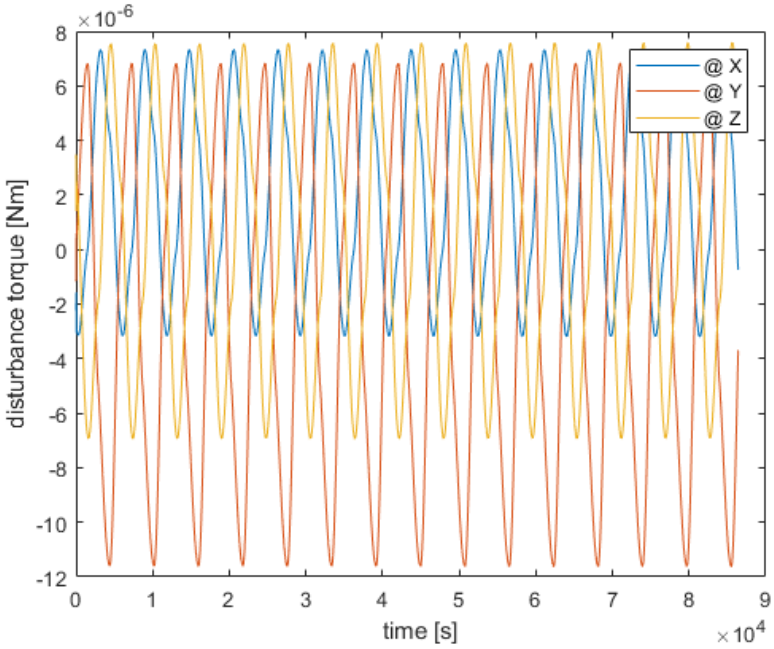

Figure 45: Disturbance torque acting on the spacecraft during 1 day of operation at nominal orbit. The torques are expressed in body axes.

A Matlab and Simulink model (shown in figure 46 as an example) has been appositely created to check the feasibility and the performance of the attitude control system. The simulation relies on the same orbital model used for the reentry analysis, coupled with attitude determination and control. All the instruments simulated in the model are set with the performance of the selected instrument reported in tables 13 and 14. The only actuators considered for the debris pointing analysis are the four reaction wheels disposed one along each body axis and one redundant wheel with same components along the three axes. The ideal control law chosen for the task is a proportional derivative control, taking into account the pointing error and the angular velocity of the spacecraft. The control law is then expressed as [70]:

$$u_{id} = -k_1\omega_e - k_2 A_{eV} + \omega \times (J\omega) + J(A_e\dot{\omega}_D - \Omega_e A_e \omega_D) \tag{22}$$

The error is computed through the error matrix, defined as the product between the attitude of the spacecraft and the desired attitude matrix.

$$A_e = A_{BN} \cdot A_D^T \tag{23}$$

A vectorial form of the error matrix is defined as:

$$A_{eV} = \begin{vmatrix} -A_{ediff}(2,3) & A_{ediff}(1,3) & -A_{ediff}(1,2) \end{vmatrix} \tag{24}$$

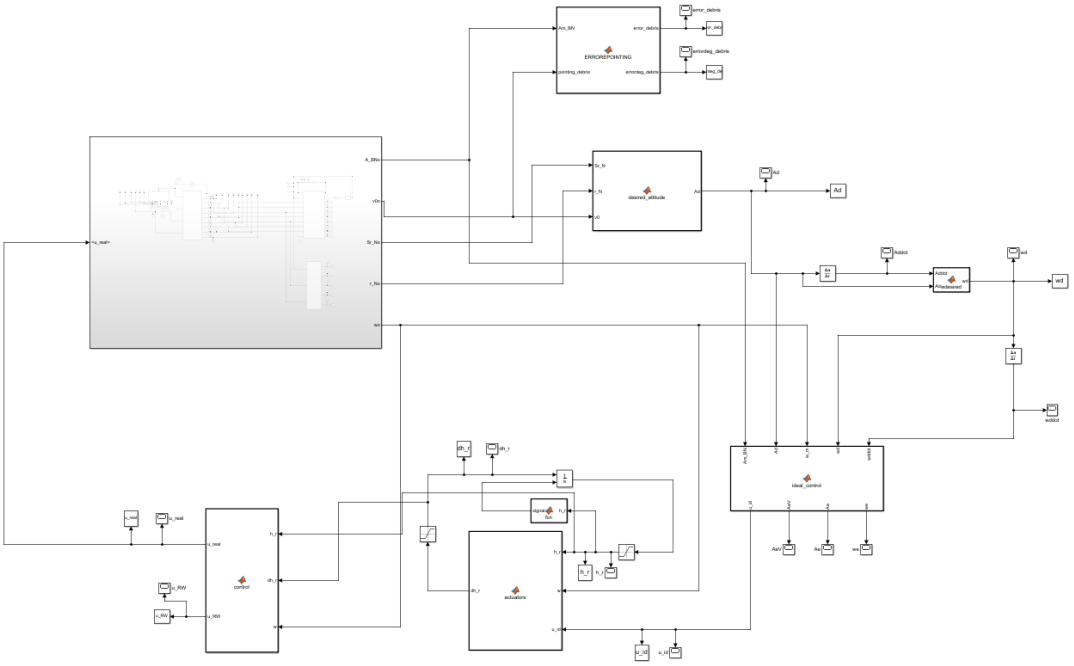

Figure 46: Simulink model for the reentry analysis phase

where A_{ediff} is computed as $A_{ediff} = A_e^T - A_e$. Finally, the angular velocity errors ω_e and Ω_e are:

$$\omega_e = \omega - A_e \omega_D \tag{25}$$

$$\Omega_e = \begin{vmatrix} 0 & -\omega_e(3) & \omega_e(2) \\ \omega_e(3) & 0 & -\omega_e(1) \\ -\omega_e(2) & \omega_e(1) & 0 \end{vmatrix} \tag{26}$$

Where J is the inertia matrix of the CubeSat and k_1 and k_2 are tuning parameters, that are taken equal to $k_1 = 0.1$ and $k_2 = k_1^2/2$. The ideal control law is then adapted to the actuators considered, giving the control law for the reaction wheels, that in this case is the control torque on the wheel. It is computed as:

$$\dot{h}_r = A^p[(Ah_r) \times \omega - u_{id}] \tag{27}$$

where A^p is the pseudo inverse of the reaction wheels configuration matrix. From the actuator control law, the real control torque acting on the spacecraft is computed taking into account the actuator dynamic, maximum torque and maximum momentum storage as:

$$u_{real} = -A\dot{h}_r + (Ah_r) \times \omega \tag{28}$$

The results show that the attitude control system can ensure pointing accuracy during

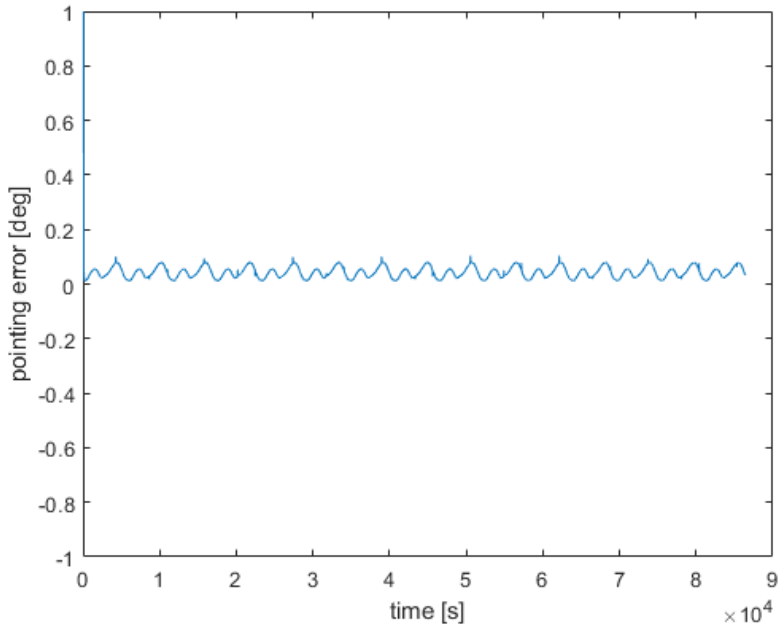

Figure 47: Pointing error during debris analysis phase for 1 day of operations.

the science phase with a smaller error than expressed in requirements, as shown in figure 47. The control torque necessary for this phase for every wheel, shown in figure 48a, is well under the maximum control torque (1.5 mNm) of the reaction wheels. In figure 48b is instead shown the resultant control moment acting on the spacecraft given by the four wheels.

6.3.3 Collision avoidance slew manoeuvre

To check the compliance of the attitude system with the collision avoidance manoeuvre requirement to perform a slew manoeuvre in less than a quarter of orbit a 90° deg slew manoeuvre is performed. The initial condition for the manoeuvre is the x face of the spacecraft in Earth pointing direction, and the target attitude is a pointing in the velocity direction. To do that, the same model and control algorithm previously described in section 6.3.2 have been used. In figures 49a, 49b, 50a and 50b the results of the analysis are shown.

The reaction wheels allow the spacecraft to perform the slew manoeuvre in less than 100 seconds. The maximum slew rate reached is 4 deg/s, figure 49a shows the variation of the angular velocity during the manoeuvre, and the smooth increasing and decreasing in the angular velocity of the spacecraft. This is very important to ensure the correct pointing once reached the desired direction, to avoid overshooting or chattering, that would delay the possibility to perform the collision avoidance manoeuvre. The collision avoidance manoeuvre slew requirement is then fully respected by the attitude system.

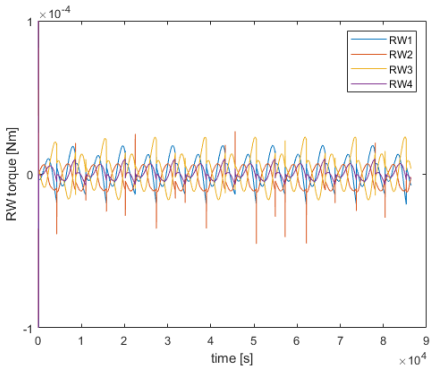

(a) Control torque for every reaction wheel.

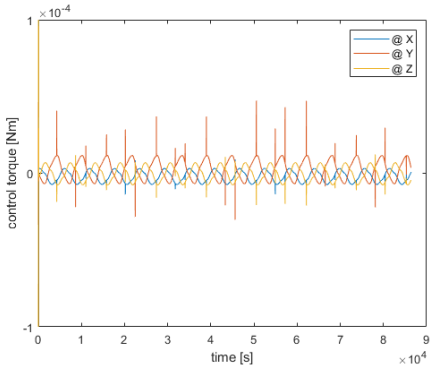

(b) Real control torque acting on the spacecraft given by the four reaction wheels.

Figure 48: Attitude control results for nominal debris analysis phase

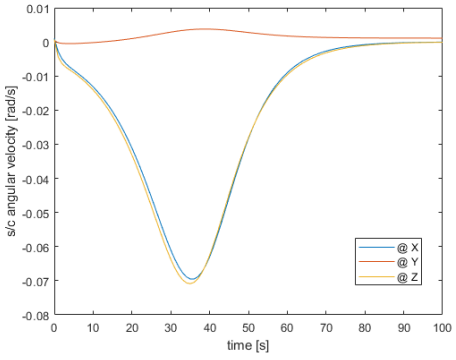

(a) Spacecraft angular velocity during slew manoeuvre.

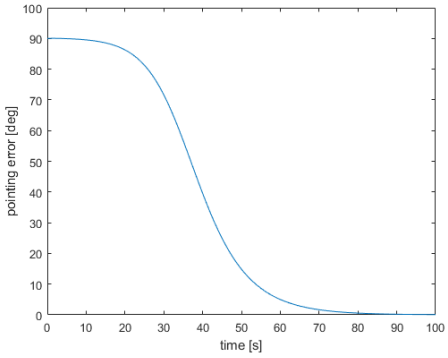

(b) Pointing error during slew manoeuvre.

Figure 49: Slew manoeuvre for CAM

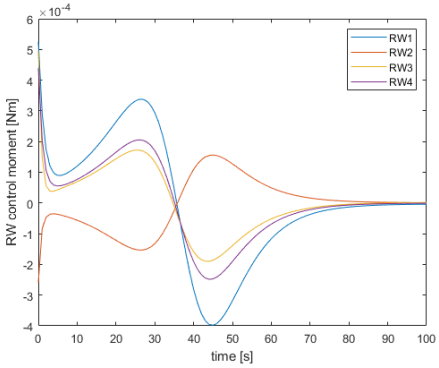

(a) Reaction wheels control moment for the slew manoeuvre.

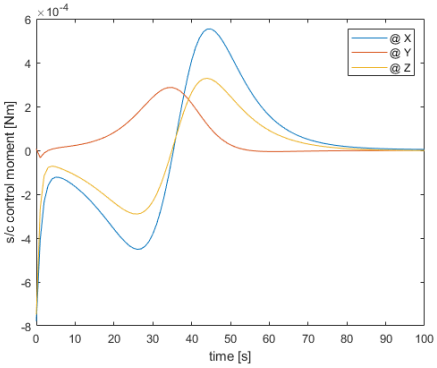

(b) Real control torque acting on the spacecraft during the slew manoeuvre.

Figure 50: Slew manoeuvre control for CAM

6.3.4 Reentry phase

To study the behaviour of the attitude control system during the reentry phase, a simulation of the orbital natural decay coupled with attitude control has been performed. The orbital model is the same model used for the reentry phase in section 5, and follows the orbit natural evolution from the elliptical orbit with apogee at 564.1 km and perigee at 199.1 km, after the last engine firing, until complete loss of control of the spacecraft, which occurs around 100 km. The orbital behaviour is the same described in section 5, with the same circularisation process and decay time. The attitude control system model is the same used for the attitude analysis of the debris science phase in section 6.3.2, with the same desired attitude matrix and control law. The velocity pointing has been chosen because the reentry analysis sensors need to be pointed in the velocity direction, and moreover it is not excluded that debris analysis can be protracted down to the reentry, furnishing valuable information even in the lower altitudes. Even in this case, only the reaction wheels are considered as actuators. At the beginning of the deorbit phase, no issues regarding the attitude control of the spacecraft arise. The attitude control system could balance the perturbations effects along all the orbit. The attitude behaviour of the spacecraft is shown in figures 51, 52a, 52b and 53 for the first part of the reentry phase. The results are expressed in body coordinates. From the plots of the simulation output the spacecraft is able to guarantee the pointing accuracy both at the apogee and at the perigee during the first part of the reentry.
When the spacecraft continue its descent toward reentry, at about 80/90 km altitude the atmosphere perturbations become so intense that the control system is no more able to react and the satellite starts tumbling with no control possibility. At this point, both science and communications become difficult or completely unfeasible, and the spacecraft continues its uncontrolled descent until break up and burning in the atmosphere occur. In figure 54 is reported the orbit evolution for the last days of reentry. The perigee altitude remains almost constant during all the reentry phase, and this is an advantage the

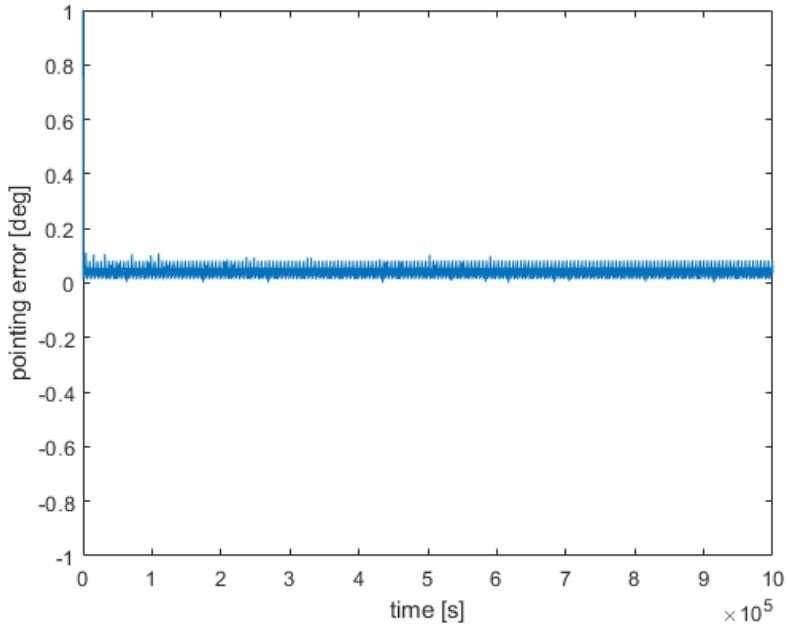

Figure 51: Pointing error during the reentry phase for the first 10 days

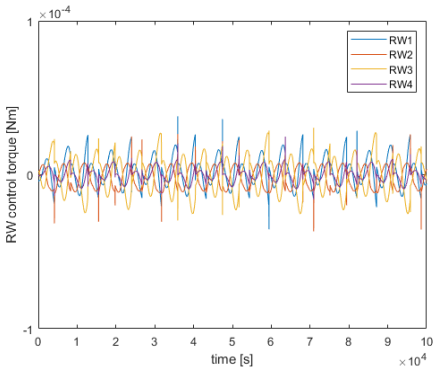

(a) Reaction wheels torque during the first day of reentry phase.

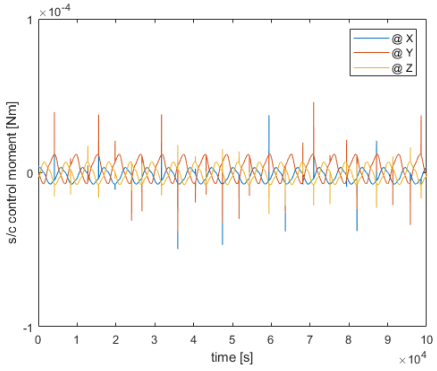

(b) Real control torque acting on the spacecraft during the first day of the reentry phase.

Figure 52: Reentry phase attitude control

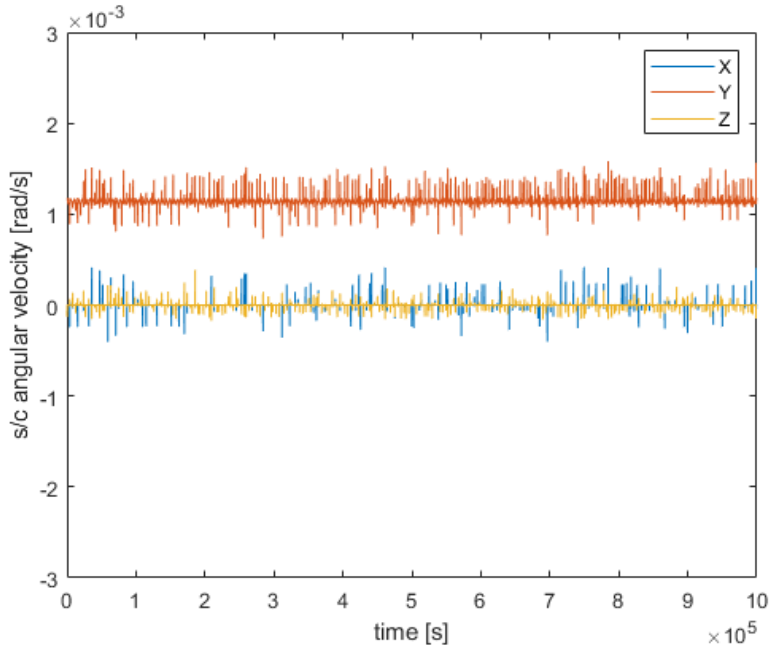

Figure 53: angular velocity of the spacecraft during the first 10 days of reentry phase

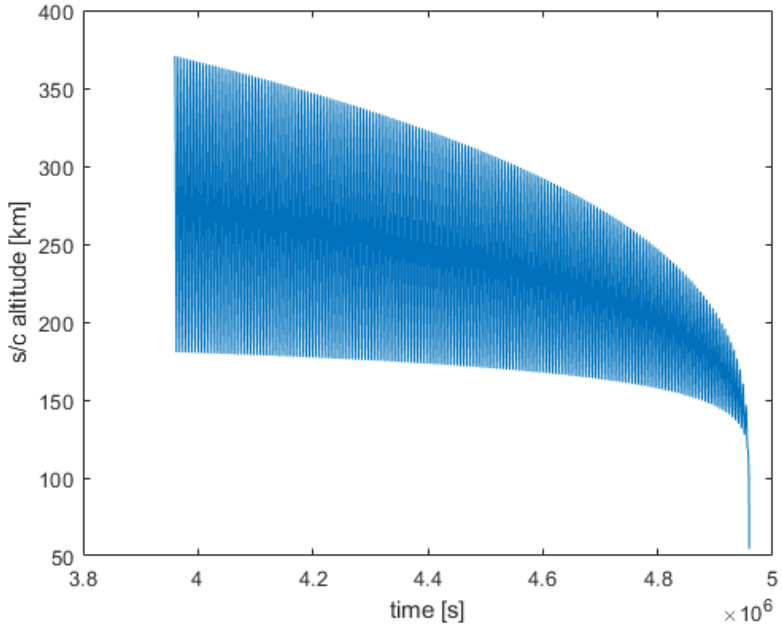

Figure 54: Orbit evolution during the last part of the reentry phase.

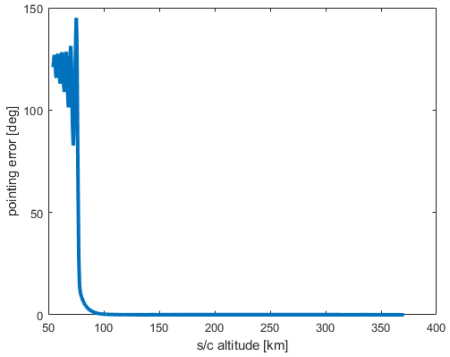

(a) Pointing error with respect to spacecraft altitude.

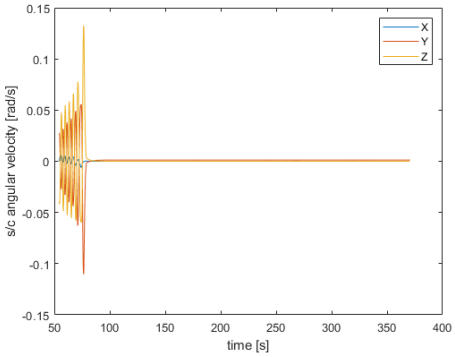

(b) Spacecraft angular velocity with respect to altitude.

Figure 55: Spacecraft attitude during the last phase of the reentry

attitude control which is not subjected to increasing atmospheric perturbations. Only when apogee decreases under the 200 km, the s/c re-enters in few days and the attitude is strongly affected by the drag perturbation, which causes the spacecraft tumbling, and the attitude is subjected to a strong effort. In figure 55a is plotted the pointing error with respect to spacecraft altitude, and in figure 55b is shown the spacecraft angular velocity depending on the altitude. The attitude control system maintain the spacecraft pointing until an altitude lower than 100 km. This is a positive result for the reentry phase science, which can extend its analysis range. Moreover, if pointing control can be ensured also under 100 km height, the telecommunication system can rely on pointing accuracy for the transmissions. In figure 56a and 56b the control torque of the reaction wheels and the control moment acting of the spacecraft is shown for the last part of the reentry phase, starting from $4 \cdot 10^6$ seconds until the reentry. As expected from the error and angular velocity results, under 100 km the reaction wheels are not able to give enough control moment to maintain the pointing attitude, since the maximum torque of the actuator is not enough to control it.

6.3.5 Reaction wheels desaturation

A preliminary design of the reaction wheels desaturation strategy has been carried out for the debris science phase and for the reentry phase. The deasaturation model has been implemented using Matlab and Simulink, adopting the same orbital and attitude model used for the pointing phase as in section 6.3.2. The objective of the simulation is to desaturate the reaction wheels keeping at the same time the velocity pointing attitude during the debris analysis phase. The ideal control law used is the same proportional derivative control based on angular velocity and attitude error used for regular pointing as shown in equation 22. A different actuation system is considered. The four reaction wheels are assumed completely saturated at the beginning of the simulation, hence it is not possible to rely on them. This is the worst case scenario, taken asbaseline for

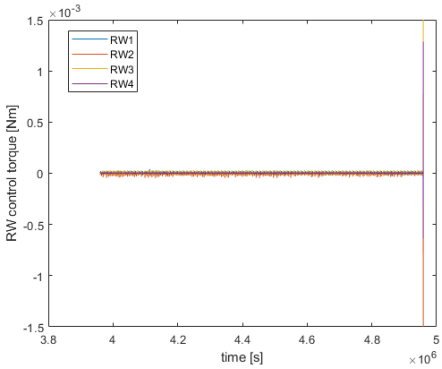

(a) Control torque for the reaction wheels during the last part of the reentry.

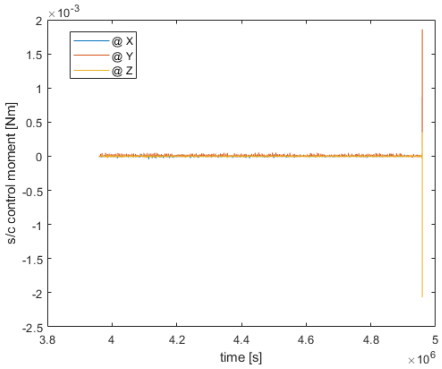

(b) Control moment acting on the spacecraft during the last part of the mission.

Figure 56: Attitude control during the last phase of the reentry

the design of the manoeuvre. During the simulation they are desaturated at a constant rate, all together or one at a time, depending on the desaturation strategy adopted, and the torque generated on the spacecraft by the reaction wheel desaturation is computed. The actuators chosen for the desaturation, that are the magnetorquers and the cold gas thruster, takes charge of balancing the known desaturation torque resulting from the reaction wheels deceleration, adding it to the ideal control law torque to keep the pointing accuracy required. The desaturation torque acting on the single reaction wheel is considered constant and computed as [70]:

$$\dot{h}_r = -M_{max} sign(h_r) \tag{29}$$

Where M_{max} is a constant appositely chosen to be compatible with the support actuators capability, in order to not give a torque that the other actuators can not counteract. The disturbance torque acting on the spacecraft is then computed using the reaction wheel control moment law:

$$u_{RW} = -A\dot{h}_r + (Ah_r \times \omega) \tag{30}$$

This torque is computed during the desaturation manoeuvre. The control law of the support actuators is given by $u = -u_{RW} + u_{id}$, where u_{id} is the ideal control moment to grant the pointing accuracy of the spacecraft. As first try only three orthogonal magnetorquer rods have been chosen to desaturate the reaction wheels. This approach did not provide good results to desaturate the four wheels at the same time, because three magnetorquer rods can not give three independent momentum torque around the 3-axis, so it was impossible to reproduce the ideal control law with the real control moment given by the magnetorquers, and the spacecraft started to tumble and completely lost the pointing direction. A second approach to cope with the limitation of the magnetorquers is to consider a configuration with two magnetorquer rods, one aligned with x-axis and one along y-axis of the body frame, and a cold gas thruster actuator that gives momentum around the z-axis has been adopted. This configuration proved to be

an effective desaturation control strategy, being able to control the spacecraft during the desaturation, ensuring at the same time pointing accuracy if a low rate desaturation is performed. The magnetic dipole and the cold gas thruster torque are computed as [70]:

$$\begin{vmatrix} m_x \\ m_y \\ T \end{vmatrix} = \frac{1}{b_z} \begin{vmatrix} 0 & -1 & 0 \\ 1 & 0 & 0 \\ b_x & b_y & b_z \end{vmatrix} (-u_{RW} + u_{id}) \tag{31}$$

m_x and m_y are the magnetic dipole of the magnetorquers in the x and y-axis respectively, and T is the torque requested by the thruster in the z-axis. b is the magnetic field measured by the magnetometer in the body frame. The torque given by the thruster is available from the third row of the vector, and the torque given by the magnetorquer rods is given by:

$$u_m = m \times b \tag{32}$$

For the magnetorquers maximum momentum dipole and for the thruster maximum thrust and minimum impulse bit have been taken into account the performance of the iMTQ platform reported in table 14.

Desaturation during the Debris Analysis Phase. During the debris analysis phase at nominal altitude, the saturation process of the reaction wheels is shown in figure 57 for one day of operations. During the simulation, once a reaction wheel reached saturation, instant desaturation has been considered. This however is a preliminary assumption, and should be verified with the desaturation time of every single wheel. For future investigations and more advanced design in the project phase, a combined control model and desaturation model shall be implemented. This result allows to make important considerations on the saturation process. First of all, it is important to notice the saturation frequency. Saturation of at least one wheel occurs every 1.2 hours, that is about once per orbit. This preliminary analysis on saturation of reaction wheels shows potential issues on the control itself, due to fast saturation. Specifically, the saturation and the control effort strongly depends on the control law tuning parameters k_1 and k_2. For future analyses, an optimisation on such parameters should be performed to optimise the control law. In particular it should be assessed whether a proper selection of k_1 and k_2 could relax the saturation time up to one event per day, for easier missions operations. Furthermore, it is unlikely that all the reaction wheels saturate together, and differential desaturation can be performed, since there is always a redundant wheel that can lean on the torque of the saturated wheel during its desaturation. However, the preliminary design has been carried out for the worst case scenario in which all the wheels are saturated at the same time. To desaturate the reaction wheels, three main strategy are proposed. As pointed out, for these simulations the starting point is to have all the four reaction wheels saturated at the same time in order to consider the worst case scenario. The first strategy is to desaturate the four wheels with a single manoeuvre. On the wheels a constant torque of 1e-5 Nm is applied for the desaturation. The manoeuvre is 1900 s long, about 31 minutes. In figure 58 the momentum storage of the wheels is shown. As expected, it decrease at a constant rate until complete desaturation.

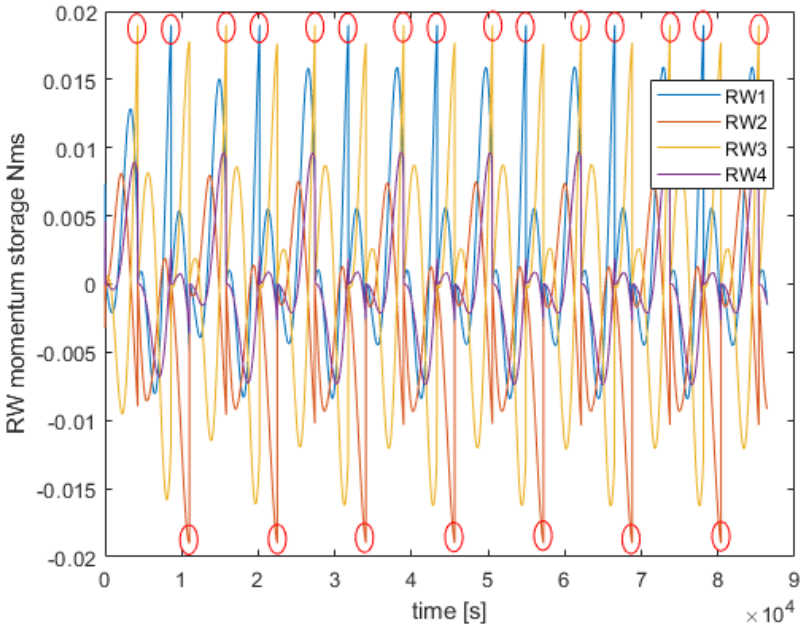

Figure 57: Reaction wheels momentum storage during debris analysis phase at nominal altitude

At the beginning of the manoeuvre, the spacecraft loses initially the velocity pointing accuracy required for the debris analysis phase, as shown in figure 59a. However, the control and the pointing accuracy is reconstituted before the end of the desaturation, at about 1400 seconds as shown in figure 59b. The maximum pointing error during the desaturation is less than 35° deg, and the debris analysis can still be performed, even with a reduction in the performances.

The magnetorquers and thruster control moment necessary for the manoeuvre is shown in figure 60. To accomplish the task, with a simple analog to digital conversion for the thruster actuation, a first approximation of the number of impulses required for the manoeuvre and the total firing time has been computed. The conversion takes into account the minimum impulse bit, the maximum and minimum thrust multiplied by the half of the distance from the centre of mass, taken as 0.2263/2 m. The algorithm compute the required thrust and the firing time by weighting the ideal control moment with the ideal firing time, in order to reach the same impulse level, as shown in equation 33.

$$\Delta t_{ON} = \frac{u_{cont,i}\Delta t}{F} \tag{33}$$

Where $u_{cont,i}$ is the continuous control, and F is the thrust given by the thruster. The result is that for the manoeuvre 751 impulses are needed, with a total firing time of 10.65 seconds. The second strategy considered wants to reduce the desaturation time. To do that, only one wheel at a time is desaturated, but at a faster rate. The desaturation

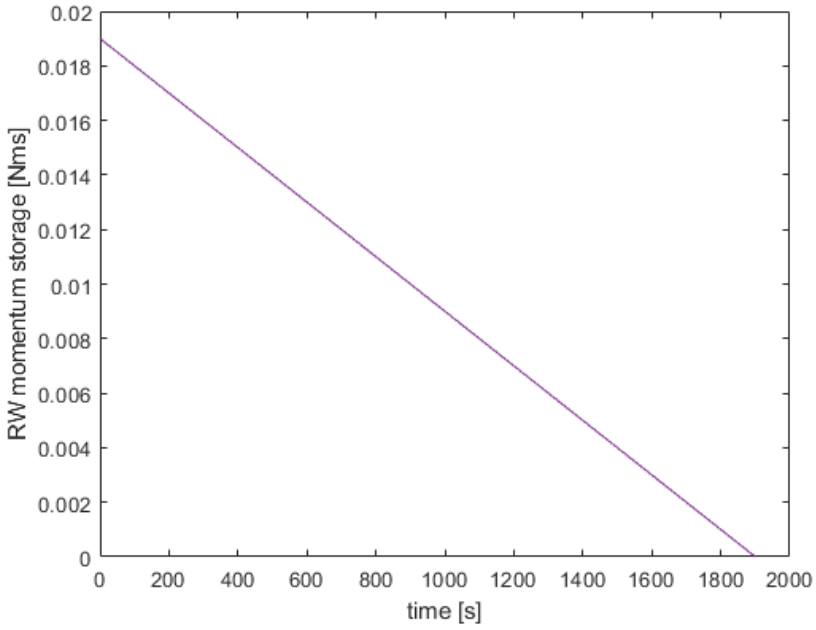

Figure 58: Reaction wheels momentum storage during desaturation strategy 1

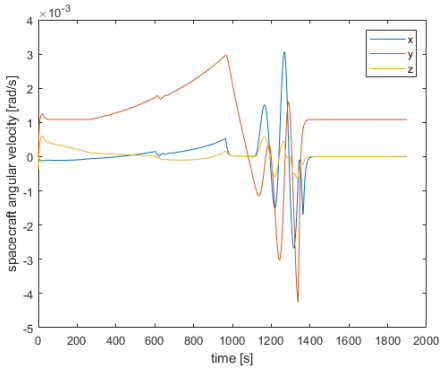

(a) Spacecraft angular velocity during desaturation strategy 1.

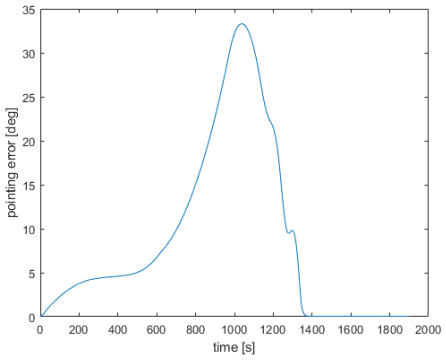

(b) Pointing error during desaturation strategy 1.

Figure 59: Spacecraft attitude during wheel desaturation strategy 1

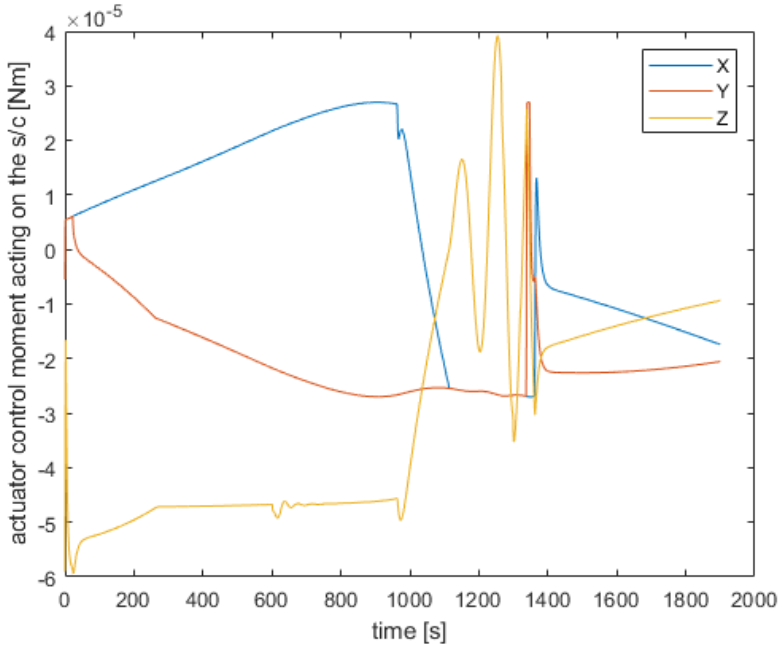

Figure 60: Magnetorquers and thruster control moment during desaturation strategy 1

torque acting on the wheel is set as 1e-4 Nm, therefore to completely desaturate the wheel only 190 seconds are needed, about 3 minutes. In figure 61 the pointing errors corresponding to the desaturation of the four wheels are reported. In this case, the actuators are not fully able to counteract the torque generated by the reaction wheel. The pointing error remains restrained under 40° deg, and once the reaction wheel is desaturated is straightforward to restore the spacecraft pointing, considering also the fact that simultaneously saturation of the wheels does not happen. In figures 62a and 62b are reported as an example the momentum storage, the control moment of the actuators and the angular velocity of the spacecraft during the desaturation of the fourth wheel, the one along the bisector of the 3-axes, representing the worst case scenario. During this manoeuvre the thruster shall perform 191 impulses for a total firing time of 12.27 seconds. Since the loss of pointing accuracy is caused by the poor control torque given by the magnetorquers, which is not able to counteract the reaction wheels desaturation torque, the last possibility identified for a fast desaturation manoeuvre relies on a custom magnetorquers rod, which are able to give 20 Am^2 of dipole moment. If such an actuator is mounted, it is possible to desaturate the 4 wheels all together with an applied torque of 1e-4 Nm. This would mean a complete desaturation in 3 minutes. Furthermore, thanks to the increased control authority of the enhanced magnetorquers, pointing accuracy is ensured during all the manoeuvre with a maximum error less than 8° deg, as illustrated in figure 63. This means that debris analysis can be performed during the manoeuvre. However, future project design shall perform further investigation and considerations on the power, mass and dimensions requirements of such an instrument, to check if the

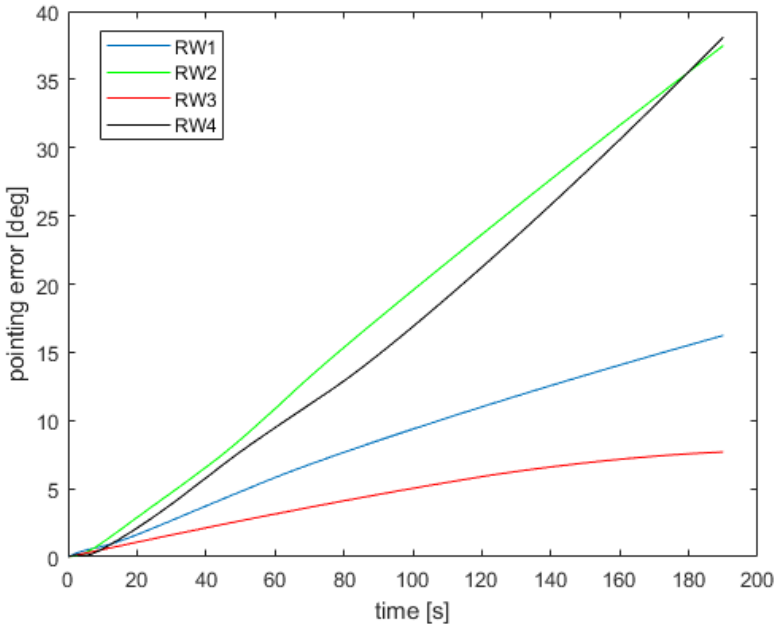

Figure 61: Pointing errors during second strategy reaction wheels desaturations

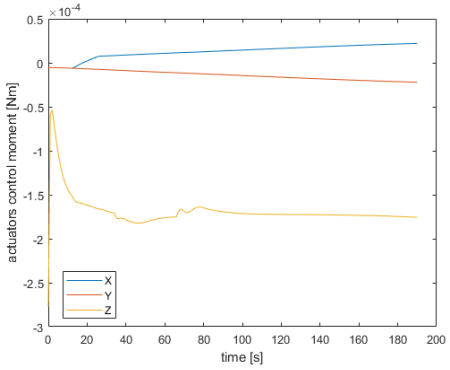

(a) Actuators control moment during reaction wheel 4 desaturation.

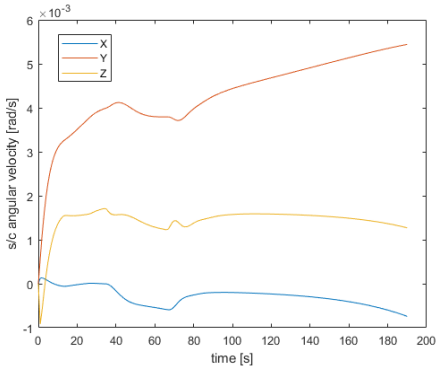

(b) Spacecraft angular velocity during wheel 4 desaturation.

Figure 62: Spacecraft attitude during wheel 4 desaturation.

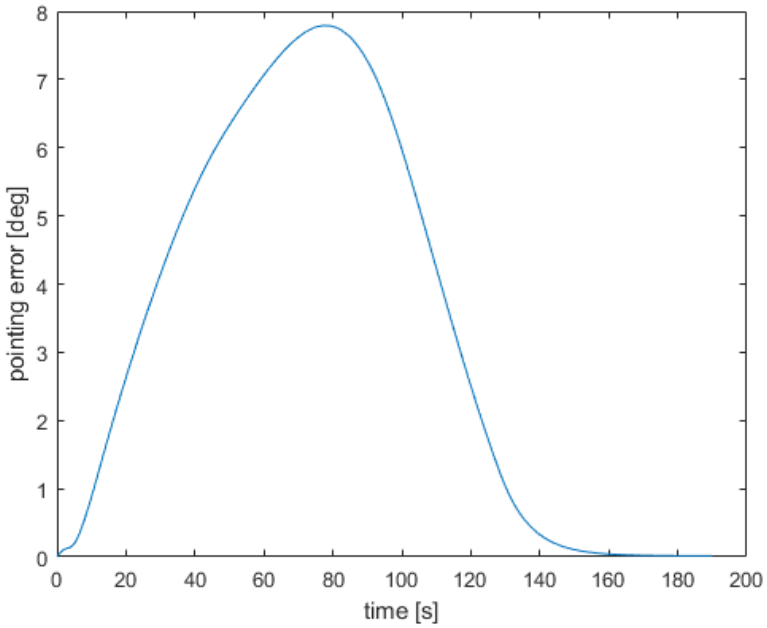

Figure 63: Pointing error during reaction wheels desaturation strategy 3

power system is able to ensure that amount of power and can fit into a 12 U satellite. In figures 64a and 64b the results of the simulation are reported. During this manoeuvre, the thruster performs 190 impulses for 6.88 seconds.

In table 15 a summary on the strategies used for reaction wheels desaturation during debris analysis is presented.

Desaturation during the Re-entry Analysis Phase. During the reentry phase the reaction wheels saturation occur with more frequency than the nominal debris analysis phase, due to the increase of the magnitude of the perturbations. The saturation frequency of the initial part of the reentry is shown in figure 65a. Same considerations made for the nominal debris analysis saturation are valid. In this case, saturation occur about every 1.14 h. No other differences are found with respect to the operative 600 km orbit.

For the last part of the reentry, when the orbit is lower and lays beneath 200 km altitude, the reaction wheels saturation frequency becomes more severe. Before reaching 100 km height, the reaction wheels saturate in 0.95 h, which means in little more than half an orbit. Approaching the Karman line at 100 km, which is a standard altitude taken as the convention for separation between space and atmosphere [102], the situation becomes even worse, and the saturation frequency becomes so high that would be impossible to keep the spacecraft control with such an actuation. The reaction wheels momentum storage and the spacecraft altitude are shown in figure 65b and 38 respectively.

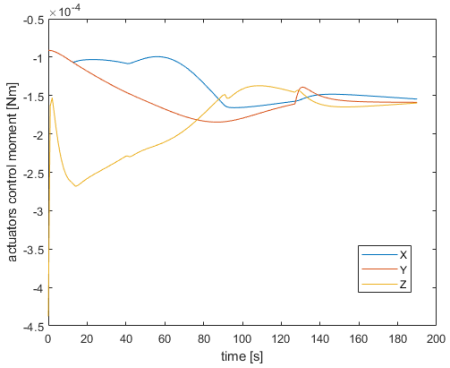

(a) Actuators control moment during reaction wheels desaturation strategy 3.

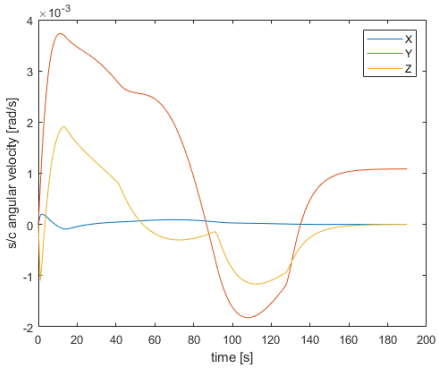

(b) Spacecraft angular velocity during reaction wheels desaturation strategy 3.

Figure 64: Spacecraft attitude during wheel desaturation strategy 3

strategy	**actuators**	**RW desaturated**	**max pointing error [deg]**	**desaturation time [s]**
1	0.2 Am^2 magnetorquers + 1 cold gas	4	35°	1900
2	0.2 Am^2 magnetorquers + 1 cold gas	1	40°	190
3	20 Am^2 magnetorquers + 1 cold gas	4	8°	190

Table 15: Reaction wheels desaturation strategies for debris analysis phase

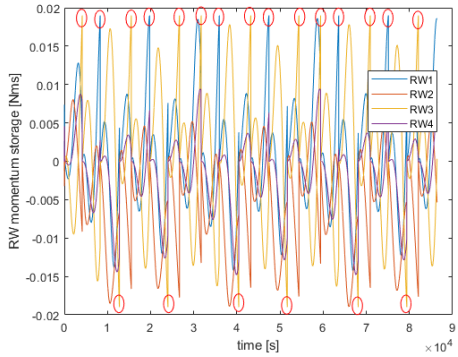

(a) Reaction wheels momentum storage during the first day of reentry phase.

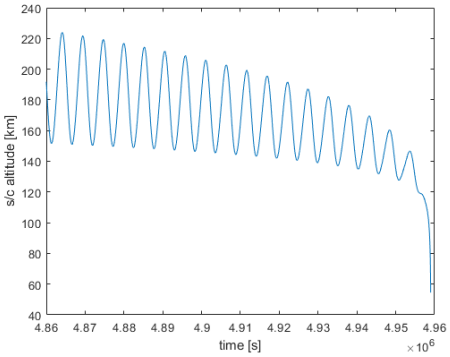

(b) Reaction wheels momentum storage during the last part of the reentry phase.

Figure 65: Reaction wheels momentum storage during reentry phase

The desaturation model is exactly the same as the one used for the debris analysis phase desaturation. In the preliminary design of the manouvre, two representative conditions have been analysed and compared. During the most part of the reentry phase the spacecraft flies at an altitude between 200 and 600 km, until the drag forces reduces the apogee height and proceed to orbit circularising. The first desaturation manoeuvre considered is performed at an altitude of 200 km, representing the worst case scenario for that part in terms of perturbations. After the lowering of the apogee, the spacecraft starts a constant descent until reentry. As worst case scenario, an altitude of 110 km has been considered as desaturation altitude for this last phase. For both the altitudes, the 3 alternatives presented before are investigated. The first strategy has proved more effective at 200 km than at 600 km, as seen from the pointing error for 200 km altitude in figure 66a. This is due to the fact that the magnetic field increases as altitude decreases, and the magnetorquers are more effective since, with the same dipole moment, they are able to generate more control torque. The pointing is lost only for 15 minutes, which is less than one quarter of orbital period, and for an angle lower than 15° deg. In figure 68a and 67a are reported the results for the relative spacecraft angular velocity and actuator control moment during the desaturation. For the manoeuvre, 500 impulses are required by the cold gas thruster, for a total operating time of 6.09 s.
Similar considerations can be made for the desaturation at 110 km. In figure 66b is shown the pointing error during this manoeuvre; it is very similar to the pointing error of the 200 km case. Similar results are obtained also for the actuator control moment and spacecraft angular velocity, respectively in figure 67b and 68b.

As for the desaturation during the debris analysis phase, a second strategy is investigated to reduce the manoeuvre time. The second strategy performed at 200 km gives a pointing errors very similar to the case at operative altitudes, with a maximum of 35° deg error for the fourth reaction wheel desaturation, which represents the worst case as in the previous case at operative altitude. Since higher torque is acting on the wheel

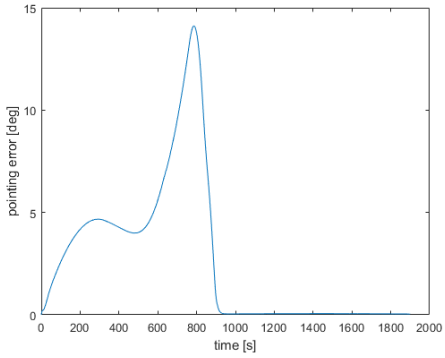

(a) Pointing error during first strategy desaturation manoeuvre at 200 km.

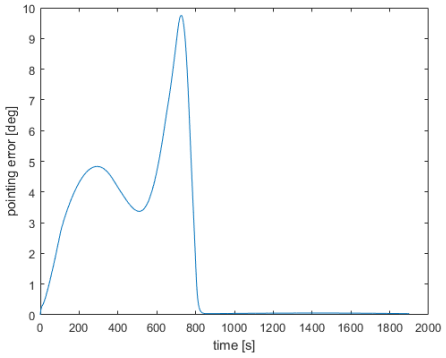

(b) Pointing error during first strategy desaturation manoeuvre at 110 km.

Figure 66: Pointing error during first strategy desaturation at reentry

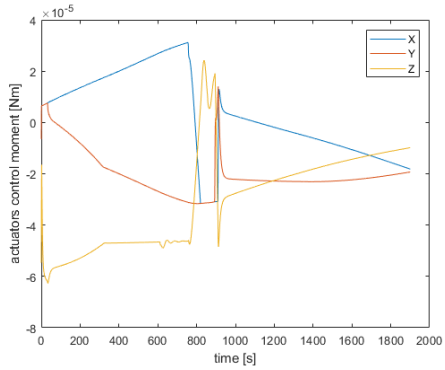

(a) Actuators control moment during first strategy desaturation manoeuvre at 200 km.

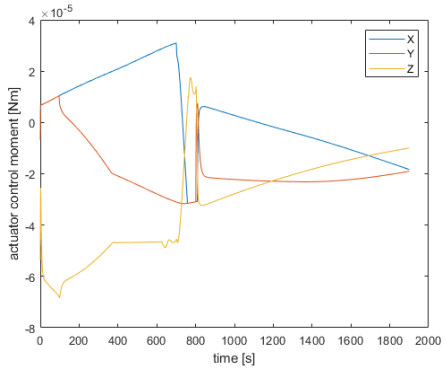

(b) Actuators control moment during first strategy desaturation manoeuvre at 110 km.

Figure 67: Actuators control moment during first strategy desaturation at reentry

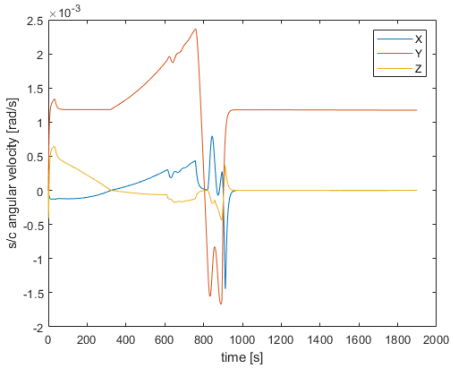

(a) Spacecraft angular velocity during first strategy desaturation manoeuvre at 200 km.

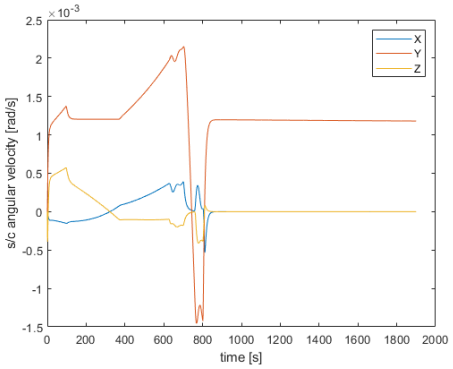

(b) Spacecraft angular velocity during first strategy desaturation manoeuvre at 110 km.

Figure 68: Spacecraft angular velocity during first strategy desaturation at reentry

for the desaturation, it is more demanding for the magnetorquers and thruster, and the spacecraft starts to tumble, however, the short duration of the manoeuvre allows to keep the error restrained, and a successive slew can easily restore the pointing. In figures 69a and 69b are reported the actuators control moment and the spacecraft angular velocity. The thruster shall produce 191 impulses with a total time of 11.8 seconds.

At 110 km this approach does not produce an efficient result as at 200 km. The increased level of aerodynamic perturbations make the spacecraft to start tumbling, and the actuators are not strong enough to avoid this. In figure 70 are shown the pointing error for the desaturation of the 4 wheels at 110 km altitude. The maximum error is registered for the desaturation of the third wheel, the one along the z body frame axis. An 180° deg error means a complete lack of control of the spacecraft, which is free to tumble under the action of the perturbances. The spacecraft angular velocity and actuators control moment are reported in figures 71a and 71b for this worst case. The actuators reach the maximum torque possible, and the angular velocity of the spacecraft keep increasing with no control. It is not possible then to control the spacecraft in this region with such a control architecture. The full-scale control is reached either for the magnetorquers and the cold gas thruster. The thruster performs 190 firings but for more than 40 second total duration. This is would be too demanding for the propellant mass. In this region then it is probable that the spacecraft would be uncontrollable once reaction wheels saturation is reached. This second strategy should then be excluded by the possible choice for wheel desaturation in very low orbit.

The last strategy investigated is the one with the enhanced magnetorquers. This however is a preliminary analysis, and the feasibility to equip the spacecraft with such an instrument shall be evaluated with further investigations. At 200 km height the strategy is very effective, keeping the attitude control in an error lower than 5° deg during all the manoeuvre, as shown in figure 72a. Actuator control moment and spacecraft angular velocity are shown respectively in figures 73a and 74a. To the thruster 191 impulses and

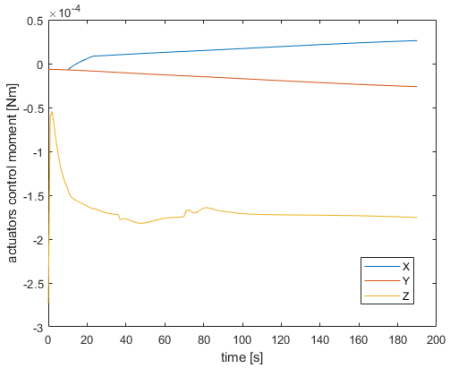

(a) Actuators control moment during wheel 4 desaturation at 200 km and second strategy considered.

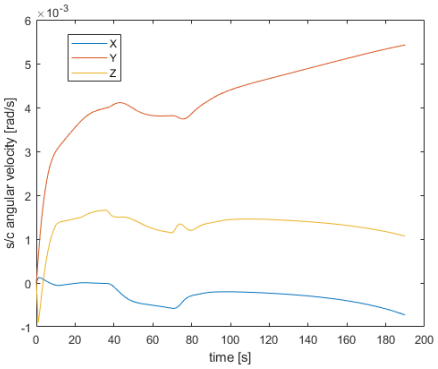

(b) Spacecraft angular velocity during fourth wheel desaturation for second strategy at 200 km.

Figure 69: Attitude control during fourth wheel desaturation for second strategy at 200 km.

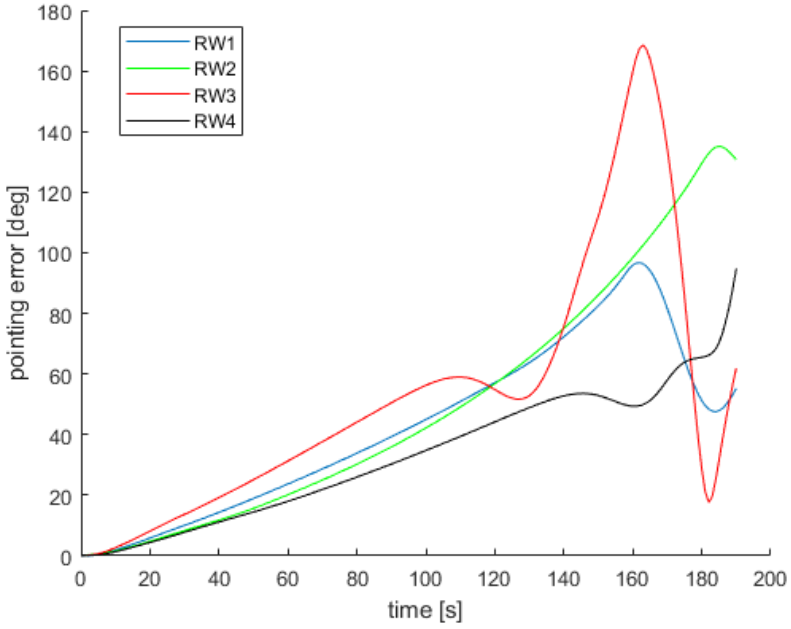

Figure 70: Pointing errors during the second strategy desaturation at 110 km

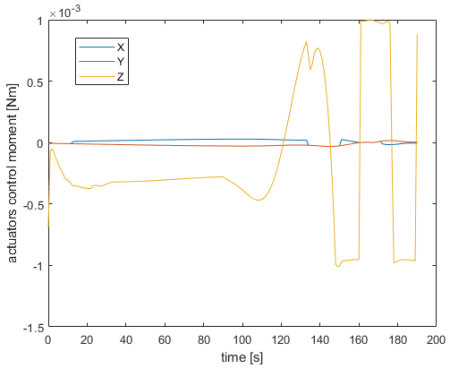

(a) Actuators control moment during wheel 3 desaturation at 110 km and second strategy considered.

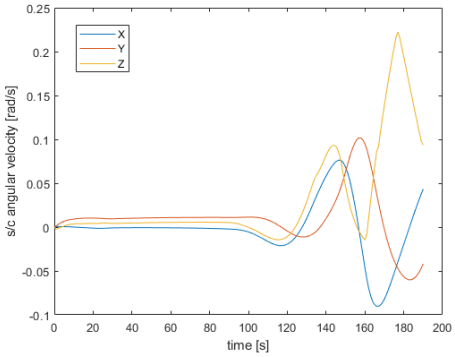

(b) Spacecraft angular velocity during third wheel desaturation for second strategy at 110 km.

Figure 71: Attitude control during third wheel desaturation for second strategy at 110 km.

42.8 total firing time are demanded. Even in this case, the propellant requirement can become too significant for a 10 kg CubeSat, and further investigation is needed.
For the same manoeuvre performed at 110 km, the augmented magnetic dipole of the magnetorquers determines even better pointing accuracy during the manoeuvre, as seen in figure 72b. The total control torque given by the actuators and the spacecraft angular velocities are shown in figure 73b and 74b. The thruster is requested to perform 191 impulses for a total firing time of 44.45 seconds. Event in this case, the thruster contribution can result in an high propellant mass requirement.

In table 16 a summary on the strategies used for reaction wheels desaturation during reentry analysis is presented.

Desaturation Analysis conclusions. Different desaturation scenarios have been evaluated. During the debris phase the main decision driver is the duration of the manoeuvre. If a long manoeuvre, in the order of thirty minutes, can be admitted, the first strategy is an affordable and effective way to perform the desaturation, without interrupting the debris analysis. However, without introducing too much penalty on the propellant requirement of the thruster, the second alternative allows a fast wheels desaturation, which is always preferable. The third possibility would be useless in the debris analysis phase, since the desaturation can be performed with cots magnetorquers, and the higher cost and power requirement for a custom magnetorquer rod is not justified by the improvement in performance at 100 km altitude. During the reentry phase the increasing magnetic field improve the magnetorquers control authority, but the longer manoeuvre is penalised by an high saturation frequency. Since at 200 km the combination of two magnetorquers and a thruster is able to grant pointing accuracy, a solution can be to use these actuators during all the lower part of the reentry. However, a further

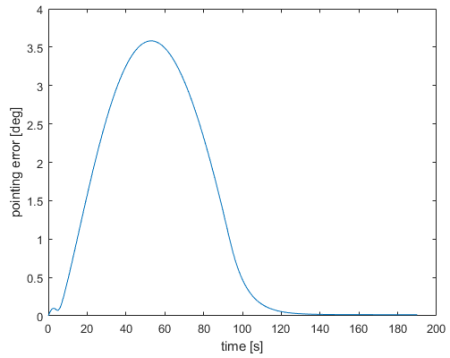

(a) Pointing error during the last desaturation strategy at 200 km.

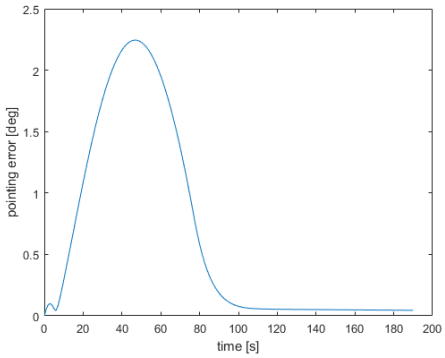

(b) Pointing error during the last desaturation strategy at 110 km.

Figure 72: Pointing error during the last desaturation strategy for reentry phase.

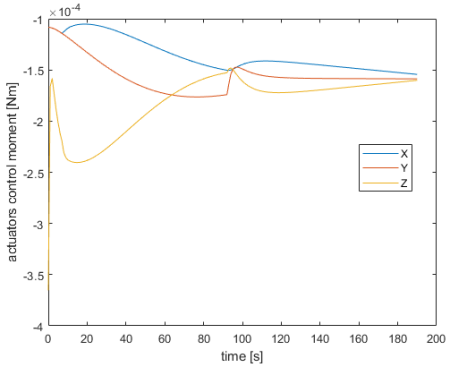

(a) Actuators control moment during the last desaturation strategy at 200 km.

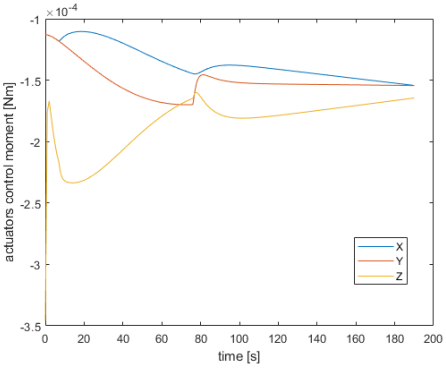

(b) Actuators control moment during the last desaturation strategy at 110 km.

Figure 73: Actuators control moment during the last desaturation strategy for reentry phase.

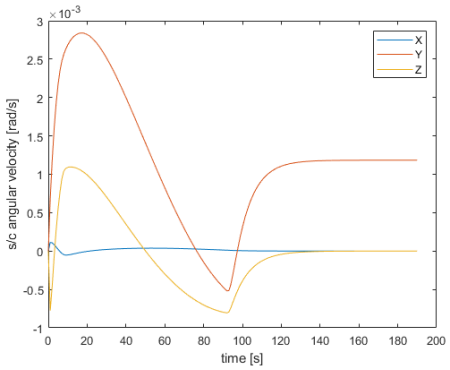

(a) Spacecraft angular velocity during the last desaturation strategy at 200 km.

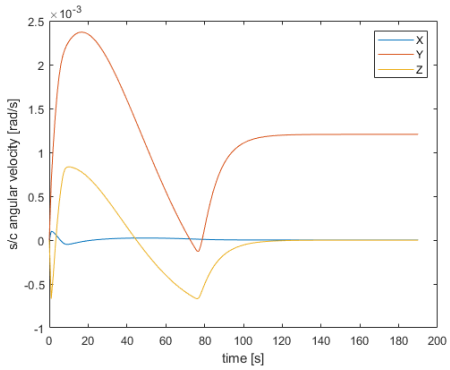

(b) Spacecraft angular velocity during the last desaturation strategy at 110 km.

Figure 74: Spacecraft angular velocity during the last desaturation strategy for reentry phase.

strategy	**actuators**	**RW desaturated**	**max pointing error [deg]**	**desaturation time [s]**
1	0.2 Am^2 magnetorquers + 1 cold gas	4	15°	1900
2	0.2 Am^2 magnetorquers + 1 cold gas	1	35° at 200 km ; 180° at 110 km	190
3	20 Am^2 magnetorquers + 1 cold gas	4	3.5°	190

Table 16: Reaction wheels desaturation strategies for reentry analysis phase

analysis should be performed to evaluate the power budget including such magnetometer, and the propellant budget including the delta-v needed to desaturate the reaction wheels. A synergistic combination of the reaction wheels and the other actuators if carefully designed could result in the best solution for the reentry phase attitude control, and this type of solution should be implemented in future works regarding this project. Once the spacecraft approaches to 100 km, the approach can no longer control the attitude of the spacecraft, because the magnetorquers and the thruster are no more able to counteract the disturbance torque given by the atmosphere. For this reason, if a controlled reentry until altitudes lower than 100 km is pursued, a more detailed analysis should be performed, including the trade-off on the enhanced magnetometer. Further problems for this last case can arise from the propellant mass budget of the cold gas thruster, which can exceed the CubeSat weight requirements. In this thesis has been demonstrated the possibility to control the CubeSat in the nominal phases of the mission with the proposed system architecture; future analysis and models shall identify the optimum configuration for the lowest orbit altitudes, performing also a trade off on the target altitude to which the spacecraft shall have a controlled attitude.

6.4 Preliminary selection of platform subsystem components

For the non critical platform subsystems a preliminary component selection is presented, based on the currently available on the market. This thesis does not provide a detailed analysis for such subsystem, and thus they should be investigated in future works.

6.4.1 Position and Orbit Determination and Control

This subsystem includes all sensors and software necessary to control the spacecraft orbit. In the requirement discussion in section 3 is specified the need to determine satellite position and velocity with high accuracy, during the main phase of the mission to precisely check the autonomous CAM and assess the outcome of the manoeuvre, and during the reentry phase in order to collect reliable data on the orbit evolution and compare them with the predictions of the reentry models. A standard common approach to design the navigation system for satellite is to rely on GNSS antenna receiver, which can provide very accurate estimation of the satellite current position. The trade-off analysis on the component should be done considering the accuracy needed by the CAM algorithm. For the purpose, two GPS receiver are suggested, with related receiving patch antennas, and for redundancy two are then mounted. Possible selections for the GNSS transceivers and antenna components are listed in table 17; they all work with data from both GPS constellation and GALILEO constellation, and the LEO accuracy satisfies the mission requirements for CAM and reentry analysis phases.

For orbital control there are two alternatives: the first alternative consists in using the CAM engine to perform also orbital control manoeuvres. This requires adequate pointing of the spacecraft at the moment of the firing, with consequently interruption of the science phase. This is the best choice from the point of view of system mass

and compactness, but can results in poor manoeuvre efficiency [103]. Station keeping and perturbations rejection use very low thrust and usually requires firings in different directions during the mission. The second alternative is to use a dedicated propulsion system, as the one in table 17, made by multiple thrusters capable of very low thrust (0.1 N) specifically designed for CubeSat station keeping and attitude control; these thrusters indeed can be used also in aid of the attitude control system, for faster desaturation manoeuvres or during the lower reentry orbit, to allow even deeper controlled atmosphere descent. This however required further investigation to be assessed. At this point the mass and volume reduction deriving from the adoption of the first possibility is preferred, so in this thesis it is assumed to use the main propulsion system also for orbit control, but this selection should be investigated with further analysis on the mission profile.

6.4.2 Command and Data Handling

The command and data handing (C&DH) subsystem is made by all electronics and software used to receive and distribute commands and to store and forward payload data and spacecraft telemetry. The main drivers for the design of the subsystem are the instrument data interface, the processing requirements, the data storage volume and timing accuracy. A very preliminary selection on the possible OBC has been proposed, but further analysis would be needed to confirm whether the processing requirements from the payload are compatible with this selection. The component selection suggested in table 18 refers to a very preliminary data budget assessment. The ARMADILLO payload [2] has been taken as baseline for this preliminary analysis. It uses as microprocessor the Phytec phyCORE-LPC3250 SOM (System on a Module) [109], and a 2 SD memory card to collect payload data. The processors in table 18 have similar or even superior processor performance and have been chosen and their requirements are known.

6.4.3 Telemetry, Tracking and Command

Telemetry, tracking and command system (TT&C) is used to communicate with the ground or other spacecrafts. The TT&C major design drivers are the data rate and distance, the frequency, the ground station selection, and the duty cycle. As baseline, the TT&C architecture from similar CubeSat mission has been identified, but further analysis must be performed to trade-off the system with respect to the drivers. The most demanding phase of the mission from the data rate viewpoint is the reentry phase. The science payload collects data from both spacecraft and atmosphere, and the telecommunication system should be able to send the data to a visible ground station. During the re-entry phase the link time between the ground station and the CubeSat shall be carefully analysed. Furthermore, the high temperatures generated by the reentry in the atmosphere and the ionised gases could affect the communication with errors. To be sure to download the necessary data in a short period of time, transmissions in the X-band are considered [112], in order to improve the data transmission in a short time. The baseline transmitter, as in table 19, is able to a link rate up to 100 Mbps. The

Instrument	**mass [kg]**	**dim. [mm]**	**power [mW]**	**properties**	**provider**
GNSS200	0.003	20x14.5x3.1	165	accuracy: 8m , TBD m/s ; GPS+GAL	Hyperion Technologies [104]
SGR-Ligo	0.09	92x87x12	500	accuracy: 5m , 0.1 m/s , 100 nanosec ; GPS+GLO+GAL	Surrey Satellite Technology [105]
GNSS Patch	0.018	70x70x15	48	peak gain: 5.5 dBi ; signal gain up to 32.5 dB ; GPS+GAL	ISIS [106]
piPATCH-MAX	0.089	74x74x13	110	SNR: 50 ; GPS+GLO+GAL	SkyFox Labs [107]
Monopropellant Propulsion Module	1010	100x100x100	22000	liquid green propellant ; 0.1-1 N thrust ; 224 Isp ; 59 m/s ΔV	MOOG [108]

Table 17: PODC hardware selection

Parameter	**IMT-OBC**	**iOBC**
mass [g]	38	76
dimensions [mm]	96x90x10	96x90x12.4
power [mW]	300	400
characteristics	200 MHz ; freeRTOS (other option on demand)	400 MHz ; freeRTOS or KubOS Linux
memory	16 MB RAM (64 MB available) ; 64 MB Flash NOR memory ; 8 GB Flash NAND memory	64 MB SDRAM ; 1 MB code storage ; 256 kB critical data storage ; 2 SD cards data storage
company	IMT [110]	ISIS [111]

Table 18: C&DH hardware selection

spacecraft is also equipped with a VHF/UHF transceiver, for telemetry, tracking and low power consumption communications. Further analysis are needed to trade-off the subsystem drivers and identify the proper component architecture from the baseline.

6.4.4 Electric power system

The electric power system should generate and store power, as well as power distribution. Electric power is produced with a set of solar panels. The main driver for the design of solar arrays is the power consumption and the payload duty cycle. A first iteration on the solar panels area needed for the mission has been performed referring to the power budget reported in section 6.6; the peak power requested by the spacecraft occurs during CAM phase, and it is about 50 W. To satisfy such a request, by considering a cell efficiency of 30%, a cell area of 0.123 m^2 is needed. This would be possible only if deployable solar panels are used. If only body mounted solar panels are used, considering for example the Azur space solar cells [119], and two side of the spacecraft equipped with 16 cells per side, having each cell up to 1.15 W of peak power the resulting peak power generation for perpendicular Sun incidence on the panels would be of 36.8 W. If a 45° deg incidence angle with Sun rays is assumed, as shown in figure 75, the power generated reduces to 26.02 W [70]. To cover for peak power, a battery pack would be used. The mission indeed is a LEO Sun synchronous orbit, and the eclipse time is not a concern. During the CAM, that is the most demanding phase of the mission from the power point of view, is about 23.31 W. Considering 20 minutes of manoeuvre duration, a 1.2 battery conversion factor the capacity used from the battery is 9.32 Wh [70]. Considering a typical value of 15% of depth of discharge, the capacity required from the batteries results 62.26 Wh. A suggestion on the battery pack selection is the NanoPower BPX from GOMspace [121], which has a capacity of 77 Wh. Furthermore, it can be matched to the GOMspace NanoPower P60 system [122]; the complete system contains a P60 Dock motherboard and a combination of an Array Conditioning Unit (ACU) and Power Distribution Unit (PDU) daughterboards. The properties of the EPS hardware are reported in table 20.

Instrument	**mass [kg]**	**dimensions [mm]**	**power [mW]**	**properties**	**provider**
UHF/VHF transceiver	0.075	90x96x15	480-4000	TX: 435-438 MHz or 400.15-402 MHz ; other ranges on request ; RX: 145.8-146 MHz and 148-105.05 MHz ; 9.6 Kbps	ISIS [113]
Xlink	0.2	90x65x28	15000	TX: 8025-8500 MHz ; RX: 7145-7250 MHz ; downlink 25+ Mbps ; uplink: 64+ Kbps	IQ spacecom [114]
UHF Antenna III	0.085	-	-	Omnidirectional ; 435-438 MHz	EnduroSat [115]
Xpatch	0.0022	-	output power 4000	gain: 6dB ; HPBW: 74° deg ; 8025-8400 MHz	EnduroSat [116]
4x4Xpatch	0.053	-	output power 4000	8025-8400 MHz ; HPBW: 18° deg ; gain: 16 dB	EnduroSat [117]
smallsatxband	0.065	72.6x72.6x11	3000	8025-8400 MHz ; HPBW 40° deg ; gain: 11.5 dB	Anywaves [118]

Table 19: TT&C hardware selection

Instrument	**mass [kg]**	**dimensions [mm]**	**capacity [Wh]**	**properties**	**provider**
NanoPower BPX	0.5	93x86x41	77	Li-ion ; autonomous heater ; 33.6 V 1 motherboard, 1 ACU, 1 PDU ; 3	GOMspace [121]
NanoPower P60	0.191	90x96x12.3	-	configurable output voltages ; current and voltage measurement	GOMspace [122]

Table 20: EPS hardware selection

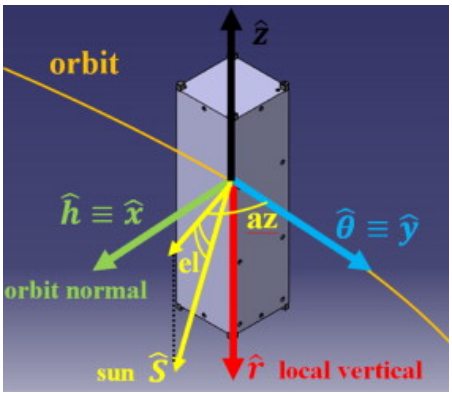

(a) Sun incidence angle on body mounted solar panels. Credit: [120]

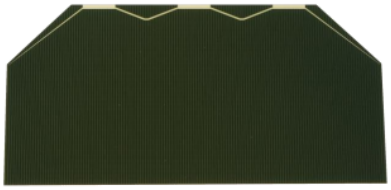

(b) Azur Space Quadruple Junction GaAs Solar Cell. Credit: Azur Space

Figure 75: Spacecraft solar array

6.5 Payloads

For every mission objective the CubeSat is equipped with a dedicated payload. The choice of the payload is made after evaluating different technologies and alternatives, based on literature research of the state of the art and similar missions. This thesis aims at providing a preliminary overview of possible payload technology to put on the CubeSat mission.

6.5.1 Debris analysis

The high level mission architecture choice for the debris analysis is in the detection method; the big distinction that can be made is between active debris detection through a dedicated sensor or passive debris detection. The latter is usually adopted when pieces of large satellites are retrieved at the end of life, and a statistical debris population analysis is assessed by studying the damages of the returned structures. One example of this procedure is the debris population study performed on the parts retrieved from the Hubble telescope [123] [124]. This method however gives only average values based on the orbit and lifetime of the spacecraft, and no precise analysis on the debris population can be done. Furthermore, to applied this method it is necessary to retrieve the spacecraft, and this would mean to have a structure that survives the reentry, with the need of an heavy thermal shielding and a controlled reentry, that would complicate the mission for no justifiable reasons. For these reasons, this method is discarded, and an in-situ active detection solution is sought. There are many different missions involving this type of payloads, and the technology working principle of the sensor can be of various type [7], for example:

- impact detectors
- acoustic sensor

- charged capacitors
- optical impact flash
- particle charge detectors
- laser curtains
- telescopic observation of reflected sunlight

Between these technologies, the most common are the impact detectors. They have been extensively used in many missions and with a variety of different configurations. One frequently used detector uses a polyvinylidene fluoride (PVDF) piezoelectric film as the impact target and detects the charge generated on the film from local impact depolarisation. A PVDF detector consists of a metal-coated and permanently polarized polyvinylidene fluoride film. When a micrometeorite or a debris impact the detector, a portion of the metal surface layer is removed and the debris penetrate in some of the permanently polarized PVDF dielectric material underneath. This generates a charge signal whose amplitude determines the magnitude of the impact [125] [126]. Because of their low demand on spacecraft resources PVDF films were used as dust detectors on a number of missions and spacecrafts, including Argos [127] and Stardust [128], Vega [129] or Cassini [42].
In the Earth environment, the Advanced Research and Global Observation Satellite (ARGOS) is equipped with the SPADUS instrument, which uses two arrays of PVDF dust sensors in a time of flight (TOF) arrangement that provides measurements of flux, velocity and trajectory of natural meteoroids in the order of 1e-9 kg, as well as space debris particles [130]. The SPADUS detectable particles mass range goes from 5e-11 g to 1e-5 g, which corresponds to a dimension range of 3.3 μm to 200 μm. The overall instrument mass 23.6 kg and the power consumption is 6.3 W.
The Cassini instrument, called the Cosmic Dust Analyser, is able to detect particles as small as 1e-6 m in diameter. When a dust particle enter the CDA, its charge, speed, size and direction are determined by the instrument. The instrument is also able to determine the particles composition, after the particle annihilates into smaller parts smashing into the instrument's detector. The CDA had two types of sensors: an high rate detector, used to study the Saturn's rings and to count the number of particles the instrument encounters, with a resolution of 10,000 particles per second; a dust analyser, with the form of a big bucket, as shown in figure 76, capable of detecting only one particle per second, but retrieving information on its charge, speed, flight direction, mass and chemical composition. The instrument's overall dimensions are 81 cm x 67 cm x 45 cm for a weight of 16.36 kg; the peak power is 18.38 W, and the data rate of the instrument is 0.524 kbits/s [42].
Highly reliable impact momentum sensors were realised with Giotto's Dust Impact Detection System (DIDSY) [131] in the dusty environment of Halley's comet. DIDSY employed various impact detection principles, most notably five piezoelectric crystals mounted at various positions of Giotto's 3 m^2 front and rear shields.

Figure 76: Cassini CDA instrument. Credit: NASA

The lander Philae, which is part of the Rosetta mission that landed on comet 67P/Churymov-Gerasimenko, was equipped with piezoelectric sensors on the Dust Impact Monitor (DIM) instrument [132]. The purpose of the DIM is to measure dust and ice particles released from the surface of the comet's nucleus. The DIM sensor detects a particle when it impacts the sensitive surface of the instrument. This creates an electric signal which amplitude and duration is analysed by the instrument's electronic system, determining the number of impacting particles, which means determining the flux, the rough distribution of their impact direction and the evolution of this parameters in time. Assuming plausible particle densities, the mass and velocity of the particles can also be derived. The instrument is specifically designed for detect dust particles ejected fro the comet, hence its detectable particle range goes from 0.2 mm to 5 mm radius, for a mass from 3e-8 kg to 5e-5 kg. The ejected particles velocity range is between 0.25 m/s and 2 m/s, so the impact energy is included in the range from 2e-9 J to 2e-5 J. The sensor has a total sensitive area of 70 cm^2. Onboard Rosetta orbiter, another dust impact instrument was present: the GIADA (Grain Impact Analyser and Dust Accumulator) instrument. It is aimed to analyse physical and dynamical properties of individual particles ejected by the nucleus and to monitor the dust flux and spatial distribution as a function of time. GIADA is composed of different modules: an optical detection system, to monitor the light scattered by single particles entering the instrument, an impact sensor, to detect the momentum carried by the particles, and five micro-balances, to measure the dust flux from different directions. The velocity of the particles can be determined by the time of flight when they cross the 100x100 mm^2 light curtain created by the optical instrument, composed by four laser diode. From the optical analysis, also information on particle size can be retrieved [133]. The IS is 100x100 mm^2 aluminium diaphragm (thickness = 0.5 mm) exposed to the dust impacts. When an impact occurs, an acoustic wave propagates along the plate, that is converted in electrical signals by five lead zirconate titanate ceramic piezoelectric (PZT) sensors (resonant frequency f = 200 kHz), placed below the centre and each corner of the plate. The output voltage depends, through the coefficient of restitution, on the momentum of the impinging particle [134].
A CubeSat scale impact dust detector is mounted aboard the ARMADILLO CubeSat. The instrument is a Piezoelectric Dust Detector (PDD); even if similar to previous cited impact detectors, the PDD is the first of its kind. The device indeed will gather in-situ sub-millimetre space particle data on a picosatellite with a mass of less than four kilograms. ARMADILLO is the first CubeSat mission dedicated to in-situ particles detection using a small impact payload [2]. In collaboration with UT-Austin, Baylor University's CASPER (the Center for Astrophysics, Space Physics and Engineering Research) has agreed to provide a space debris sensor to fly on picosatellite ARMADILLO as an experiment. The instrument fits within the CubeSat form factor and measures the velocity, impulse, and time of each impact, providing information about mass and size, frequency of occurrence, source (man-made or natural) and limited information on the direction of the particle based upon the known satellite attitude. The detection starts when a sub-millimetre size particle pass through two ionised mesh grids, the first grounded to the spacecraft and the second at a voltage of -100 V. The particle is detected when it

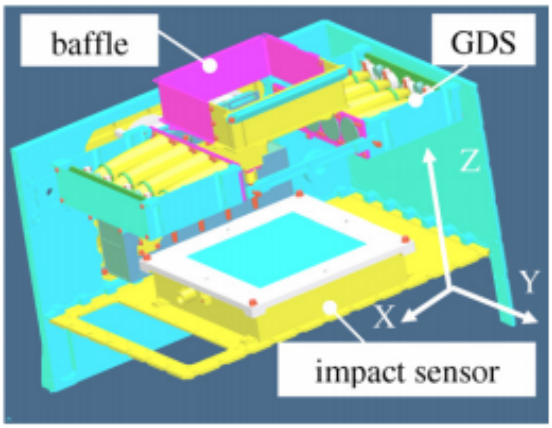

Figure 77: Internal configuration of GIADA instrument. Credit: Galileo Avionica

pass the second grid, because it forms a capacitor with the piezo plate. Once the particle pass through the second grid, it impacts the piezoelectric element on the base plate of the device, and this will create a plasma. The charges of the plasma are then separated within the capacitor, which creates a signal on the grid channel. The signal due to the deformation of the piezo plate is taken from the back electrode. Analysis of the signals of the grid and the piezo can return the mass, velocity and impact energy of the particle. Since the particles detected are in the sub-millimetre range, they disintegrate after the impact with the piezo element, avoiding an undesired particles accumulation on the instrument. After post process of the data, the PDD allow the reconstruction of source and nature of the impacting particles, whether man-made or natural [2]. The minimum energy that the PZT plates (STEMiNC piezo material SM410) [135] can sense is 100 nJ. If an impact velocity of 10 km/s is assumed, particles smaller than 1 μm in diameter would have an energy below 100 nJ, so most particles with a diameter smaller than 1 μm will not be able to be detected by the instrument. The PDD weighs 393 g for a total volume of less than 500 cm^3. The required power is 2.98 W and the estimated data rate is about 150 kB/day.
The impact detectors described have a strong limitation dictated by size. A new design of acoustic impact detector is proposed by Corsaro et al. [7], and is shown in figure 79 [7]; the instrument working principle consists in two thin membranes that are the impact targets, made of two thin polymer films adhered to support frameworks. The membranes have to be thin enough to not slow or disrupt the particles of interest that pass through the membrane. The impact on each membrane generates acoustic signals that are detected by a set of sensors located near the membrane edge. The signal is then analysed in order to identify the time and location of the impact on each membrane, from which the direction and velocity of the particle can be retrieved. The advantages of the dual membrane sensor are the low mass of the instrument, since the target area is a thin film and the possibility to fold and unfold the sensitive area membrane, allowing a stowed configuration for transport and then a large deployed area during operations. Thanks

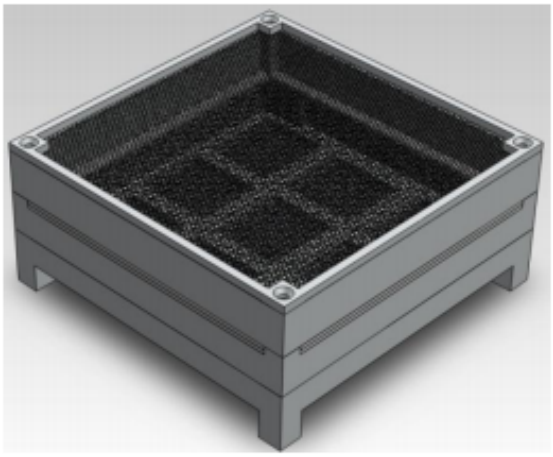

Figure 78: ARMADILLO Piezoelectric Dust Detector. Credit: UT-Austin [2]

to the folding configuration of the instrument, multiple units could also be stacked for transport and distributed to cover wider areas, with high improvement in science possibilities. Suitable membrane materials include Kapton and Mylar, which are readily available in thin films ranging from 2 to 100 μm. They have high tear strength, low creep, and are qualified for use in space. The instrument however is still at design and testing level, and has never flown. The acoustic challenge is to develop a sensor system capable of accurately measuring impact signals generated on large films by particles 50 μm in diameter or larger.
The US Naval Research Laboratory is developing an optical debris spotter since 2014. The sensor under development consists in a light source, for example a low power laser, that thanks to a conic mirror creates a light sheet in order to detect debris particles through the light scattered, reflected, transmitted and absorbed by the particle passing through the light sheet. A CCD camera detects the scattered light, registering the object passage through the light curtain. A continuous detection is ensured by the permanently illuminated light sheet. The instrument allows to retrieve the position of the intersection between the particle and the light sheet thanks to the knowledge of the light sheet geometry and the angles of the scattering event with respect to the camera that have been derived from the signal location on the sensor. Furthermore, even size and shape of the debris particle can be retrieved from the size and shape of the scattering event on the sensor. This concept, implemented with a low power laser, is expected to be able to detect debris passing by the spacecraft within a range of a few meters. The sensitive area of the instrument, formed by the light sheet, is mainly dependent on the light source intensity, size and scattering properties of the particles, and distance from the sensor [136]. The power required by the light source is estimated depending on the size of the debris to be detected: it would take a 1.25 mW output power source to detect a 1 cm particle at the distance of 1 m, or alternatively it would take a 12.5 W source to detect a 0.01 cm particle at the same distance. The instrument size of a

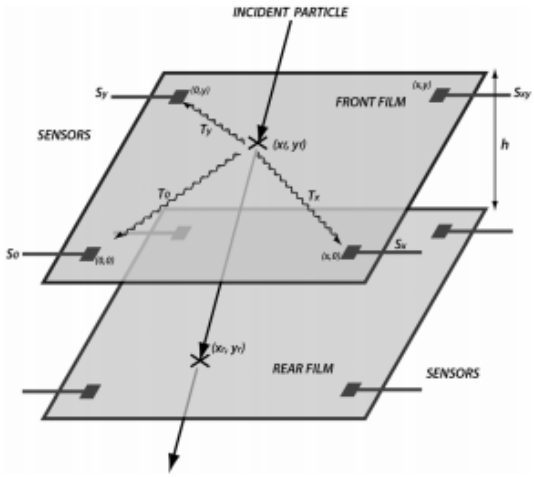

Figure 79: Illustration of the instrument concept. [7]

basic Optical Orbital Debris Spotter system is estimated to be approximately 10x10x20 cm in size, have a mass of approximately 2 kg, and a power consumption of about 10 W plus the light source power. The characteristics of this instrument, determined by a low size, weight and power requirements, give it great flexibility that allows development of modular or single devices for implementation into subsystems under development or rapidly deployable new spacecraft systems, or moreover as a secondary payload on a large mission [136]. When implemented on a dedicated nanosatellite or CubeSat, an optical orbital debris spotter unit could be considered disposable, permitting deployment of the system into otherwise highly risky, dense debris environments, enabling access to otherwise difficult to obtain debris field data.
As reported in section 2, the NASA ODPO has designe the DRAGONS instrument to fill the gap in knowledge for orbital debris population in the sub centimetre scale. The working principle of the instrument has been explained in section 2. The ODPO proposed DRAGONS to fly on the ISS as an external payload in 2013. The proposal was accepted in 2015, and the plan was to deploy from the ISS a 1 m^2 DRAGONS instrument in 2016 for a three year mission. The mission objective was a comprehensive system performance testing, resulting in a positive outcome. DRAGONS proved its ability to accurately measure particles velocity and direction ranging from 50 to 1000 μm in diameter. DRAGONS modular, inexpensive, and lightweight design enables it to be installed on most spacecraft in both LEO and GEO. It is one of the first technologies that enable the measurement of both particle velocity and angle of attack of MMOD.
In table 21 a summary of the baseline payloads is presented. ARMADILLO's PDD has been chosen between all other instruments as baseline payload for the mission. The payload is specifically designed for a CubeSat, with low power requirement, small dimensions and low weight, and moreover rely on flight proven technology. It allows to measure particles mass, size, source (man made or natural) and coarse direction. The optical and

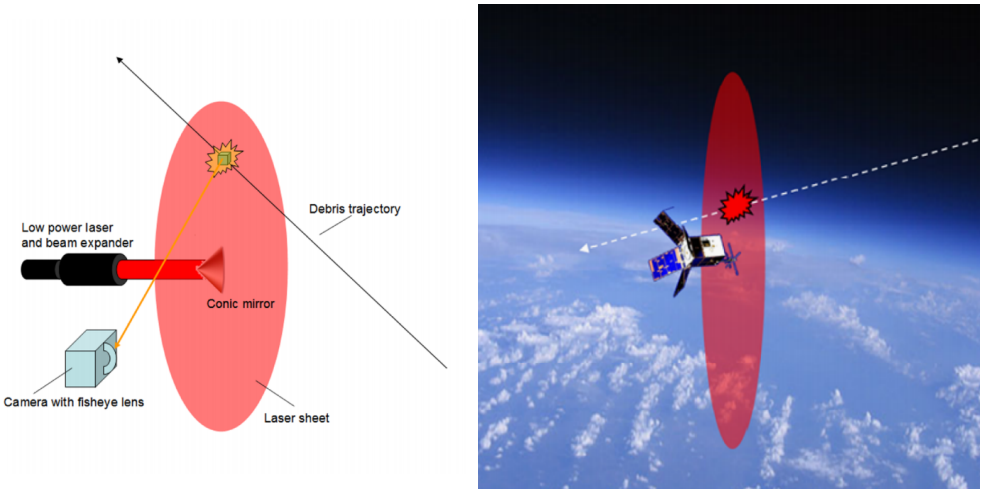

(a) Representative components for an optical orbital debris spotter

(b) Concept for employment of the orbital debris spotter

Figure 80: The NRL orbital debris spotter concept. Credit: Naval Research Laboratory

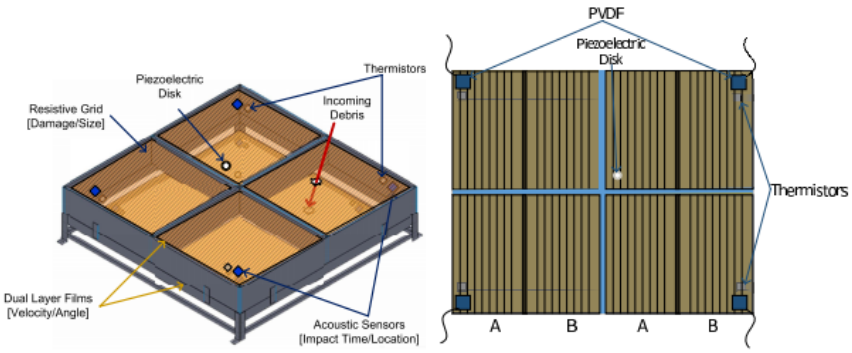

Figure 81: DRAGONS instrument sensor. Credit: NASA ODPO

Instrument	**mass [kg]**	**dimensions [mm]**	**power [mW]**	**data rate [kbits/s]**	**main characteristics**
SPADUS	23.6	-	6300	-	particle mass range: 5e-11 g - 1e-5 g ; particles dimension range: 3.3 μm - 200 μm ; information retrieved: flux, velocity, and trajectory
CDA	16.36	810 x 670 x 450	18380	0.524	information retrieved: charge, speed, flight direction, mass and chemical composition ; information retrieved: mass, velocity ; particles dimension range: 0.2 mm - 5 mm ; particles mass range 3e-8 kg - 5e-5 kg ; particles energy range: 2e-9 J - 2e-5 J ; sensitive area: 70 cm^2 information retrieved: flux, distribution ; composed by different modules: optical detection, impact sensor, micro-balances ; designed for CubeSats ; information retrieved: mass, size, source, direction ; minimum energy impact: 100 nJ ; minimum particles dimension 1 μm
DIM	-	-	-	-	
GIADA	-	-	-	-	
PDD	0.393	80x80x40	2980	150 kB/day	
acoustic detector	-	-	-	-	deployable ; large area possible ; light ; information retrieved: direction, velocity ; low TRL
optical detector	2	100x100x200	10000+	-	very wide area ; no impact needed ; information retrieved: size, shape
DRAGONS	-	-	-	-	1 m^2 sensitive area ; impact, acoustic, optical technology combined ; particles range: 50 μm - 1000 μm

Table 21: Debris payloads comparison

Instrument	**mass [kg]**	**dimensions [mm]**	**power [mW]**	**data rate [kB/day]**
CAM	0.08	96x90x15	400	20

Table 22: CAM payload characteristics

acoustic systems have high science potential, but their low TRL is not compatible with the concept of this thesis work, which is proposing a first mission to demonstrate the effectiveness of CubeSat science for orbit sustainability. Acoustic and optical detectors however shall be taken into account for future missions, to expand the science capability.

6.5.2 Collision Avoidance Manoeuvre

The collision avoidance manoeuvre payload will implement the algorithm developed at Politecnico di Milano by the COMPASS project [137] to compute via analytic instruments the best collision avoidance manoeuvre directly on-board the satellite. The inputs of the program are the information of the conjunction warning, which are the particle position and velocity and its uncertainties. The system then compute the optimum manoeuvre based on risk and propellant cost, an provide the command to the actuators, that perform the manoeuvre. It is based in machine learning algorithms, trained on ground with historical and synthetic CAM datasets. The CAM design module implements semi analytical models for the efficient computation of maximum deviation or minimum collision probability impulsive CAMs. The CAM algorithm is currently at TRL 4; a preliminary estimation on the payload parameters are based on the onboard computer performance, and are shown in table 22.
To perform the in-orbit tests a minimum ΔV of 5 m/s has been chosen, based on the preliminary analysis made with the DRAMA tool, in order to be able to perform at least three autonomous collision avoidance manoeuvre during the mission. The baseline for the CAM phase is to perform three CAM manoeuvre with a synthetic object, representative of three possible real scenarios for the missions.

6.5.3 Reentry analysis

To perform reentry analysis different alternatives have been evaluated, as reported in section 4. The chosen architecture is a reentry analysis performed using a sensor net on the spacecraft, for altitudes between 200 km and 100 km. To characterise the reentry environment and spacecraft response to aerodynamic loads, it is necessary to retrieve information on atmosphere density, aerodynamic loads on the spacecraft and structures heating and internal loads. The collected data are transmitted thanks to the telecommunication system previously presented. With these information a model of the reentry can be reproduced. The spacecraft should be able to retrieve information about atmosphere temperature, pressure, structures temperature and the acceleration acting on the satellite. Indeed, with the measurement of atmosphere temperature and pressure, after post processing the data, it is possible to elaborate the atmosphere density at different

altitudes through the ideal gas law. A direct measurement of the density would require an elaborated expensive payload, which is not suitable for a CubeSat mission, while temperature and pressure sensors are readily available on the market. A suggestion on pressure and temperature sensors is given in table 23, with the respective performance and characteristics.
To study the thermomechanical loads acting on the structure the spacecraft is equipped with inertial measurement units based on MEMS technology, to register the reentry accelerations, combined with temperature sensors and strain gauge to measure internal heat loads and displacements. Also in this case, a first guess on component selection is presented in table 23.
A first guess on the overall payload characteristic is presented in the last row of table 23, that can be used for preliminary budgets analysis.

6.6 Mission Budgets

A preliminary mass, power and ΔV budget has been assessed for the mission concept presented in this work. The ΔV budget has been presented in section 6.2. The target was to achieve a maximum of 150 m/s of required ΔV, and the computed marginalised ΔV is 147.7 m/s, which is in line to what expected. The mass target for the mission is 10 kg. The average subsystems mass distribution and relative percentage for a small satellite LEO mission with on-board propulsion capabilities [70] is shown in figure 82a. This values have been taken into account as key performance drivers of the subsystems design. If a single subsystem weighs more than what expected, it should be revised and modified to be compliant with the mission weight. The target weights are reported in figure 82b. The initial power estimated for the mission has been defined after a comparison on the literature with mission having a weight between 10 and 25 kg. The average is about 50 W, and has been taken as a reference value. However, this is not a real target or requirement to be respected. The driving parameter is to have a power budget that minimise deployable solar panels area, that would increase the exposed area during the debris analysis, increasing the risk, and would create issues during the reentry phase, augmenting the disturbance torque driven by the aerodynamic forces. The average power distribution percentage for small LEO spacecraft with on board propulsion is reported in figure 83 [70], and these values are taken as key performance drivers for the design of the subsystems as well as the mass distribution.

6.6.1 Mass budget

The preliminary mass budget considers the contribution from the preliminary analysis of each subsystem components. In table 24 the total mass of the subsystem components previously presented and the marginalised value are reported. In figure 84 a comparison between the target weight of the subsystem defined by literature and the weight of the preliminary design of the subsystems for the mission is presented. The main differences between the values are located in the propulsion system, attitude determination and control system, electric power system and payload. The high value of the propulsion

Instrument	**mass [kg]**	**dimensions [mm]**	**power [mW]**	**data rate [kbit/s]**	**measurement range**	**performance**	**company**
905 MicroPirani	0.009	-	220	-	1e-3 to 1e+5 [Pascal]	accuracy: 5%	MKS [138]
HFS-3	0.028	28.5x35.1x0.18	-	-	-200° to 150° C	two sensitivity levels	Omega [139]
ADIS16485	0.048	47x39.6x14	500	-	-5 g to 5 g	$\pm 0.05°$ orthogonal alignment error ; 6°/hr in-run bias stability ; $0.3°/\sqrt{hr}$ angular random walk ; 0.01% non linearity	Analog Devices [140]
overall reentry payload	≤ 0.5	95x95x80	5000	125	-	-	-

Table 23: Reentry payload characteristics

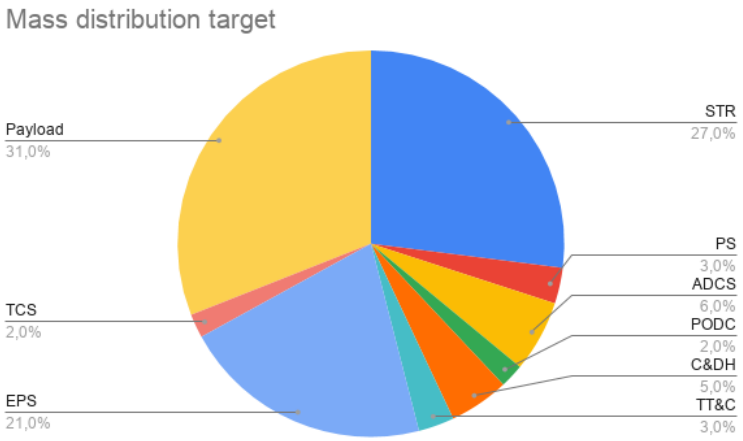

(a) Average mass distribution for small LEO spacecraft with propulsion [70]

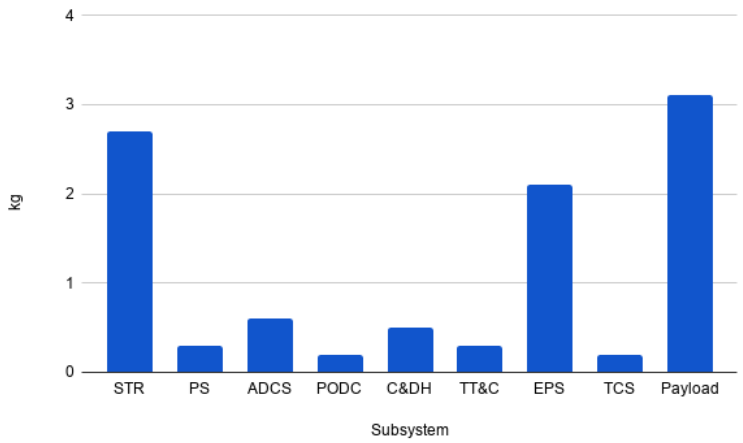

(b) Subsystems weight for a 10 kg spacecraft

Figure 82: Target subsystems weight

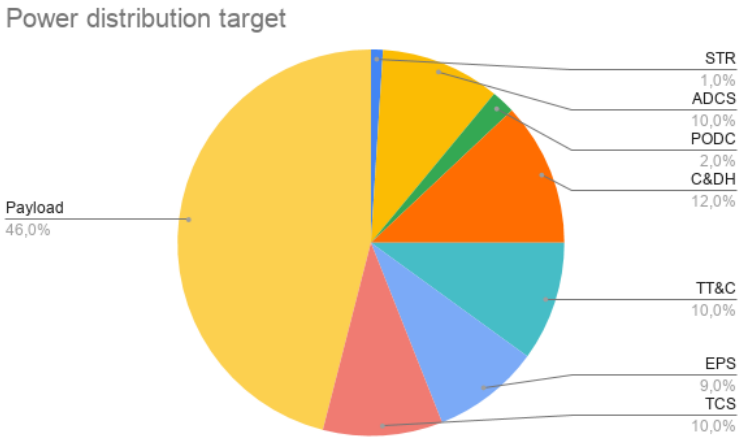

Figure 83: Average power distribution on small LEO spacecraft with on-board propulsion

Subsystem	**total mass [g]**	**total mass with 20% margin [g]**
STR	1750	2100
PS	1410	1692
ADCS	1392	1670.4
PODC	116	139.2
C&DH	76	91.2
TT&C	413	495.6
EPS	691	829.2
Payload	1008	1209.9
Total	**6856**	**8227.5**

Table 24: Mission preliminary mass budget

system mass for this mission is justified by the fact that the spacecraft has to perform a powered de-orbiting, hence the need to equip the spacecraft with a bigger propulsion system. Also for the attitude determination and control system case, the mission is particularly challenging from the attitude viewpoint, and this is reflected by the heavier hardware. Both the electric power system and Payload are instead underestimated. In both cases the design is still in a preliminary phase, and more detailed plans shall be carried out by future works.

6.6.2 Power budget

The power budget of the mission is again assembled on the power request of the subsystems components selection previously presented. In table 25 a summary of the power required by each subsystem is presented. To determine the power required to the EPS

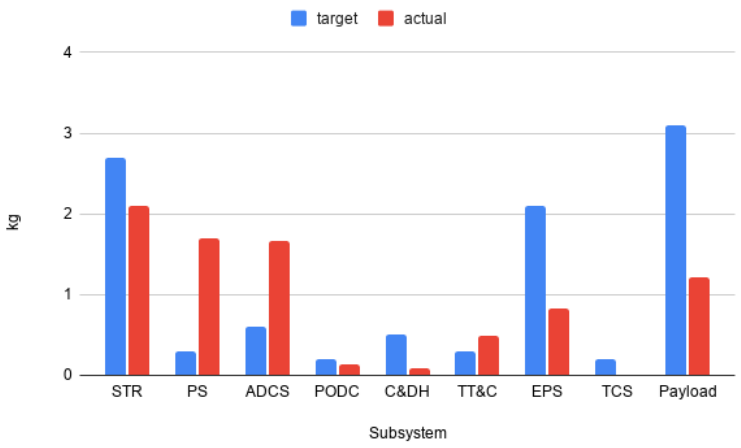

Figure 84: Comparison between target and actual weight of the subsystems

Subsystem	**total power [mW]**	**total power with 20% margin [mW]**
STR	0	0
PS	12500	15000
ADCS	14140	16968
PODC	658	789.6
C&DH	400	480
TT&C	23000	27600
EPS	-	-
Debris detection payload	3000	3600
Autonomous CAM	400	480
Reentry analysis payload	5000	6000

Table 25: Preliminary power request by each subsystem

during the different mission phases, the subsystems are then divided into 4 groups, each one representing 1 of the 4 main operations of the mission, as reported in table 26. Each group represents the active subsystems during that phase, and the relative power request. The result of the analysis shows that the power request is lower than 50 W in every mission phase. The highest power demand is due to the telecommunication system. This is because the X-band has been chosen. If further analysis on the TT&C system highlight the possibility to reduce the data rate and use a S-band communication system or completely rely on the UHF/VHF communication, the power demand on the subsystem can be significantly reduced. In figure 85 the percentage power level for every subsystem is presented, to be compared to the literature average reported in figure 83. From the target budget and the current budget a bad power management is highlighted.

Subsystem	**Debris science phase [mW]**	**Telecom [mW]**	**CAM and propulsion [mW]**	**Reentry analysis [mW]**
STR	-	-	-	-
PS	-	-	15000	-
ADCS	16968	16968	16968	16968
PODC	789.6	789.6	789.6	789.6
C&DH	480	480	480	480
TT&C	-	27600	-	-
EPS	-	-	-	-
Debris detection payload	3000	-	-	-
Autonomous CAM	-	-	480	-
Reentry analysis payload	-	-	-	6000
Total	**21237.6**	**45837.6**	**33717.6**	**24237.6**

Table 26: Preliminary power budget

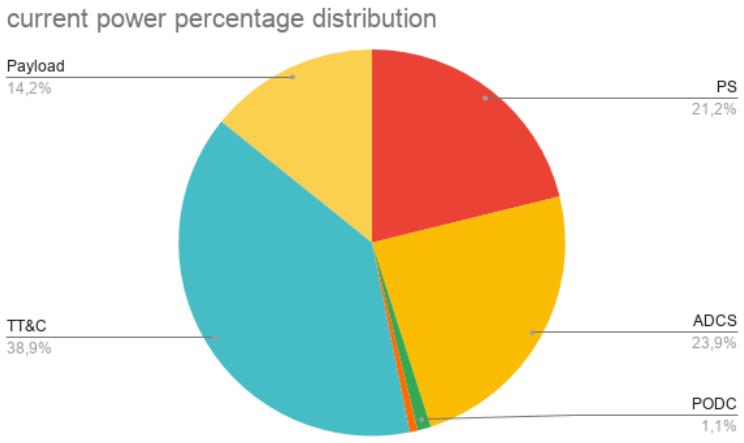

Figure 85: Preliminary power subsystems distribution

7 Conclusions

This thesis discusses the preliminary design of a CubeSat science mission in LEO orbit, focusing on the mission analysis and attitude control of the spacecraft. The operative orbit of the mission has been selected after a debris impact analysis, performed using the MASTER and DRAMA tool. The objective of the analysis was to identify suitable orbit parameters in order to guarantee the minimum of 100 debris impact by the detection payload, as stated in the requirements of the mission. The orbital range of the Sun synchronous orbits ranging from 550 to 1200 km has been then highlighted as potential selection pool for the operative orbit of the mission. Further trade-off on orbit parameters regard the ΔV budget for the reentry, the time to reentry and the time spent in the region between 200 and 100 km height. Considerations on the decay time of the orbit and required ΔV to deorbit the spacecraft, have led the final choice toward a 600 km Sun synchronous orbit. At this point, the orbit profile has been completed with the design of the reentry, through a multi-objective optimisation with the aim to maximise the time spent below 200 km and minimise the ΔV, that has been divided in 5 impulsive manoeuvres at the apogee of the orbit. For the entire mission profile, a preliminary attitude control has been proposed, and the results confirm the possibility to control the spacecraft in 3-axis during the entire mission, down to 100 km. Moreover, different reaction wheels desaturation strategies have been proposed, showing the feasibility of the manoeuvre in the different scenarios. A preliminary subsystems design has been carried out, along with a preliminary mass and power budget for the mission. The main characteristics that the three payload should have to satisfy mission requirements have been pointed out, proposing the payload architecture and performance to be implemented for the mission.
CubeSats have great potential for both science and commercial missions, reducing the costs and improving at the same time the compliance with space sustainability guidelines. The LEO environment characterisation coming from the data analysis of the debris science payload and the reentry analysis payload could constitute an important contribution for a better knowledge of the space environment, providing high fidelity models of space debris distribution and atmospheric reentry. Moreover, the selection of small thrust propulsion is effective on CubeSats, but future drag augmentation devices could ensure fast reentry with no propellant needed.
CubeSats represent a great opportunity to expand a sustainable and wise use of space and space science, widening the stakeholders pool reducing operation costs and giving standard components to rely on.

7.1 Future works

This thesis represent a feasibility study and preliminary mission design. The main open points that need to be further investigated in future development of the mission regard the subsystem design. The attitude control system architecture and its effectiveness until the reentry phase have been proved with simulations and models; also the reaction wheels saturation and desaturation manoeuvre has been investigated, proposing three different

alternatives. Future works should refine the analysis implementing the desaturation directly in the pointing simulation, in order to have a comprehensive and complete model. Further analysis are also needed to better estimate if the propellant mass is compliant with a single propulsion module, or if two are needed, according to the cold gas attitude thruster demand and the preliminary ΔV budget presented for the design of the propulsion system. Another future analysis will be the link budget and the TT&C subsystem. After estimating a precise and reliable link budget, the ground stations for mission service will be defined, and depending on the orbit profile a communication concept of operations has to be designed. In this way, the TT&C subsystem can be optimised, and a link strategy can be set for the debris science phase and the reentry phase. In this way, the need of an X-band transceiver could be confirmed; if instead the link budget has been overestimated and future analysis point out that the X-band transmissions are not required, a more common S-band transceiver can be chosen for the mission, solution that would determine a less power demand. The OBC design that has been presented is a preliminary design, and a more detailed analysis should be carried out in future works in order to estimate the system requirements to accomplish the tasks, considering as input other subsystems configuration. Moreover, the power budget of the mission will be revised, and the preliminary design of the EPS will be completed. The total area of the solar panels should be set in order to include it in the attitude and reentry analysis. The future design of the payloads will start from the baselines identified in this thesis, with particular attention to the key performance identified to be compliant with the mission requirements.

Bibliography

[1] M. Ramsey, D. Ash, J. Bowen, A. Sadilek, E. Bunker, B. Harden, V. Pisacane, A. Chris, T. Musmanno, H. Ngo, F. Giovane, J. Liou, G. Stansbery, V. Pisacane, R. Corsaro, M. Burchell, Debris Resistive Acoustic Grid Orbital Navy Sensor (DRAGONS), in: Infotech@Aerospace 2011, American Institute of Aeronautics and Astronautics, Reston, Virigina, 2011. doi:10.2514/6.2011-1600.
URL http://arc.aiaa.org/doi/10.2514/6.2011-1600

[2] K. M. Brumbaugh, H. C. Kjellberg, E. Glenn Lightsey, A. Wolf, R. Laufer, In-situ sub-millimeter space debris detection using cubesats, Advances in the Astronautical Sciences (2012).

[3] Q. Funke, B. Virgili, V. Braun, T. Flohrer, H. Krag, S. Lemmens, K. Merz, Current collision avoidance service by ESA's space debris office, 7th European Conference on Space Debris (2017).

[4] B. Bastida Virgili, T. Flohrer, H. Krag, K. Merz, S. Lemmens, CREAM — ESA's Proposal for Collision Risk Estimation and Automated Mitigation, in: First International Orbital Debris Conference, Vol. 2109, 2019, p. 6031.

[5] E. De Pasquale, L. Francillout, J. J. Wasbauer, J. Hatton, J. Albers, D. Steele, ATV Jules Verne reentry observation: Mission design and trajectory analysis, in: IEEE Aerospace Conference Proceedings, 2009. doi:10.1109/AERO.2009.4839703.

[6] W. Ailor, I. Dupzyk, J. Shepard, M. Newfield, REBR: An innovative, cost-effective system for return of reentry data, in: A Collection of Technical Papers - AIAA Space 2007 Conference, 2007. doi:10.2514/6.2007-6222.

[7] R. D. Corsaro, F. Giovane, J.-C. Liou, M. J. Burchell, M. J. Cole, E. G. Williams, N. Lagakos, A. Sadilek, C. R. Anderson, Characterization of space dust using acoustic impact detection, The Journal of the Acoustical Society of America (2016). doi:10.1121/1.4960782.

[8] D. Griggs, M. Stafford-Smith, O. Gaffney, J. Rockström, M. C. Öhman, P. Shyamsundar, W. Steffen, G. Glaser, N. Kanie, I. Noble, Sustainable development goals for people and planet, Nature 495 (7441) (2013) 305–307.

[9] T. Maury, P. Loubet, M. Trisolini, A. Gallice, G. Sonnemann, C. Colombo, Assessing the impact of space debris on orbital resource in life cycle assessment: A proposed method and case study, Science of the Total Environment (2019). doi:10.1016/j.scitotenv.2019.02.438.

[10] Esa's annual space environment report, ESA Space Debris Office (2020). URL https://www.sdo.esoc.esa.int/environment_report/Space_Environment_Report_latest.pdf

[11] E. Portal, Orbital debris. URL https://directory.eoportal.org/web/eoportal/satellite-missions/o/orbital-debris

[12] M. Mejía-Kaiser, iadc Space Debris Mitigation Guidelines, in: The Geostationary Ring, 2020. doi:10.1163/9789004411029_014.

[13] L. Hall, The History of Space Debris, Space Traffic Management Conference (2014).

[14] A. I. Nazarenko, Prediction of the space debris spatial distribution on the basis of the evolution equations, Acta Astronautica (2014). doi:10.1016/j.actaastro.2014.02.023.

[15] D. Mehrholz, L. Leushacke, W. Flury, R. Jehn, H. Klinkrad, M. Landgraf, Detecting, tracking and imaging space debris, ESA Bulletin(0376-4265) (2002).

[16] ESA, The current state of space debris (2020). URL https://www.esa.int/Safety_Security/Space_Debris/The_current_state_of_space_debris

[17] K. Fletcher, Space debris: The esa approach (03 2017).

[18] S. L. Report, Orbital launch summary by year. URL https://www.spacelaunchreport.com/logyear.html

[19] J. Mason, J. Stupl, W. Marshall, C. Levit, Orbital debris-debris collision avoidance, Advances in Space Research (2011). arXiv:1103.1690, doi:10.1016/j.asr.2011.08.005.

[20] D. J. Kessler, N. L. Johnson, J. C. Liou, M. Matney, The Kessler Syndrome: Implications to future space operations, in: Advances in the Astronautical Sciences, 2010.

[21] D. J. Kessler, B. G. Cour-Palais, COLLISION FREQUENCY OF ARTIFICIAL SATELLITES: THE CREATION OF A DEBRIS BELT., J Geophys Res (1978). doi:10.1029/JA083iA06p02637.

[22] D. J. Kessler, B. G. Cour-Palais, Collision frequency of artificial satellites: The creation of a debris belt, Journal of Geophysical Research: Space Physics 83 (A6) (1978) 2637–2646. arXiv:https://agupubs.onlinelibrary.wiley.com/doi/pdf/10.1029/JA083iA06p02637, doi:10.1029/JA083iA06p02637.
URL https://agupubs.onlinelibrary.wiley.com/doi/abs/10.1029/JA083iA06p02637

[23] T. S. Kelso, Analysis of the Iridium 33-Cosmos 2251 collision, in: Advances in the Astronautical Sciences, 2010.

[24] ESPI, "espi report 71 - towards a european approach to space traffic management - full report, European Space Policy Institute (ESPI) (2020).

[25] S. H. Park, H. D. Kim, G. Park, Orbit, orbital lifetime, and reentry survivability estimation for orbiting objects, Advances in Space Research (2018). doi:10.1016/j.asr.2018.08.016.

[26] Z. Wu, R. Hu, X. Qu, X. Wang, Z. Wu, Space debris reentry analysis methods and tools, Chinese Journal of Aeronautics (2011). doi:10.1016/S1000-9361(11)60046-0.

[27] N. Bobrinsky, L. Del Monte, The space situational awareness program of the European Space Agency, Cosmic Research (2010). doi:10.1134/S0010952510050035.

[28] NASA, Space debris and human spacecraft.
URL https://www.nasa.gov/mission_pages/station/news/orbital_debris.html

[29] B. Weeden, The numbers game (7 2009).
URL https://www.thespacereview.com/article/1417/1

[30] B. Weeden, P. Cefola, J. Sankaran, Global Space Situational Awareness Sensors, Proceedings of the Advanced Maui Optical and Space Surveillance Technologies Conference (2010).

[31] ESA, Space debris.
URL https://www.esa.int/Safety_Security/Space_Debris/About_space_debris

[32] V. Mayorova, V. Leonov, D. Grishko, Analysis of approaches to the near-earth orbit cleanup from space debris of the size below10 cm, Aerospace Scientific Journal 16 (01 2016). doi:10.7463/aersp.0116.0833914.

[33] L. C. G. Shepherd, A. F. S. Command, Space surveillance network, in: Shared Space Situational Awareness Conference, Colorado Sprincs, CO, 2006.

[34] E. Portal, Midcourse space experiment.
URL https://directory.eoportal.org/web/eoportal/satellite-missions/m/msx

[35] J. Utzmann, A. Wagner, J. Silha, T. Schildknecht, P. Willemsen, F. Teston, T. Flohrer, Space-based space surveillance and tracking demonstrator: mission and system design (2014).

[36] E. P. Directory, Sbss (space-based surveillance system).
URL `https://directory.eoportal.org/web/eoportal/satellite-missions/s/sbss`

[37] P. Maskell, L. Oram, Sapphire: Canada's Answer to Space-Based Surveillance of Orbital Objects, in: C. Paxson, H. Snell, J. Griffin, K. Kraemer, S. Price, M. Kendra, D. P. E. Mizuno (Eds.), Advanced Maui Optical and Space Surveillance Technologies Conference, 2008, p. E5.

[38] P. H. Krisko, The new NASA orbital debris engineering model ORDEM 3.0, in: AIAA/AAS Astrodynamics Specialist Conference 2014, 2014.

[39] A. P. Ingersoll, Pioneer 10 and 11 observations and the dynamics of Jupiter's atmosphere, Icarus (1976). `doi:10.1016/0019-1035(76)90052-X`.

[40] E. J. Smith, R. G. Marsden, The Ulysses Mission, Scientific American (1998). `doi:10.1038/scientificamerican0198-74`.

[41] E. Grün, H. Fechtig, M. S. Hanner, J. Kissel, B. A. Lindblad, D. Linkert, D. Maas, G. E. Morfill, H. A. Zook, The Galileo Dust Detector, Space Science Reviews (1992). `doi:10.1007/BF00216860`.

[42] R. Srama, T. J. Ahrens, N. Altobelli, S. Auer, J. G. Bradley, M. Burton, V. V. Dikarev, T. Economou, H. Fechtig, M. Görlich, M. Grande, A. Graps, E. Grün, O. Havnes, S. Helfert, M. Horanyi, E. Igenbergs, E. K. Jessberger, T. V. Johnson, S. Kempf, A. V. Krivov, H. Krüger, A. Mocker-Ahlreep, G. Moragas-Klostermeyer, P. Lamy, M. Landgraf, D. Linkert, G. Linkert, F. Lura, J. A. Mcdonnell, D. Möhlmann, G. E. Morfill, M. Müller, M. Roy, G. Schäfer, G. Schlotzhauer, G. H. Schwehm, F. Spahn, M. Stübig, J. Svestka, V. Tschernjawski, A. J. Tuzzolino, R. Wäsch, H. A. Zook, The Cassini cosmic dust analyzer, Space Science Reviews (2004). `doi:10.1007/s11214-004-1435-z`.

[43] H. Klinkrad, J. Alarcon, N. Sánchez-Ortiz, Collision avoidance for operational esa satellites, European Space Agency, (Special Publication) ESA SP 587 (2005) 509.

[44] N. Sanchez-Ortiz, R. Dominguez-Gonzalez, J. C. De Oliveira, J. Gelhaus, H. Krag, ESA DRAMA ARES and CROC: Evaluation of cross section and estimated collision alerts, in: Proceedings of the International Astronautical Congress, IAC, 2013.

[45] H. Klinkrad, P. Beltrami, S. Hauptmann, C. Martin, H. Sdunnus, H. Stokes, R. Walker, J. Wilkinson, The ESA Space Debris Mitigation Handbook 2002, in: Advances in Space Research, 2004. `doi:10.1016/j.asr.2003.01.018`.

[46] T. Floher, S. Lemmens, B. Bastida Virgili, H. Krag, H. Klinkrad, E. Parilla, N. Sanchez, J. Oliveira, F. Pina, DISCOS – Current Status and Future Developments, in: Proceedings of the 6h European Conference on Space Debris, ESOC, Darmstadt, Germany, 2013.

[47] T. Flohrer, H. Krag, K. Merz, S. Lemmens, CREAM - ESA's Proposal for Collision Risk Estimation and Automated Mitigation, in: S. Ryan (Ed.), Advanced Maui Optical and Space Surveillance Technologies Conference, 2019, p. 57.

[48] H. Krag, K. Merz, T. Flohrer, S. Lemmens, B. B. Virgili, Q. Funke, V. Braun, ESA's modernised collision avoidance service, in: SpaceOps 2016 Conference, 2016. doi:10.2514/6.2016-2449.

[49] G. Salemme, R. Armellin, P. Di Lizia, Continuous-thrust collision avoidance manoeuvres optimization, in: AIAA Scitech 2020 Forum, 2020. doi:10.2514/6.2020-0231.

[50] J. H. Grinstead, P. Jenniskens, A. M. Cassell, J. Albers, M. W. Winter, Airborne observation of the Hayabusa sample return capsule re-entry, in: 42nd AIAA Thermophysics Conference, 2011. doi:10.2514/6.2011-3329.

[51] K. A. Trumble, I. Cozmuta, S. Sepka, P. Jenniskens, M. Winter, Postflight aerothermal analysis of stardust sample return capsule, Journal of Spacecraft and Rockets (2010). doi:10.2514/1.41514.

[52] M. Winter, G. Herdrich, Spectroscopic observation of the stardust re-entry in the near UV, in: Collection of Technical Papers - 39th AIAA Thermophysics Conference, 2007.

[53] P. Jenniskens, D. Kontinos, M. Wright, J. Olejniczak, G. Raiche, P. Wercinski, P. Desai, C. Taylor, M. Mcharg, S. Abe, R. Rairden, J. Albers, M. Winter, J. Wolf, D. Revelle, P. Gural, R. Dantowitz, F. Rietmeijer, A. Hildebrand, Preparing for the meteoritic return of stardust, Dust in Planetary Systems 643 (2006) 7–10.

[54] A. M. Cassell, M. W. Winter, G. A. Allen, J. H. Grinstead, M. E. Antimisiaris, J. Albers, P. Jenniskens, Hayabusa re-entry: Trajectory analysis and observation mission design, in: 42nd AIAA Thermophysics Conference, 2011. doi:10.2514/6.2011-3330.

[55] M. Yoshikawa, J. Kawaguchi, A. Fujiwara, A. Tsuchiyama, Hayabusa Sample Return Mission, 2015. doi:10.2458/azu_uapress_9780816532131-ch021.

[56] F. M. Capristan, J. J. Alonso, Range safety assessment tool (rsat): An analysis environment for safety assessment of launch and reentry vehicles, in: 52nd Aerospace Sciences Meeting, 2014, p. 0304.

[57] W. Ailor, W. Hallman, G. Steckel, M. Weaver, Analysis of reentered debris and implications for survivability modeling, in: European Space Agency, (Special Publication) ESA SP, 2005.

[58] W. Ailor, I. Dupzyk, J. Shepard, M. Newfield, REBR: An Innovative, Cost-Effective System for Return of Reentry Data. arXiv:https://arc.aiaa.org/doi/pdf/10.2514/6.2007-6222, doi:10.2514/6.2007-6222.
URL https://arc.aiaa.org/doi/abs/10.2514/6.2007-6222

[59] ESA, Space safety/space traffic management programmes.
URL https://www.esa.int/About_Us/Ministerial_Council_2016/Space_Safety_Space_Traffic_Management_Programmes

[60] H. Krag, ESA's Space Safety Programme, in: First International Orbital Debris Conference, Vol. 2109, 2019, p. 6147.

[61] H. Schaub, L. E. Jasper, P. V. Anderson, D. S. McKnight, Cost and risk assessment for spacecraft operation decisions caused by the space debris environment, Acta Astronautica (2015). doi:10.1016/j.actaastro.2015.03.028.

[62] F. Schäfer, R. Putzar, Triple wall ballistic limit equation, in: European Space Agency, (Special Publication) ESA SP, 2005.

[63] UNOOSA, Space debris mitigation guidelines of the committee on the peaceful uses of outer space (2010).
URL https://www.unoosa.org/pdf/publications/st_space_49E.pdf

[64] A. Poghosyan, A. Golkar, Cubesat evolution: Analyzing cubesat capabilities for conducting science missions, Progress in Aerospace Sciences 88 (2017) 59–83.

[65] ESA, Cubesat concept - deployer standards for an enlarged cubesat family.
URL https://earth.esa.int/web/eoportal/satellite-missions/c-missions/cubesat-deployer

[66] U. N. R. Laboratory, Nrl patents compact orbital debris sensor (2015).
URL https://www.nrl.navy.mil/news/releases/nrl-patents-compact-orbital-debris-sensor

[67] W. Bauer, O. Romberg, C. Wiedemann, G. Drolshagen, P. Vörsmann, Development of in-situ Space Debris Detector, Advances in Space Research (2014). doi:10.1016/j.asr.2014.07.035.

[68] B. Lim, S. Statham, S. Misra, J. Clark, K. Donahue, J. Steinkraus, The Radiometer Atmospheric CubeSat Experiment (RACE) pre-launch performance, in: 2015 IEEE MTT-S International Microwave Symposium, IMS 2015, 2015. doi:10.1109/MWSYM.2015.7167097.

[69] R. P. Patera, W. H. Ailor, The realities of reentry disposal, Advances in the Astronautical Sciences (1998).

[70] J. Wertz, D. Everett, J. Puschell, Space mission engineering : the new smad, 2011.

[71] ESA, Space debris user portal.
URL https://sdup.esoc.esa.int/

[72] M. Mejía-Kaiser, iadc Space Debris Mitigation Guidelines, in: The Geostationary Ring, 2020. doi:10.1163/9789004411029_014.

[73] National Geophysical Data Center, U.S. standard atmosphere (1976) (1992). doi:10.1016/0032-0633(92)90203-Z.

[74] J. R. Wertz, Spacecraft attitude determination and control, Vol. 73, 1978. doi:10.1007/978-94-009-9907-7.

[75] T. P. Brito, C. C. Celestino, R. V. Moraes, Study of the decay time of a CubeSat type satellite considering perturbations due to the Earth's oblateness and atmospheric drag, in: Journal of Physics: Conference Series, 2015. doi:10.1088/1742-6596/641/1/012026.

[76] D. Selva, D. Krejci, A survey and assessment of the capabilities of Cubesats for Earth observation (2012). doi:10.1016/j.actaastro.2011.12.014.

[77] J. Puig-Suari, C. Turner, R. Twiggs, CubeSat: the development and launch support infrastructure for eighteen different satellite customers on one launch, 15TH Annual/USU Conference on Small Satellites (2001).

[78] J. Bouwmeester, J. Guo, Survey of worldwide pico- and nanosatellite missions, distributions and subsystem technology, Acta Astronautica (2010). doi:10.1016/j.actaastro.2010.06.004.

[79] California Polytechnic State University, CubeSat Design Specification Rev. 13, The CubeSat Program, California Polytechnic State (2014).

[80] NASA, State of the Art of Small Spacecraft Technology, State of the Art of Small Spacecraft Technology (2018).

[81] T. P. University, Russia's first 3d-printed satellite preparing to launch into outer space.
URL https://tpu.ru/en/about/tpu_today/news/view?id=3069#:~:text=Satellite%20launch%20into%20outer%20space,the%20size%20of%2030x11x11%20sm.

[82] M. S. University, Printsat.
URL http://www.ssel.montana.edu/printsat.html#:~:text=Mission%20Overview,a%20material%20for%20space%20structures.

[83] Design and development of the unsw qb50 cubesat - ec0.

[84] N. R. Council, Orbital Debris: A Technical Assessment, The National Academies Press, Washington, DC, 1995. doi:10.17226/4765.
URL https://www.nap.edu/catalog/4765/orbital-debris-a-technical-assessment

[85] M. M. Paul Stephen Dempsey, Suborbital Flights and the Delimitation of Air Space Vis-à-Vis Outer Space: Functionalism, Spatialism and State Sovereignty, XLII Annals of Air & Space Law 197 (2017) (2020).
URL https://ssrn.com/abstract=3558150

[86] N. Spacemind, Sm12.
URL https://www.npcspacemind.com/solutions/nanosatellite-hardware/cubesat-structure/sm12-12u/

[87] ISIS, 8-unit cubesat structure.
URL https://www.isispace.nl/product/8-unit-cubesat-structure/

[88] ESA, Cubesat concept - deployer standards for an enlarged cubesat family.
URL https://earth.esa.int/web/eoportal/satellite-missions/c-missions/cubesat-deployer

[89] NanoAvionics, Cubesat propulsion system epss.
URL https://nanoavionics.com/cubesat-components/cubesat-propulsion-system-epss/

[90] D. Aerospace, Cubesat propulsion module.
URL https://www.dawnaerospace.com/products/p/cubesat-propulsion-module

[91] E. Portal, Armadillo (attitude related maneuvers and debris instrument in low (l) orbit).
URL https://directory.eoportal.org/web/eoportal/satellite-missions/a/armadillo

[92] N. systems, Sun sensors: Ncss-sa05.
URL https://www.newspacesystems.com/portfolio/sun-sensors/

[93] BST, Star tracker-st200.
URL https://www.berlin-space-tech.com/portfolio/star-tracker-st200/

[94] Sensonor, Stim202.
URL https://www.sensonor.com/products/gyro-modules/stim202/

[95] N. systems, Magnetometer.
URL https://www.newspacesystems.com/portfolio/magnetometer/

[96] D-Orbit, D-sense: multi-sensor adcs module.
URL https://www.dorbit.space/d-sense

[97] ISIS, Isis magnetorquer board.
URL https://www.isispace.nl/product/isis-magnetorquer-board/

[98] GOMspace, Reaction wheel for nanosatellites.
URL https://gomspace.com/shop/subsystems/attitude-orbit-control-systems/nanotorque-gsw-600.aspx

[99] B. Wie, Space vehicle dynamics and control, American Institute of Aeronautics and Astronautics, 2008.

[100] NOAA, International geomagnetic reference field.
URL https://www.ngdc.noaa.gov/IAGA/vmod/igrf.html

[101] NASA, Earth albedo and emitted radiation.
URL https://ntrs.nasa.gov/archive/nasa/casi.ntrs.nasa.gov/19710023628.pdf

[102] J. C. McDowell, The edge of space: Revisiting the Karman Line, Acta Astronautica (2018). arXiv:1807.07894, doi:10.1016/j.actaastro.2018.07.003.

[103] R. Ranjan, S. K. Chou, F. Riaz, K. Karthikeyan, Cold gas micro propulsion development for satellite application, in: Energy Procedia, 2017. doi:10.1016/j.egypro.2017.12.758.

[104] H. Technologies, Gnss200.
URL https://hyperiontechnologies.nl/products/gnss200/

[105] S. S. Technology, Sgr-ligo.
URL https://www.sstl.co.uk/getattachment/Media-Hub/Featured/Navigation/SGR-Ligo-Datasheet-2018-V2-Read-Only.pdf?lang=en-GB

[106] ISIS, Gnss patch antenna.
URL https://www.isispace.nl/product/gnss-patch-antenna/

[107] S. Labs, pipatch-max/fm.
URL https://www.skyfoxlabs.com/product/20-pipatch-max

[108] Moog, Monopropellant propulsion module.
URL https://www.moog.com/content/dam/moog/literature/Space_Defense/spaceliterature/propulsion/moog-monopropellant-propulsion-module-datasheet.pdf

[109] arm, Phytec 01. phycore-arm9/lpc3250 system on module (som).
URL https://www.keil.com/boards/tpcl/630.htm

[110] I. M. Tecnologia, Cubesat on-board computer.
URL http://www.imtsrl.it/obc-cubesat-it.html

[111] ISIS, Isis on board computer.
URL https://www.isispace.nl/product/on-board-computer/

[112] U. D. o. C. Ntia, Manual of Regulations and Procedures for Federal Radio Frequency, Channels (2009).

[113] ISIS, Isis vhf uplink/uhf downlink full duplex transceiver.
URL https://www.isispace.nl/product/isis-uhf-downlink-vhf-uplink-full-duplex-transc

[114] I. spacecom, X band transceiver.
URL https://www.iq-spacecom.com/images/downloads/XLink_Datasheet_07_2020.pdf

[115] EnduroSat, Uhf antenna iii.
URL https://www.endurosat.com/cubesat-store/all-cubesat-modules/uhf-antenna/?v=cd32106bcb6d

[116] EnduroSat, X-band patch antenna.
URL https://www.endurosat.com/cubesat-store/all-cubesat-modules/x-band-patch-antenna/?v=cd32106bcb6d

[117] EnduroSat, X-band 4x4 patch array.
URL https://www.endurosat.com/cubesat-store/all-cubesat-modules/x-band-4x4-patch-array/?v=cd32106bcb6d

[118] N. Factory, Smallsat x-band antenna.
URL https://newspace-factory.com/product/cubesat-x-band-antenna/

[119] A. Space, Space solar cells.
URL http://www.azurspace.com/index.php/en/products/products-space/space-solar-cells

[120] F. Santoni, F. Piergentili, S. Donati, M. Perelli, A. Negri, M. Marino, An innovative deployable solar panel system for cubesats, Acta Astronautica 95 (2014) 210 – 217. doi:https://doi.org/10.1016/j.actaastro.2013.11.011.
URL http://www.sciencedirect.com/science/article/pii/S0094576513004037

[121] GOMspace, High capacity lithium-ion battery pack with a heater for cubesats.
URL https://gomspace.com/shop/subsystems/power/nanopower-bpx.aspx

[122] GOMspace, Modular power system for large nanosatellites.
URL https://gomspace.com/shop/subsystems/power/nanopower-p60.aspx

[123] A. T. Kearsley, G. A. Graham, J. A. McDonnell, E. A. Taylor, G. Drolshagen, R. J. Chater, D. McPhail, M. J. Burchell, The chemical composition of micrometeoroids impacting upon the solar arrays of the Hubble Space Telescope, Advances in Space Research (2007). doi:10.1016/j.asr.2006.05.011.

[124] A. T. Kearsley, J. L. Colaux, D. K. Ross, P. J. Wozniakiewicz, L. Gerlach, P. Anz-Meador, T. Griffin, B. Reed, J. Opiela, V. V. Palitsin, G. W. Grime, R. P. Webb, C. Jeynes, J. Spratt, T. Salge, M. J. Cole, M. C. Price, M. J. Burchell, Hypervelocity impact in low earth orbit: Finding subtle impactor signatures on the Hubble Space Telescope, in: Procedia Engineering, 2017. doi:10.1016/j.proeng.2017.09.746.

[125] A. Shua, S. Bugiel, E. Grun, J. Hillier, M. Horányi, T. Munsat, R. Srama, Cratering studies in Polyvinylidene Fluoride (PVDF) thin films, in: Planetary and Space Science, 2013. doi:10.1016/j.pss.2013.05.001.

[126] J. A. Simpson, A. J. Tuzzolino, Polarized polymer films as electronic pulse detectors of cosmic dust particles, Nuclear Inst. and Methods in Physics Research, A (1985). doi:10.1016/0168-9002(85)90145-7.

[127] A. J. Tuzzolino, T. E. Economou, R. B. McKibben, J. A. Simpson, S. Benzvi, L. Blackburn, H. D. Voss, H. Gursky, Final results from the space dust (SPADUS) instrument flown aboard the earth-orbiting ARGOS spacecraft, Planetary and Space Science (2005). doi:10.1016/j.pss.2005.03.008.

[128] A. J. Tuzzolino, T. E. Economou, R. B. McKibben, J. A. Simpson, J. A. McDonnell, M. J. Burchell, B. A. Vaughan, P. Tsou, M. S. Hanner, B. C. Clark, D. E. Brownlee, Dust Flux Monitor Instrument for the Stardust mission to comet Wild 2, Journal of Geophysical Research E: Planets (2003). doi:10.1029/2003je002086.

[129] J. A. Simpson, R. Z. Sagdeev, A. J. Tuzzolino, M. A. Perkins, L. V. Ksanfomality, D. Rabinowitz, G. A. Lentz, V. V. Afonin, J. Erö, E. Keppler, J. Kosorokov, E. Petrova, L. Szabó, G. Umlauft, Dust counter and mass analyser (DUCMA) measurements of comet Halley's coma from vega spacecraft, Nature (1986). doi:10.1038/321278a0.

[130] A. J. Tuzzolino, R. B. McKibben, J. A. Simpson, S. BenZvi, H. D. Voss, H. Gursky, The Space Dust (SPADUS) instrument aboard the Earth-orbiting ARGOS spacecraft: I - Instrument description, Planetary and Space Science (2001). doi:10.1016/S0032-0633(01)00012-5.

[131] J. A. McDonnell, The Giotto dust impact detection system, Journal of Physics E: Scientific Instruments (1987). doi:10.1088/0022-3735/20/6/033.

[132] K. J. Seidensticker, D. Möhlmann, I. Apathy, W. Schmidt, K. Thiel, W. Arnold, H. H. Fischer, M. Kretschmer, D. Madlener, A. Péter, R. Trautner, S. Schieke, SESAME - An experiment of the Rosetta Lander Philae: Objectives and general design, Space Science Reviews (2007). doi:10.1007/s11214-006-9118-6.

[133] E. Mazzotta Epifani, E. Bussoletti, L. Colangeli, P. Palumbo, A. Rotundi, S. Vergara, J. M. Perrin, J. J. Lopez Moreno, I. Olivares, The grain detection system for

the GIADA instrument: Design and expected performances, Advances in Space Research (2002). doi:10.1016/S0273-1177(02)00133-3.

[134] F. Esposito, L. Colangeli, V. Della Corte, P. Palumbo, Physical aspect of an "impact sensor" for the detection of cometary dust momentum onboard the "Rosetta" space mission, Advances in Space Research (2002). doi:10.1016/S0273-1177(02)00132-1.

[135] G. R. Frank Odom III, Piezo dust detector (2014).
URL https://www.baylor.edu/casper/doc.php/237649.pdf

[136] C. Englert, J. Bays, K. Marr, C. Brown, A. Nicholas, T. Finne, Optical orbital debris spotter, Acta Astronautica 104 (2014) 99–105. doi:10.1016/j.actaastro.2014.07.031.

[137] J. L. Gonzalo, C. Colombo, Collision avoidance algorithms for space traffic management applications, 2020.

[138] MKS, 905 micropirani vacuum pressure transducer kit.
URL https://www.mksinst.com/f/905-micro-pirani-vacuum-sensor-kit

[139] Omega, Thin-film heat flux sensors.
URL https://br.omega.com/omegaFiles/temperature/pdf/HFS-3_HFS-4.pdf

[140] A. Devices, Six degrees of freedom inertial sensor.
URL https://www.analog.com/media/en/technical-documentation/data-sheets/ADIS16485.pdf

[141] E. Portal, Sapphire space surveillance.
URL https://earth.esa.int/web/eoportal/satellite-missions/s/sapphire-space-surveillance

[142] E. S. . Security, The current state of space debris (10 2020).
URL https://www.esa.int/Safety_Security/Space_Debris/The_current_state_of_space_debris

[143] ESA, Space situational awareness.
URL https://www.esa.int/About_Us/ESAC/Space_Situational_Awareness_-_SSA

[144] ESA, Space debris: The esa approach.
URL http://esamultimedia.esa.int/multimedia/publications/BR-336/offline/download.pdf

[145] ESA, Space debris: Assessing the risk.
URL https://www.esa.int/About_Us/ESOC/Space_debris_assessing_the_risk

[146] F. Alby, E. Lansard, T. Michal, Collision of Cerise with space debris, European Space Agency, (Special Publication) ESA SP (1997).